UNIVERSITÀ
DI PAVIA

Dipartimento di Biologia e Biotecnologie "L. Spallanzani"

New insights in Aicardi-Goutières Syndrome: association between a RNU7-1 variant and novel pathologic mechanisms

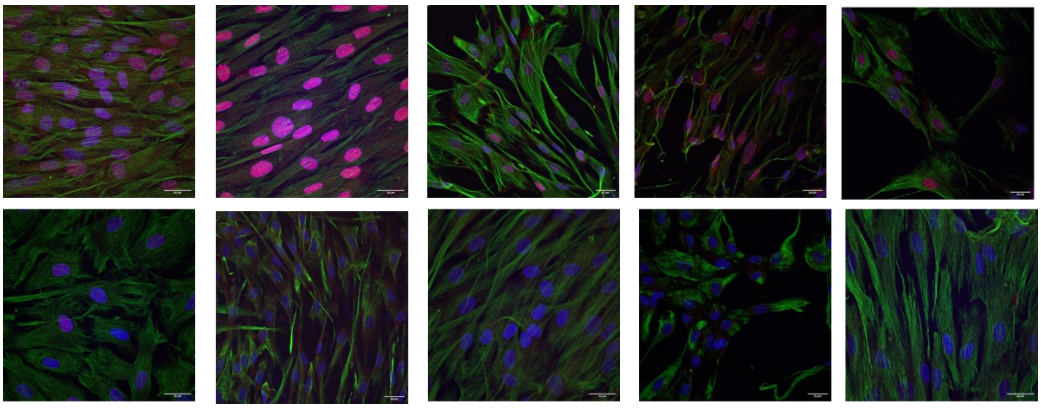

Erika Maghraby

Dottorato di Ricerca in
Genetica, Biologia Molecolare e Cellulare
Cycle XXXVII – A.A. 2023-2024

1. TABLE OF CONTENTS

2. **ABSTRACT** 1
3. **ABBREVIATIONS** 3
4. **INTRODUCTION** 6
   - 4.1 Aicardi-Goutières Syndrome: overview 6
   - 4.2 Clinical manifestations 6
     - *4.2.1 Neurological signs* 7
     - *4.2.2 Extra-neurological signs* 8
   - 4.3 Diagnostic criteria 8
     - *4.3.1 Neuroradiological aspects* 9
     - *4.3.2 Cerebrospinal fluid (CSF)* 10
     - *4.3.3 Interferon signature* 10
   - 4.4 AGS and Type I interferonopathies 11
     - *4.4.1 Mechanisms of interferon induction* 12
   - 4.5 Genetic insights of AGS 13
     - *4.5.1 TREX1 (AGS1)* 14
     - *4.5.2 RNASEH2B (AGS2), RNASEH2C (AGS3), RNASEH2A (AGS4)* 14
     - *4.5.3 SAMHD1 (AGS5)* 15
     - *4.5.4 ADAR1 (AGS6)* 16
     - *4.5.5 IFIH1 (AGS7)* 16
     - *4.5.6 LSM11 (AGS8) and RNU7-1 (AGS9)* 17
     - *4.5.7 Frequencies of mutations and genotype-phenotype correlations* 18
   - 4.6 Pathogenesis 19
     - *4.6.1 Implication of RNU7-1 in AGS pathogenesis* 20
     - *4.6.2 Mitochondria* 22
   - 4.7 Therapeutic options for Aicardi-Goutières Syndrome 24
     - *4.7.1 Reverse transcriptase inhibitors* 25
     - *4.7.2 JAK-STAT inhibitors* 25
     - *4.7.3 Hydroxychloroquine* 26
     - *4.7.4 Metformin* 26
5. **AIMS** 28
6. Materials and methods 29

6.1 Study subjects 29
6.2 Isolation and characterization of human dermal fibroblasts 29
6.3 Cell culture 29
6.4 Hydroxychloroquine treatment 30
6.5 RNA analysis 30
6.5.1 Total RNA extraction 30
6.5.2 RNA subcellular fractioning 30
6.5.3 RNA quantification 31
6.5.4 Reverse transcription 31
6.5.5 Real-Time PCR 32
6.5.6 RNA immunoprecipitation 33
6.5.7 Total protein extraction 33
6.5.8 Subcellular fractioning 33
6.5.9 Bradford protein assay 33
6.5.10 Western Blot Analysis 34
6.5.11 Immunocytochemistry 34
6.5.12 ELISA assay 35
6.5.13 Nascent protein labeling (Click-It assay) 35
6.6 Mitochondrial assays 36
6.6.1 Mitotracker assay 36
6.6.2 Mitosox assay 36
6.7 MTT assay 36
6.8 Transmission Electron Microscopy (TEM) analysis 37
6.9 RNA sequencing workflow 37
6.10 Statistical analysis for *in vitro* experiments 39
7. **RESULTS** 40
7.1 Setup of the experimental model 40
7.1.1 Fibroblast characterization 40
7.1.2 Metabolic state and membrane permeability assay 41
7.2 Impact of RNU7-1 pathologic variant on U7 snRNA 41
7.2.1 Folding prediction of U7 snRNA following RNU7-1 mutation 41

7.2.2 Investigation of U7 snRNA expression and localization in primary fibroblasts carrying mutations in RNU7-1 42

7.3 Impact of RNU7-1 pathologic variant on other AGS-related genes 43

7.4 Investigation of AGS canonic features 43

7.4.1 Production of IFNα in fibroblasts carrying mutations in RNU7-1 43

7.4.2 Evaluation of interferon signature in AGS9 fibroblasts 44

7.5 Effects of Hydroxychloroquine on interferon signaling and cell viability 46

7.5.1 Hydroxychloroquine reduces interferon signature and secretion of IFNα 46

7.5.2 Hydroxychloroquine improves overall metabolism of AGS9 cells 47

7.6 Importance of the cGAS-STING signaling cascade in IFN production 47

7.7 Investigation of AGS specific features following RNU7-1 variation 48

7.7.1 RNU7-1 variations affect expression of U7 snRNP-related genes 49

7.7.2 Variations of RNU7-1 impair physical association between U7 snRNA and ZFP100 50

7.8 Identification of novel molecular pathways involved in AGS9 pathology ... 50

7.8.1 RNA-sequencing analysis highlights differences in AGS9 transcriptome 50

7.8.2 AGS9 fibroblasts present alterations in multiple neural pathways 52

7.8.3 Transcriptional changes in AGS9 cells affect chromatin modifications .. 53

7.9 Variations in RNU7-1 gene affect histone mRNA maturation and translation 54

7.9.1 Misprocessing of RDH pre-mRNAs in AGS9 fibroblasts 54

7.9.2 Histone translation is reduced because of RNU7-1 pathologic variations 55

7.10 TEM analysis reveals morphological alterations in AGS9 fibroblasts 56

7.10.1 AGS9 fibroblasts present dysfunctions in mitochondrial metabolism 57

7.10.2 Nascent protein synthesis is decreased in AGS9 cells 58

8. **DISCUSSION** 60

9. **REFERENCES** 64

10. **LIST OF PUBLICATIONS** 78

11. **POSTERS AND ORAL PRESENTATIONS** 79

2. ABSTRACT

Aicardi-Goutières syndrome (AGS) is a rare genetic disorder that mainly affects the nervous system of pediatric individuals. Specifically, this disease causes a progressive encephalopathy related to motor impairment and alteration of normal neurodevelopment. This disease is also characterized by the presence of brain calcifications due to chronic inflammation mediated by high levels of alpha interferon (IFNα). As overproduction IFNα in represents a key aspect in cerebrospinal fluid and blood of over 85% of AGS-affected patients, this condition belongs is classified amongst the type I Interferonopathies. AGS is defined as a monogenic disorder currently associated with mutations in 9 genes (*TREX1, RNASEH2A, RNASEH2B, RNASEH2C, SAMHD1, ADAR, IFIH1, LSM11* and *RNU7-1*), all of which encode for proteins or transcripts involved in nucleic acid metabolism and signaling.

In this thesis work, a pathologic variant of the *RNU7-1* gene (AGS9) was analyzed. This gene encodes for the U7 small nuclear RNA (U7 snRNA), an essential component of the U7 snRNP complex. The function of U7 snRNP is to operate the endonucleolytic cleavage of the poly-A tail in replication-dependent histones (RDHs) pre-mRNAs during their maturation process. RDHs genes encode the four core histones (H2A, H2B, H3 and H4) and the linker histone family (H1). In AGS, mutations in *RNU7-1* have been linked to defects in U7 complex synthesis, resulting in the production of aberrant RDHs isoforms that possess a poly-A tail. Therefore, newly synthesized histone proteins present dysfunctional stoichiometry that affects chromatin structure. In this condition, chromatin is recognized as a foreign genome and activates the innate immune cGAS-STING cascade, leading to increased type I IFN production and induction of transcription of interferon-stimulated genes (ISGs).

As *RNU7-1* (AGS9) is the least characterized AGS-related gene, the overall aim of this project is to dissect its role in AGS pathogenesis. To this end, this work both investigated canonical AGS features such as the potential upregulation of IFNα and ISGs, and specific outcomes of a *RNU7-1* pathologic variant in primary dermal fibroblasts obtained from an AGS9 patient and compared to a healthy age- and sex-matched control. Total RNA was extracted with TRIzoL™ reagent, and the gene expression was determined by Real-Time qPCR. ELISA, Western Blot analysis and immunofluorescence were performed to assess protein expression. MTT assay was used to investigate cell viability. RNA immunoprecipitation (RIP) was carried out to assess the physical association between proteins and target RNAs. Transmission Electron Microscopy (TEM) was used to identify eventual alterations in subcellular compartments and specific staining assays were performed to assess basal mitochondrial metabolism and nascent protein synthesis. Lastly, RNA sequencing was carried out to provide a comprehensive view of the transcriptomic differences between AGS9 and control cells.

Results of this thesis work pointed out an altered RNA morphology of U7 snRNA that leads to affects its subcellular localization in AGS9-derived fibroblasts. Moreover, altered expression of two AGS-related genes, (both the isoforms of *ADAR1* and *RNASEH2B*) in fibroblasts carrying the pathologic variant of *RNU7-1* was highlighted, confirming the strong cooperation between AGS genes in nucleic acid metabolism.

The activation of the interferon signature (IS) in response to the mutation was observed, with upregulated ISGs and increased IFN score in fibroblasts and whole blood, reinforcing the connection between the *RNU7-1* variant and interferon dysregulation. An anti-inflammatory compound, hydroxychloroquine, was then tested to determine its potential effectiveness in reducing IS and IFNα production. Results proven the decrease of both ISGs and IFNα in AGS9 cells with also a partial restore of cell viability in AGS9 fibroblasts.

As aberrant morphology of U7 snRNA could affect its functioning in U7 snRNP, RIP analysis was performed and a decrease in physical association between U7 snRNA and ZFP100 was reported.

RNA-sequencing analysis then confirmed the alteration of multiple pathways related to neuron function and interferon signaling in AGS9 fibroblasts. Moreover, transcriptional changes in AGS9 cells were related to chromatin structural components. Specifically, it was highlighted that genes involved in histone post-translational modifications were strongly affected. Aberrant RDH histone processing was also confirmed through Real-Time qPCR, western blot and immunochemistry. Moreover, TEM analysis reported a lack of chromatin in AGS9 nuclei, thus reinforcing RNAseq results.

Since TEM analysis also revealed smaller mitochondria and reduced localization of ribosomes on ER membranes in AGS9 cells, Mitotracker, Mitosox and Click-iT staining assays were carried out to assess mitochondrial activity, ROS production and nascent protein production, respectively. Results demonstrated a reduced basal mitochondrial activity together with an increase production of ROS, and a reduced nascent protein production in AGS9 fibroblasts.

In conclusion, these insights contribute to a more comprehensive characterization of AGS, shedding light on potential therapeutic targets and emphasizing the need for further research into the intricate molecular mechanisms underlying this debilitating syndrome.

3. ABBREVIATIONS

AGS: Aicardi-Goutières Syndrome

IFNα: Interferon-α

CSF: Cerebrospinal fluid

TORCH: Toxoplasma, Other, Rubella, Cytomegalovirus, Herpes simplex

CRMCC: Cerebroretinal microangiopathy with calcifications and cysts

NAs: Nucleic Acids

CT: Computed Tomography

MRI: Magnetic Resonance Imaging

CNS: Central Nervous System

SLE: Systemic Lupus Erythematosus

ISGs: Interferon-Stimulated Genes

IS: Interferon Signature

IFNs: Interferons

IU: International Unit

SPENCD: Spondyloenchondromatosis

NAs: Nucleic Acids

ssDNA: single-strand DNA

dsDNA: double-strand DNA

cGAS: Cyclic GMP–AMP Synthase

dsRNA: Double Stranded RNA

ER: Endoplasmic Reticulum

STING: Stimulator of Interferon Genes

TBK1: TANK-binding kinase 1

IRF3: Interferon Regulatory Factor 3

IRF7: Interferon Regulatory Factor 7

RLH: RIG-I-like helicase

RIG-I: Retinoic acid Inducible Gene-I

MDA5: Melanoma Differentiation Associated Protein 5

TREX1: Three-prime Repair EXonuclease 1

DNase III: DNA-specific 3'→5' exonuclease

ADARs: Adenosine deaminases acting on RNA enxymes

RLRs: RIG-I-like receptors

CARDs: Caspase Activation and Recruitment Domains

MAVS: Mitochondrial Antiviral-signaling proteins

CTD: C-terminal Domain

U7 snRNA: U7 small nuclear RNA

U7 snRNP: U7 small nuclear ribonucleoprotein

IFNAR: Interferon-α/β receptor

RDHs: Replication-Dependent Histones

HDE: Histone Downstream Element

SLBP: Stem Loop Binding Protein

ZFP100: Zinc Finger Protein 100

TLRs: Toll-like Receptors

SL: Stem Loop

SMN: Survival Motor Neuron protein

RIHs: Replication Independent Histones

mtDNA: mitochondrial DNA

OXPHOS: Oxidative Phosphorylation

TLR9: Toll-like Receptor 9

TNFα: Tumor Necrosis Factor alpha

ROS: Reactive Oxygen Species

RTIs: Reverse Transcriptase Inhibitors

HCQ: Hydroxychloroquine

PBMCs: Peripheral Blood Mononuclear Cells

AMPK: AMP-activated protein kinase

mtROS: mitochondrial-derived ROS

CEB: Cytosol Extraction Buffer mix

NEB: Nuclear Extraction Buffer mix

FACS: Fluorescence-activated Cell Sorting

WES: Whole Exosome Sequencing

IMID: IntAct Molecular Interaction Database

RIP: RNA immunoprecipitation

RNAseq: RNA-sequencing

PCA: Principal Component

DEGs: Differentially Expressed Genes

FDR: False Discovery Rate

GO: Gene Ontology

TEM: Transmission Electron Microscopy

4. INTRODUCTION

4.1 Aicardi-Goutières Syndrome: overview

Aicardi-Goutières Syndrome (AGS) is a rare and genetically determined pediatric disorder firstly discovered in 1984 by the two neurologists from whom it was named, Jean Aicardi and Françoise Goutières (1). AGS has a prevalence between 1/93,000 and 1/167,000 living births (2), it mainly affects females and only few cases are described in Klinefelter patients (3,4). This condition is an early-onset encephalopathy associated with severe intellectual and physical disabilities that usually manifest between the first four months to 3 years of life (5). Clinical signs of AGS include developmental halt, basal ganglia calcifications, persistent lymphocytosis, and increased levels of multiple proinflammatory cytokines, especially interferon-α (IFNα) in both the serum and the cerebrospinal fluid (CSF) (6,7).

This disease was initially documented in 8 newborns from 5 different families who all manifested serious inflammatory signs (e.g. fatigue, loss of psychomotor skills, spasticity, and intermittent fever) in absence of detectable immunological stimuli (8). Since most of these symptoms are common to multiple disorders (9), the differential diagnosis of AGS is essential to exclude pathological conditions such as the TORCH complex (Toxoplasma, Other, Rubella, Cytomegalovirus, Herpes simplex), Cockayne syndrome, cerebroretinal microangiopathy with calcifications and cysts (CRMCC) and multiple metabolic disorders including parathormone metabolism disorders, biotinidase deficiency, and 3-hydroxyisobutyric aciduria (10). Along with the ordinary clinical signs, AGS individuals may display extended white matter hypodensities, chilblains, bilateral spasticity, ocular jerks, acquired progressive microcephaly, and dystonia (6).

Following the identification of other cases, it has been hypothesized that AGS was a hereditary disorder with an autosomal recessive inheritance. AGS is indeed defined as a monogenic disorder currently associated with mutations in 9 genes (*TREX1, RNASEH2A, RNASEH2B, RNASEH2C, SAMHD1, ADAR, IFIH1, LSM11* and *RNU7-1*), all of which encode for proteins or transcripts involved in metabolism and uptake of nucleic acids (11,12). The first gene linked to Aicardi-Goutières syndrome (*TREX1*) was identified in 2000 by Crow and colleagues through a genome-wide linkage study on 23 AGS patients (13). The same group of researchers also identified the rest of AGS genes, concluding with *LSM11* and *RNU7-1* in 2020 (14). Except for *TREX1* and *ADAR1*, which have both autosomal recessive and autosomal dominant inheritance, and *IFIH1*, which only has autosomal dominant inheritance, all AGS genes exhibit an autosomal recessive pattern of inheritance (7).

4.2 Clinical manifestations

AGS frequently manifests in patients between 4 to 36 months of age usually after a period of apparently normal development, but it may also appear as a neonatal form within the first week of birth (15). Pregnancy and delivery are indeed normal in approximately 80% of AGS infants (16). In most cases, the first signs of the disease are extreme irritability, a moderate intermittent febrile state (38-38.5 °C), loss of psychomotor skills, spasticity,

and microcephaly due to reduced head circumference growth, as well as signs of neurological impairment (8).

In the neonatal form, feeding difficulties, sleep-wake rhythm disturbances, hepatosplenomegaly, thrombocytopenia, and anemia were also reported (17). Prenatal onset of AGS was also hypothesized through the identification of brain calcifications and reduced growth of the head in-utero (18,19). This condition was then confirmed in 2019 when Bourgon and his collaborators described a fetus with a homozygous mutation in *TREX1* showing the typical signs of the disease (i.e. hepatosplenomegaly, microcephaly, calcifications in the basal ganglia) and died 9 days after birth (20).

4.2.1 Neurological signs

AGS infants commonly show diffuse neurological features that occur together with developmental delay (16). These symptoms include truncal hypotonia, lethargy, irritability, poor head control, and distal spasticity (21). Additionally, patients show extrapyramidal signs such as dystonia, buccal-lingual dyskinesia, persistent application of archaic reflexes, and abnormal eye movements probably associated with reduced vision (21,22). The neurological component of AGS represents a heterogenous apect of the disorder that could lead to differences in the severity of the symptoms, including between siblings (23). For instance, some AGS children may have a normal head circumference, even if the majority of the patients display a severe acquired microcephaly (Figure 1) (16).

Figure 1. Photography of a patient at the age of 3 years with microcephaly (24).

Lastly, one peculiar feature of AGS is the development of aberrant startle reflexes defined as “startle reaction”. This phenomena typically occurs as a physiological reaction to a sudden unexpected impulse (25). However, AGS patients also exhibit these reflexes in response to modest sensory stimuli (10). The genesis of startle reaction is mainly not epileptic but it is challenging to distinguish this condition from epilepsy (16).

4.2.2 Extra-neurological signs

Alongside neurological changes, AGS patients frequently exhibit extra-neurological signs. Chilblains, a skin condition of the hands, feet, and ears represent the most important extra-neurological manifestation of the disease and it affects approximately 31.2% of the patients (Figure 2) (7). AGS affected subjects can also manifest epidermal necrosis with intraepidermal bulla and papule in addition to chilblains (13).

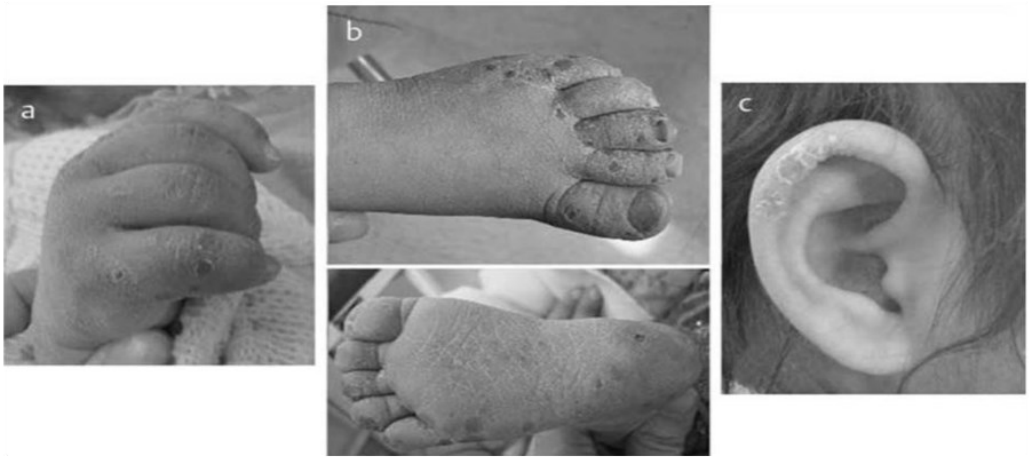

Figure 2. Chilblains with areas of necrosis and crust development were visible in a 2-year-old patient on: (a) hands, (b) feet, (c) ear. (26).

Glaucoma is the second most prevalent extra-neurological characteristic of AGS and affects about 6.3% of patients (7). Other extra-neurological signs include hypothyroidism (3.9% of patients), hypertrophic cardiomyopathy (3.3%), insulin-dependent diabetes mellitus, increased levels of autoantibodies, micropenis, transitory antidiuretic hormone deficiency, hepatosplenomegaly, hemolytic anemia, overproduction of transaminases, and transitory thrombocytopenia (7,10,16).

4.3 Diagnostic criteria

Despite recent advances in research, the diagnosis of AGS is still challenging as no biomarker has been specifically associated with this condition yet (27). For this reason, it is crucial to keep surveillance on patients over time to monitor the appearance of novel clinical or neuroradiological criteria that could help in the diagnosis of the syndrome (28). The diagnostic process of this disorder is indeed based on a combination of clinical and imaging features (10).

In the early stages of the disease, increased expression of IFNα in the CSF and serum represents an important diagnostic aspect in over 85% of AGS patients (29). Brain calcifications are also a quite specific finding for this condition, even if they are often difficult to be detected on magnetic resonance imaging (MRI) (9). For these reasons, genetic testing is crucial to confirm the AGS diagnosis (27).

4.3.1 Neuroradiological aspects

Intracranial calcifications, cerebral atrophy, and leukodystrophy are the main neuroradiological characteristics of AGS (10).
More than 90% of AGS individuals show brain calcifications in the thalami, deep white matter, and lentiform nuclei; a small percentage of patients also exhibit striatal necrosis (9). It should be emphasized that calcification is physiological during aging, and a distinction should be made between metastatic calcification, which is caused by a calcium metabolism disorder (i.e. hypo or hyperparathyroidism), and dystrophic calcification, which is caused by several pathologies affecting different brain districts (30).

Two procedures are commonly used to assess the existence, localization, and severity of brain calcifications: computed tomography (CT), which is the first-choice neuroimaging technique, and MRI.
Calcifications, which appear as calcium deposits, might have a punctate or broad pattern, and there is no association between the existence of these abnormalities and the severity of the illness (16,21) (Figure 3).

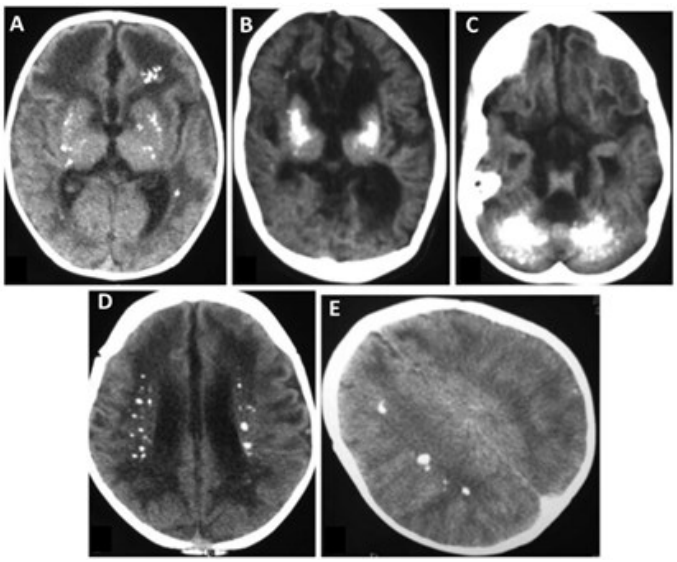

Figure 3. CT scan examples of intracranial calcification in AGS patients. (A, B) The basal ganglia, (C) dentate nuclei of the cerebellum, (D) periventricular distribution and (E) deep white matter all exhibit calcifications (15).

A diagnostic challenge in AGS is in part due to the difficulty in discriminating the disease in comparison to others, and, in part, to the clinical and radiological variability of the condition (31). Brain atrophy also demonstrated a variable distribution pattern, ranging from cortical atrophy to basal ganglia atrophy. White matter atrophy is implicated in 99.2% of AGS cases, and many individuals also exhibit substantial brainstem and cerebellar atrophy. Furthermore, absence of corpus callosum has been reported too (32) (Figure 4).

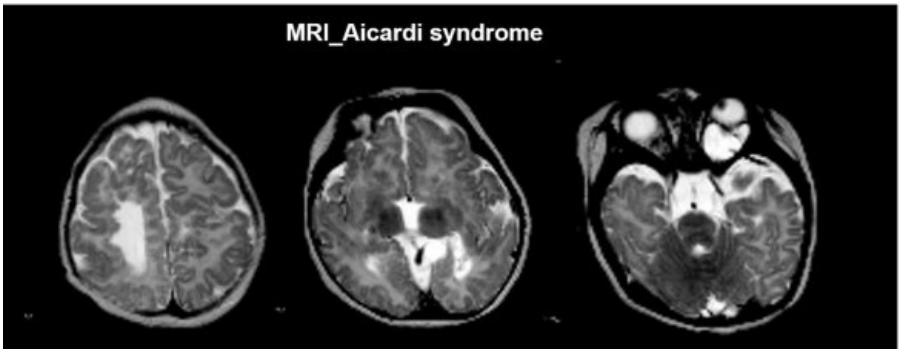

Figure 4. T2-weighted MRI scan of a three-month-old girl with Aicardi syndrome showing absent corpus callosum, ventricular asymmetry, bilateral polymicrogyria, bilateral periventricular nodular heterotopia, and closed lip schizencephaly in the left posterior parietal lobe (33).

4.3.2 Cerebrospinal fluid (CSF)

The CSF protects the central nervous system (CNS) by preserving metabolic homeostasis, providing nutrients, and regulating intracranial pressure (34). The diagnostic process in AGS includes the CSF analysis as it is essential to identify two important pathologic features: raised IFNα levels (>2 UI/ml) and persistent CSF lymphocytosis (>5-100 cells/mm^3) in absence of demonstrable infections (6). Both features are more pronounced in the early stages of the disorder and tend to decline after the first year of life (17). IFNα levels are elevated in patients' plasma as well, but this aspect is often less pronounced than in the CSF, so it does not have the same diagnostic relevance (21). Cases of affected children with both elevated IFNα levels and low lymphocyte levels have been reported in the literature, demonstrating that the two conditions do not always coexist (16).

Since discriminating AGS inflammatory markers from the ones deriving from a congenital infection can be challenging, a study on this topic has been published in 2008 by Dr. Van Heteren and colleagues. Their work examined several cytokines overexpressed in AGS patients and those produced during a viral infection, indicating CXCL10 as a potential candidate marker for the diagnosis of AGS (35). This cytokine is indeed a potent chemoattractant for activated lymphocytes that could be responsible of CSF lymphocytosis in AGS (10). On the other hand, the two factors IL-6 and CXCL8 have been found to be detectable only during viral infections (35). Other potential CSF markers in AGS have been recently discovered: neopterin and biopterin (36). These molecules both belong to the class of the pteridines, heterocyclic compounds secreted from the T Helper cells during the immune response (37,38). For this reason, the concentration of pteridines in CSF is a helpful indicator of the inflammation status in AGS (39).

4.3.3 Interferon signature

Since the increased production of IFNα unites multiple disorders, including systemic lupus erythematosus (SLE) and AGS, the term "*interferon signature*" (IS) has been introduced (29,40,41). IS refers to the upregulation of multiple interferon-stimulated genes (ISGs) during a pathologic condition, and it is often evaluated to monitor the patient-specific response to therapeutic treatments (29).

The ISGs family is composed of more than 100 members (42), but only 6 have been linked to AGS: *IFI27, IFI44, IFIT1, ISG15, RSAD2*, and *SIGLEC1* (29). Specifically, when the transcription level of those genes rises over a defined threshold level, the IS is considered positive (29). Even if the specific molecular function of each ISG has not been discovered yet, some of them have already been related to specific pathways. *IFI27*, for instance, has been linked to mitochondrial oxidative stress (43) (Figure 5). On the other hand, negative IS cannot rule out the presence of AGS as 31% of patients with gene mutations in *RNASEH2B* do not exhibit an increase in ISGs (1,11).

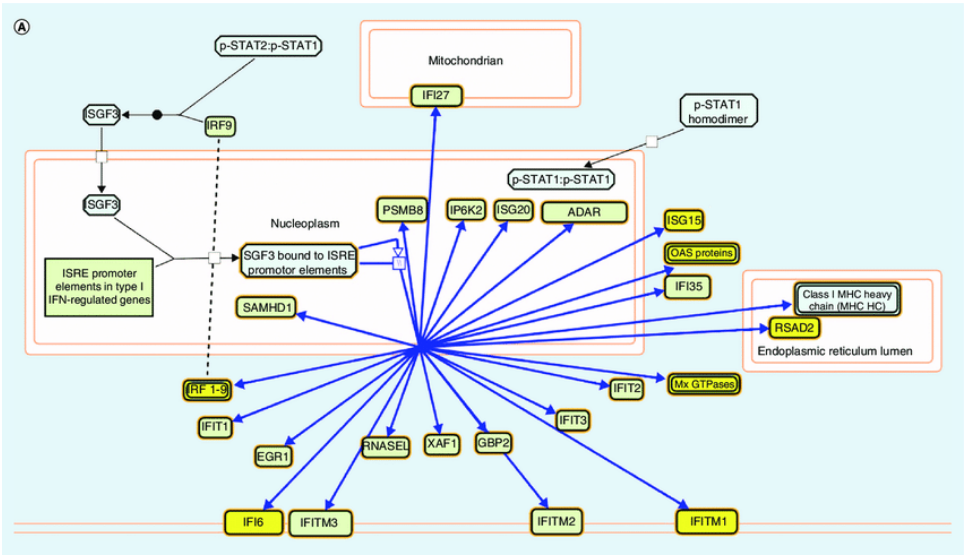

Figure 5. Molecular functions of ISGs (43).

4.4 AGS and Type I interferonopathies

Interferons (IFNs) are a family of polypeptides classified into three major groups: type I IFN (IFNα, IFNβ, IFNω, IFNε), type II IFN (IFNγ), and type III IFN (IFNλ) (44). All of them exert antiviral properties, but their specific mechanisms of action differ depending on the IFN subtype (40). Isaacs and Lindenmann firstly identified and characterized the type I IFN over 60 years ago, describing it as a soluble factor capable to prevent the spread of the influenza virus (45). IFNs are currently associated with multiple biologic activities, including cellular proliferation, differentiation, and metabolism as well as immune system activity and cancer formation (46,47). 17 different genes on human chromosome 9p encode for type I IFNs and the most abundant one is IFNα, a family composed of at least 15 subtypes (48). The physiological concentration of IFNα in the blood is lower than 2 IU (International Unit) per milliliter. During a viral infection IFNα can reach peaks of 5000 IU/milliliter (1). Almost every cell subtype can produce type I IFNs (49), but plasmacytoid dendritic cells are the principal source of them in serum (50). On the other hand, astrocytes and microglia are the major producers of this compound in CNS, where it protects the brain from viral infections (51,52). If production of IFNα exceeds the normal threshold, it leads to toxic consequences and to the condition of "interferonopathy" (53).

Considering that the constitutive upregulation of type I IFNs is relevant to the pathogenesis of AGS, this disorder belongs to the type I interferonopathies (7). SLE was the first condition connected to this family of diseases, whereas AGS was the first monogenic pathology to be related to an increase of type I IFNs.

Other conditions included within the category of type I interferonopathies are spondyloenchondromatosis (SPENCD), which is brought on by mutations in the *ACP5* gene, familial chilblain lupus, related to mutations of *TREX1* and *SAMHD1* (which are also related to AGS), and Singleton-Merten syndrome, caused by mutations in *IFIH1* (one of the genes also linked to AGS) (1).

4.4.1 Mechanisms of interferon induction

Multiple signaling cascades lead to the production of IFNα, and they all start with the recognition of immunostimulatory nucleic acids (NAs) (54). NAs that trigger the production of IFNα include endogenous damaged DNA or RNA, DNA:RNA hybrids, and viral genomes such as double stranded DNA (dsDNA), single stranded DNA (ssDNA), or double stranded RNA (dsRNA) (55). The primary intracellular DNA sensor is the guanosine monophosphate-adenosine (cGAS) which catalyzes the production of the 2′,3′-linked dinucleotide cGAMP upon DNA binding (56). The endoplasmic reticulum (ER) transmembrane adaptor protein stimulator of interferon genes (STING) is then activated by cGAMP and subsequently reaches the Golgi apparatus (57). At this point, the C-terminal tail of STING recruits and activates the TANK-binding kinase 1 (TBK1) that in turn phosphorylates the IFN regulatory factors 3 (IRF3) and nuclear NF-kB. IRF3 then translocate to the nucleus and promotes the transcription of IFNβ and the IFN regulatory factor 7 (IRF7), which is responsible for the secretion of IFNα and its autocrine signaling cascade (54,55,57).

Another pathway discovered for IFN activation includes the RIG-I-like helicase (RLH), the retinoic acid inducible gene-I (RIG-I) and the melanoma differentiation-associated gene 5 (MDA5), which together recognize viral dsRNA in the cytoplasm. RIG-I and MDA5 together activate TBK1, which phosphorylates and activates IRF3 and IRF7, allowing gene transcription of IFNα and β (58). Once produced, Type I IFNs bind to the plasma membrane-based heterodimeric interferon-α/β receptor (IFNAR). This receptor is composed of two subunits: IFNAR1, which is the main component of intracellular signal transduction, and IFNAR2, which is mainly involved in the binding of the ligand (59). The binding of type I IFNs to their receptor leads to the activation of the JAK-STAT pathway that induces the transcription of ISGs (60) (Figure 6).

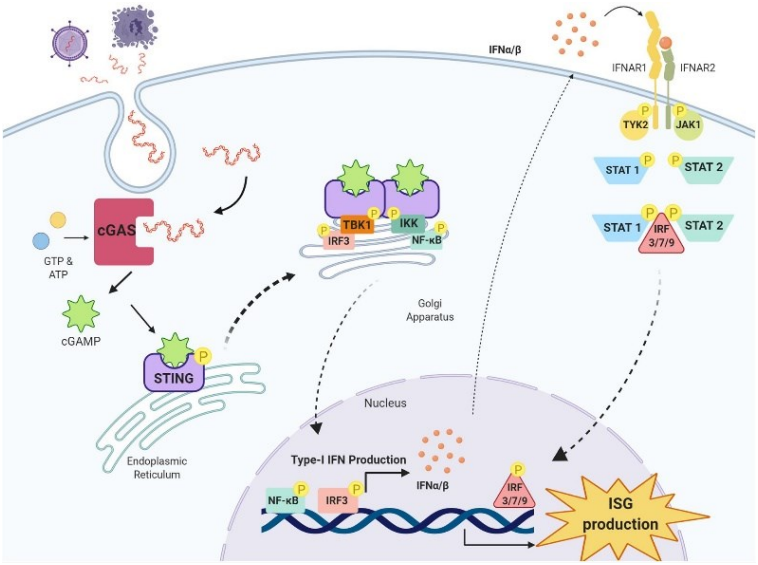

Figure 6. cGAS-STING and JAK-STAT pathways in type I IFN signaling (60).

4.5 Genetic insights of AGS

As mentioned before, AGS is a rare genetic disorder associated with mutations in 9 genes, all encoding for proteins or transcripts involved in metabolism or uptake of NAs (7) (Table 1). Despite the fact that a dominant inheritance has been emphasized for some genes, AGS is mostly defined by a recessive inheritance pattern (15).

GENE	LOCUS	INHERITANCE
TREX1 (AGS1)	**3p21**	**AR, AD**
RNASEH2B (AGS2)	**19p13**	**AR**
RNASEH2C (AGS3)	**13q14**	**AR**
RNASEH2A (AGS4)	**11q13**	**AR**
SAMHD1 (AGS5)	**20q11**	**AR**
ADAR1 (AGS6)	**1q21**	**AR, AD**
IFIH1 (AGS7)	**2q24**	**AD**
LSM11 (AGS8)	**5p12**	**AR**
RNU7-1 (AGS9)	**3q22**	**AR**

Table 1. AGS-related genes names, location on chromosomes and pattern of inheritance. AR: autosomal recessive, AD: autosomal dominant.

Moreover, recent literature descriptions of five individuals with mutations in *RNASET2* and AGS-like phenotypes raise the possibility that it may be included as a new AGS-related gene (13).

4.5.1 TREX1 (AGS1)

The first gene linked to AGS is the three-prime repair exonuclease 1 (*TREX1*) and it was identified on chromosome 3p21 by Crow and colleagues in 2000 (61). This gene encodes for the enzyme DNA-specific 3'→5' exonuclease (DNase III) that is involved in DNA repair mechanism. DNase III is indeed part of a complex that normally resides in cytoplasm, but in case of oxidative DNA damage, it migrates to the nucleus (62). Specifically, when a DNA strand breaks, the DNase III removes the mismatched 3' terminal deoxyribonucleotides by acting on single strand DNA (63). Mutations of this enzyme cause the accumulation of altered DNA that triggers the autoimmune response, leading to different autoimmune disorders, including AGS, SLE (64), retinal vasculopathy with cerebral leukodystrophy and familial chilblain lupus (62,65) (Figure 7). Since mutations in this gene may also cause an accumulation of RNA, it has been demonstrated that *TREX1* is not just a DNA exonuclease but it may also act as an exoribonuclease (60).

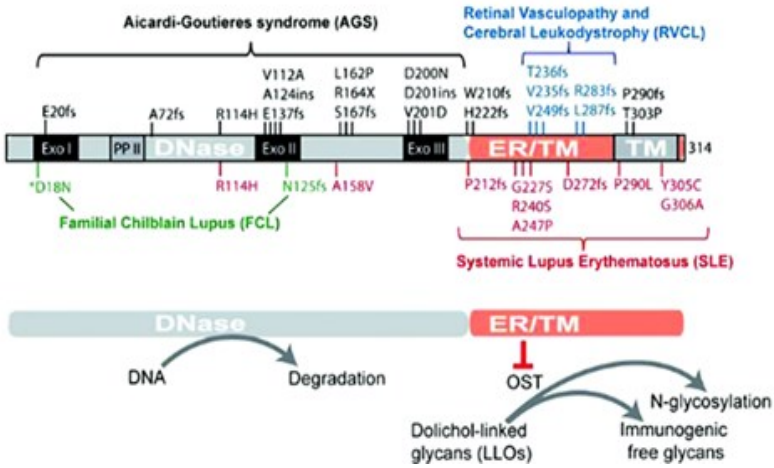

Figure 7. *TREX1* activity and point mutations associated to immune-related diseases. TM, transmembrane domain (63).

4.5.2 *RNASEH2B (AGS2), RNASEH2C (AGS3), RNASEH2A (AGS4)*

RNase H2 is an enzymatic complex composed of three subunits that operate the endonucleolytic cleavage of erroneous ribonucleotides integrated into RNA:DNA duplexes (66). The three subunits (A, B and C) of RNase H2 are encoded by *RNSEH2A* (AGS4), *RNASEH2B* (AGS2), and *RNASEH2C* (AGS3), respectively (67). *RNASEH2B* is located on chromosome 13q14 and encodes the catalytic domain of the complex; *RNASEH2C* is located on chromosome 11q13, whilst *RNASEH2A* maps on the short arm of chromosome 19 (19p13) (66) (Figure 8).

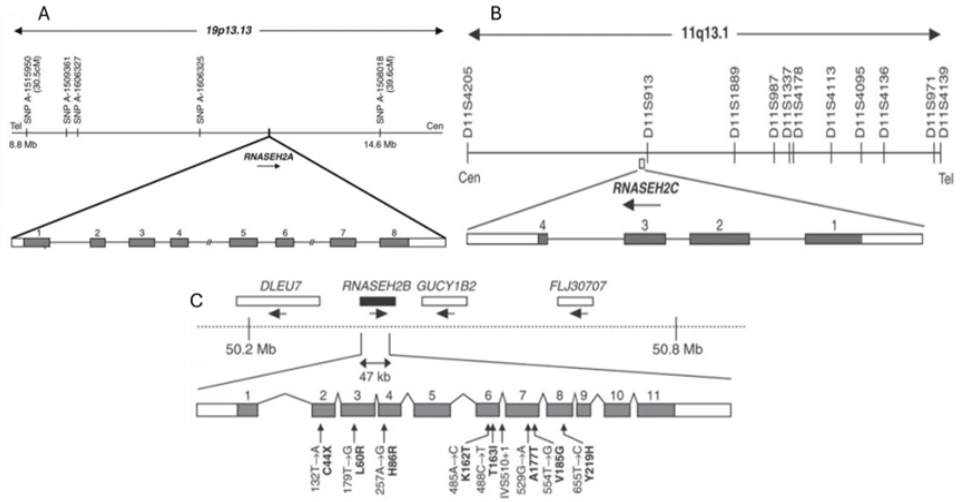

Figure 8. (A) Diagram of the AGS4 critical region and genetic map of chromosome 13q14, (B) diagram of the AGS3 critical region and genetic map of chromosome 11q13, (C) diagram of the critical region AGS2 and genetic map of chromosome 19p13 (66).

The link between RNase H2 and AGS was pointed out in 2006 (66) when Crow and colleagues identified six patients with canonical AGS symptoms. Specifically, it was discovered that biallelic mutations in *RNASEH2A, RNASEH2B* and *RNASEH2C* result in accumulation of RNA:DNA hybrids that cause the hyperactivation of the IFNα-mediated immune response (68).

4.5.3 SAMHD1 (AGS5)

SAMHD1 (AGS5) is the fifth gene related to AGS and it was identified in the long arm of chromosome 20 (20q11) by Rice and colleagues in 2009 (Figure 9).

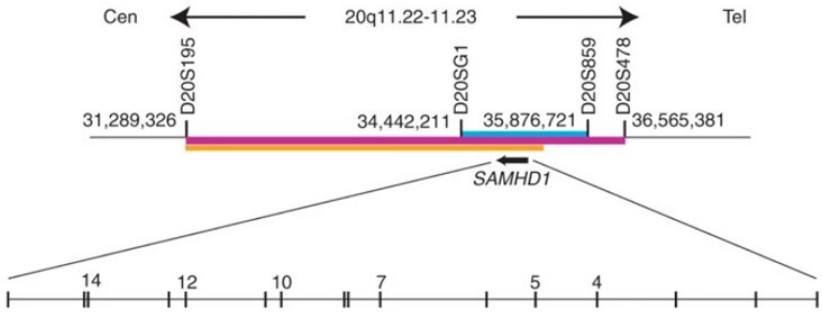

Figure 9. Diagram of the critical region *SAMHD1* and genetic map of chromosome 20q11 (69).

This gene encodes a deoxynucleotide triphosphohydrolase that helps to maintain the stability of the genome by limiting the replication of mutagenic retroelements (69). Specifically, SAMHD1 binds both ssDNA and ssRNA and prevent the effective completion of reverse transcription (70).

Inactive SAMHD1 is composed of monomers that are activated into tetramers in the presence of dGTP trough a multi-step reaction (71). Mutations in *SAMHD1* cause the migration of the enzyme from the nucleus to the cytoplasm (72).

In this condition, SAMHD1 is no longer able to prevent retrosynthesis of viral NAs, leading to an intracellular increase of "non self" genomes. As a consequence, the cGAS/STING pathway is activated and induces the production of type I IFNs that leads to the overexpression of ISGs (73).

4.5.4 ADAR1 (AGS6)

Adenosine deaminases acting on RNA (ADARs) are enzymes that catalyze the chemical conversion of adenosines to inosines in dsRNA substrates. Inosine forms two hydrogen bonds with cytosine and it is indeed recognized as guanosine by the translational cellular machinery (74). Adenosine-to-inosine (A-to-I) RNA editing effectively changes the primary sequence of RNA targets, thus discriminating "self" to "non-self" RNAs and preventing activation of innate immune response (75). Mammalian genomes encode three ADARs: ADAR1 and ADAR2, which are the catalytically active enzymes, and ADAR3, which has an inactive catalytic domain (76). In mammals, ADAR1 is encoded by a single-copy gene which maps to human chromosome 1q21 and presents two RNA isoforms: a constitutive expressed short isoform (p110), and a full-length isoform (p150) which is IFN-inducible (77). *ADAR1* structure consists of a catalytic deaminase domain at the C-terminus, three dsRNA-binding domains in the middle, and one ZDNA-binding domains at the N-terminus (Zβ). In addition, the human ADAR1 p150 isoform has an extra 295 amino acids at the N-terminus that are made up of a nuclear export signal and an extra Z-DNA/Z-RNA-binding domain known as Zα (78) (Figure 10).

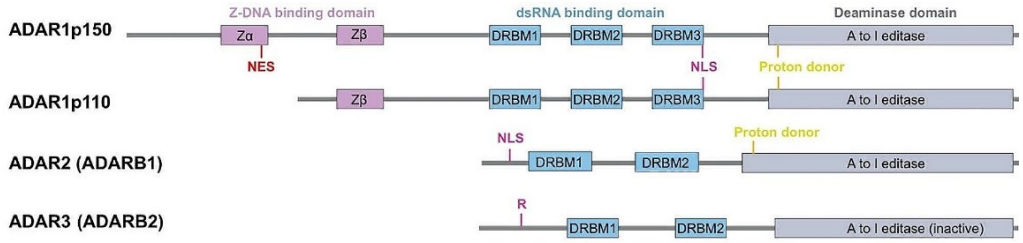

Figure 10. Organization of domains in ADAR1, ADAR2 and ADAR3 proteins. Zα, Z-RNA binding domain; NES, nuclear export signal; NLS, nuclear localization signal (79).

Mutations in *ADAR1* are associated with the development of AGS (80). Specifically, mutated ADAR1 is not able to operate A-to-I RNA editing anymore, leading to the recognition of endogenous RNAs as "non self" with subsequential activation of the innate immune system and major IFN production (81).

4.5.5 IFIH1 (AGS7)

IFIH1 (interferon induced with helicase C domain 1) is a human gene located in the long arm of chromosome 2 (2q24.2) that has been linked to AGS by Rice and colleagues in 2014 (82).

IFIH1 (sometimes referred to as AGS7) is the only AGS-related gene that exclusively exhibits a dominant pattern of inheritance, and it encodes the melanoma differentiation associated protein 5 (MDA5). MDA5 is a cytoplasmic helicase receptor that can trigger an interferon response in response to viral dsRNA (83). Specifically, this protein is one of the three RIG-I-like receptors (RLRs), and it is ubiquitously expressed at low levels in mammals (84,85). MDA5 has a central helicase domain that is responsible for the RNA-binding and RNA-dependent ATP hydrolysis, and two N terminal caspase activation and recruitment domains (CARDs) that are involved in activating mitochondrial antiviral-signaling proteins (MAVS). This enzyme also contains a DExD/H-box RNA helicase domain, and a C terminal domain (CTD) that represent additional components involved in RNA binding (85) (Figure 11).

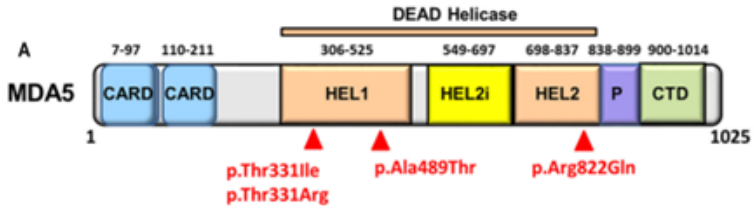

Figure 11. Protein domains organization of MDA5 and point mutations related to AGS (84).

In physiologic conditions, MDA5 signaling pathway only activates when this receptor binds "non-self" dsRNA, such as viral genomes and polynosinic RNAs (84). In this instance, MDA5 CARD tandem domains activate MAVS on the outer mitochondrial membrane, causing the activation of TBK1, the phosphorylation of IRF3 and the following induction of transcription of type I IFN and ISGs (86).

In AGS, aberrant MDA5 improperly activates its molecular pathway by interacting with cellular RNAs, determining a spontaneous signal that leads to chronic type I IFN production (87).

4.5.6 LSM11 (AGS8) and RNU7-1 (AGS9)

In 2020, Uggenti and colleagues identified two new genes associated with AGS phenotype in a recessive pattern of inheritance: *LSM11* and *RNU7-1* (14). The Sm-like protein LSM11, encoded by *LSM11,* and the U7 small nuclear RNA (U7 snRNA), encoded by *RNU7-1*, are essential components of the U7 small nuclear ribonucleoprotein (U7 snRNP) complex. The U7 snRNP complex mediates replication-dependent histones (RDHs) pre-mRNA processing (88).

RDHs genes encode the four core histones (H2A, H2B, H3 and H4) and the linker histone family (H1). The distinctive feature of RDHs is that they encode the only known eukaryotic mRNAs without a poly-A tail at the 3′ end, terminating instead with a highly conserved stem-loop structure (89). This unique 3′ end is formed by a U7-dependent endonucleolytic cleavage of the pre-mRNAs between the stem-loop and a purine-rich sequence called histone downstream element (HDE) (90). The stem loop binding protein (SLBP) and the zinc finger protein 100 (ZFP100) are also essential in this process as they stabilize the binding of the U7 complex to the histone pre-mRNA (91) (Figure 12).

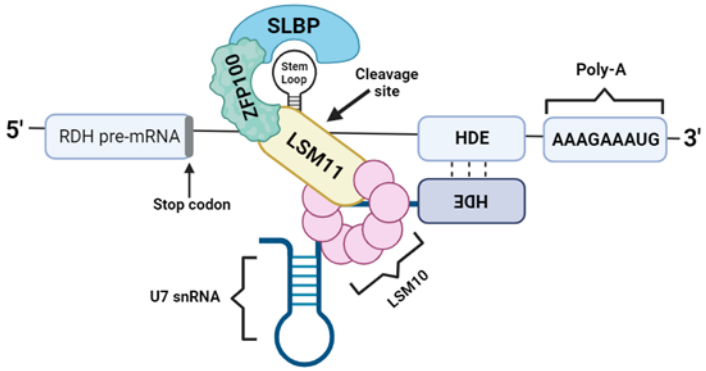

Figure 12. Schematic representation of the U7 snRNP complex involved in the processing of RDH pre mRNAs. Created with BioRender.

In AGS, mutations in *LSM11* and *RNU7-1* induce defects in U7 complex synthesis, resulting in the production of aberrant RDHs isoforms that possess a poly-A tail (92). Therefore, newly synthesized histone proteins present dysfunctional stoichiometry that affects chromatin structure. In this condition, chromatin is recognized as a foreign genome and activates the innate immune cGAS-STING cascade, leading to increased type I IFN production (14).

4.5.7 Frequencies of mutations and genotype-phenotype correlations

Around 90% of confirmed AGS cases is associated with mutation of one of the 9 genes described above. However, the incidence of mutations depends on the gene (7).

Biallelic mutations of *TREX1* were found in 22% AGS cases, 5% of patients present pathologic variations in *RNASEH2A*, and 13% express aberrant forms of *RNASEH2C*. *RNASEH2B* appears to be the most common altered gene, with a mutation frequency of 36% (10). *RNASEH2C* mutations were found in 13% of patients, *SAMHD1* mutations in 13%, and *ADAR1* mutations in 5% of cases. Only 3% of the patients investigated had dominant monoallelic mutations in *IFIH1*, whilst *LSM11* and *RNU7-1* have not been fully investigated yet due to the lack of patients presenting mutations in these genes (7) (Figure 13).

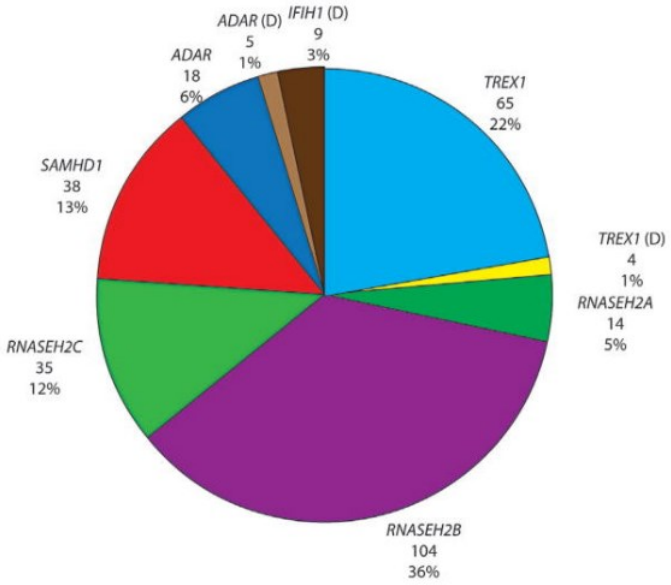

Figure 13. Frequencies of specific gene mutations in patients affected by Aicardi-Goutières syndrome (7).

Even if AGS patients with different mutations often show a common clinical status, several genotype-phenotype relationships have been discovered. For instance, patients with mutations in the *ADAR1* gene are more likely to have an early or subacute start of severe dystonia and to manifest signs of bilateral striatal necrosis (93). Moreover, AGS children with variants of *TREX1* have the highest death rate, whereas those with mutations in *SAMHD1*, *ADAR1*, and *IFIH1* are more likely to maintain some motor and communicative functions (17,82). In addition, patients with *RNASEH2B* gene mutations are more likely to have a negative interferon score (7), and these patients typically have later-onset variants of AGS with a longer life expectancy (10). On the other hand, siblings with the same gene mutation might present different phenotypes from one another (7).

4.6 Pathogenesis

Even though the function of many AGS-related genes is not fully understood, the general hypothesis in AGS pathogenesis is that defects in NAs metabolism or sensing could lead to an accumulation of endogenous DNA, RNA or DNA-RNA hybrids, that could be erroneously recognized as viral genomes by the host organism (10). In this instance, the IFNα-mediated immune response is activated as the first line mechanism of defense against potential pathogenic infections (94).

IFNα can be produced through two molecular pathways thanks to two complementary receptor systems responsible for viral detection. Both mechanisms include receptors capable to recognize “non-self” NAs: the first one includes the ubiquitous RIG-I and MDA5 receptors that detect viral dsRNA in cytoplasm, whilst the second one involves the Toll-Like receptors (TLRs) which can detect viral NAs in cell membranes and intracellular organelles (93,94). Dysfunctions in these two mechanisms lead to the inability to distinguish between viral and endogenous NAs, resulting in severe autoimmune reactions and interferonopathies like AGS (95).

As previously mentioned, all AGS-related genes are involved in the metabolism or sensing of NAs, and mutations in one of these genes can cause an increased immunological response with major IFNα production (Figure 14).

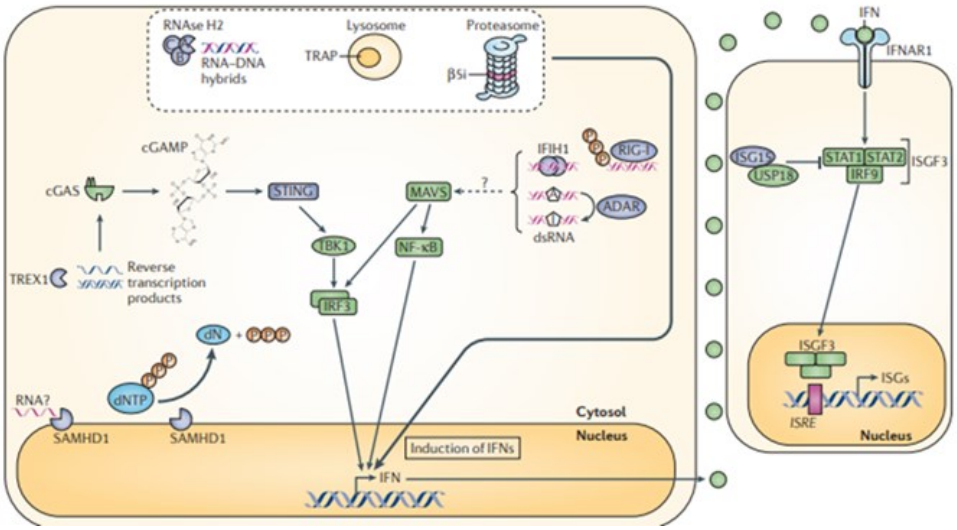

Figure 14. Mutations in AGS-related genes disrupt innate immune signaling pathways (1).

TREX1 loss-of-function mutations cause an accumulation of ssDNA and dsDNA in the cytoplasm, which in turn activates the cGAS-STING pathway and results in the production of type I IFN. In *SAMHD1* mutations, the same pathogenic process can be observed due failure in regulation of retroelements (69).

MDA5, encoded by *IFIH1,* is a sensor for exogenous dsRNA. Gain of function mutations in MDA5 result in a lower activation threshold that induces the detection of endogenous dsRNA with following activation of MAVS and IFN production. When *ADAR1* is defective, it results in the generation of aberrantly edited NAs that induce the immunological response by inducing MAVS activity (1). As regard RNASEH2, the RNase H2 complex usually acts to remove RNA: DNA hybrids, but mutations in one of its three subunits result in an increase in the intracellular content of hybrids, which can be detected by cGAS or TLR9 as foreign NAs (55,96). Even though all the previously mentioned pathologic mechanisms are generated from different upstream genes, they all result in type I IFN production.

4.6.1 Implication of RNU7-1 in AGS pathogenesis

As previously mentioned, one of the genes recently associated with AGS is *RNU7-1* (AGS9) that encodes the U7 small nuclear RNA (U7 snRNA). The U7 snRNA is an essential component of U7 snRNP, a complex necessary for RDHs pre-mRNA maturation as it operates the endonucleolytic cleavage of the poly-A tail (14). As a consequence, these transcripts terminate with a unique stem loop structure at the 3' end (97).
For this processing two cis elements are required: the stem loop (SL) and HDE, which are recognized by SLBP and U7snRNP, respectively.

The U7 snRNA is expressed at very low levels in human cells because it contains a non-canonical Sm binding site that is finely regulated throughout the cell cycle (97). The efficiency of the 3'end processing of RDHs indeed reaches a peak level during S phase, followed by a crucial decline at the end of DNA replication (92). It has been reported that mutations or depletion of U7 snRNA result in two main effects: delay in S-phase transition and aberrant U7 snRNP biogenesis (91,92).

During U7 snRNP biogenesis, the Sm binding site is crucial for a correct assembly of the complex as it contains a specific motif that recognizes other components of U7 snRNP complex (98) (Figure 15).

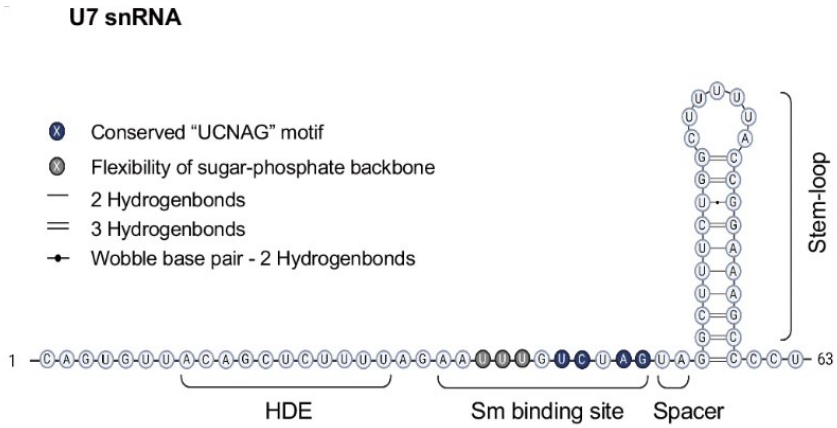

Figure 15. Secondary structure and functional domains of U7 snRNA. A correct assembly of a functional U7 snRNP requires the flexibility of the sugar-phosphate backbone mediated by uridines 23-25, a conserved UCNAG motif within the Sm binding site, a spacer between Sm binding site and stem loop and in the end a stable 3' stem-loop (91).

Newly transcribed U7 snRNA is then exported to the cytoplasm, where it is assembled with core proteins of the U7 snRNP complex (e.g. LSM10 and LSM11) in a process mediated by the survival motor neuron (SMN) protein. SMN identifies the Sm binding site of U7 RNA and enables its link with LSM10 and LSM11 (98,99). The U7 snRNP complex is then imported into the nucleus through a specific transporter and localizes in histone locus bodies where it operates the previous mentioned cut of poly-A (88,91) (Figure 16).

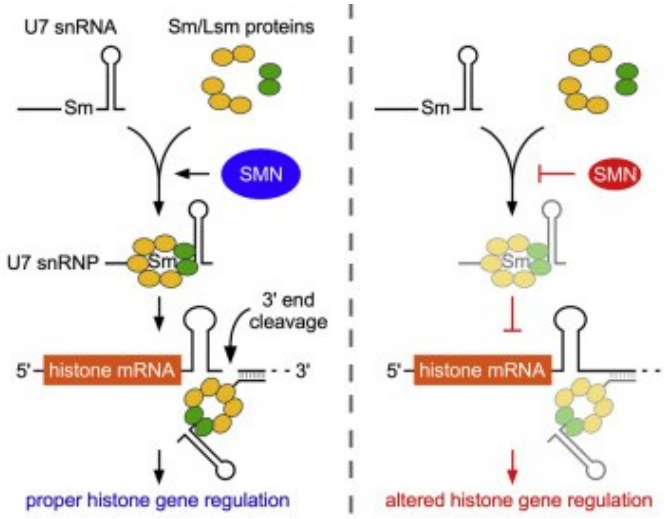

Figure 16. Regulation of biogenesis of U7 snRNP. (Left) U7 complex assembly in physiologic conditions. (Right) aberrant U7 snRNP assembly (98).

RDHs (H2A, H2B, H3, H4 and H1) are the most abundant forms of histones in metazoans. However, nucleosomes also contain other specialized variants defined replication-independent histones (RIHs) that may replace RDHs in a context-dependent manner, including DNA damage and post-mitotic cells plasticity. Since RIHs isoforms (H3.3, H2aZ, H3-cid, and macroH2a) are processed as polyadenylated mRNAs, they do not need U7 snRNP complex activity (90).

Recent knowledge demonstrated that primary cells derived from AGS-affected patients with mutations in *LSM11* or *RNU7-1* exhibited enriched polyadenylated forms of RDHs but equivalent levels of RIHs. Thus, indicating a U7 snRNP malfunctioning. The same group of research also reported that misprocessed forms of RDHs lead to aberrant histone stoichiometry, thereby influencing chromatin folding and genome accessibility. In this instance, chromatin is recognized as “non-self” and induces the host antiviral response which in turn activates the cGAS-STING cascade, triggers the MAVs, and enhances type I IFN production (14).

4.6.2 Mitochondria

Mitochondria are membrane-bound organelles that supply the cell by producing energy in the form of ATP (100). In addition, mitochondria generate heat, control cell growth and death, and store calcium for cell signaling functions. These organelles are distributed in the cytoplasm in a heterogeneous manner and their count depends on the cell type (101). Mitochondria are usually concentrated where a bigger source of energy is required and they can move within the cytoplasm by using filamentous cytoskeleton proteins to construct genuine "tracks" (102).

These organelles possess their own circular DNA defined mitochondrial DNA (mtDNA) of 16.6 kb that replicates independently of the host genome (103).

The human mtDNA is not associated to histone proteins and only encodes for 13 proteins that are primarily involved in oxidative phosphorylation (OXPHOS). Nuclear genome provides the mitochondria with the remaining proteins (100). Mitochondrial membrane is composed of two main lipid layers separated by a gap as the inner membrane is structured into ridge-like invaginations, known as *cristae*. The mitochondrial matrix, which houses the mtDNA and ribosomes, is positioned underneath the inner membrane, near to the two main protein complexes of the mitochondrial respiratory chain (F0 and F1) (104) (Figure 17).

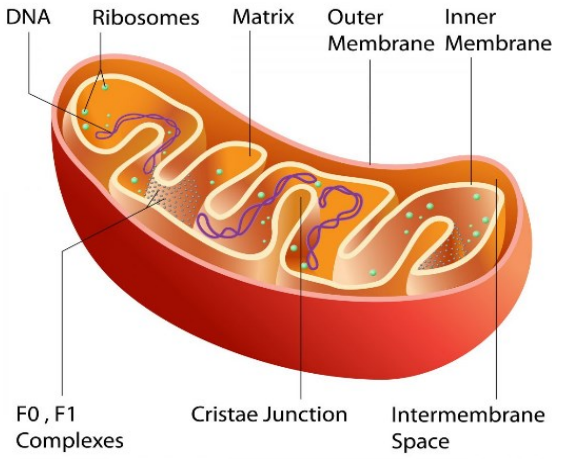

Figure 17. Structure of mitochondria (104).

4.6.2.1 Mitochondria and inflammation

Endogenous DNA usually resides in the nucleus and mitochondria of healthy cells. However, in pathologic conditions, genomic and/or mtDNA can be released into the cytoplasm where they trigger an immunological response (105). Specifically, mtDNA is recognized as a "non-self" dsDNA by cGAS, leading to the activation of the cGAS-STING signaling pathway and to the release of type I interferon (106). Moreover, double-stranded fragments of mtDNA can activate a separate innate immune response pathway involving Toll-like receptor 9 (TLR9) (107,108) (Figure 18). TLR9 is localized in the ER where it identifies exogenous DNA and binds the NF-kB factor. This cascade causes a raise in the expression of proinflammatory cytokines such as tumor necrosis factor alpha (TNFα), IL-6, and IL-1β (107).

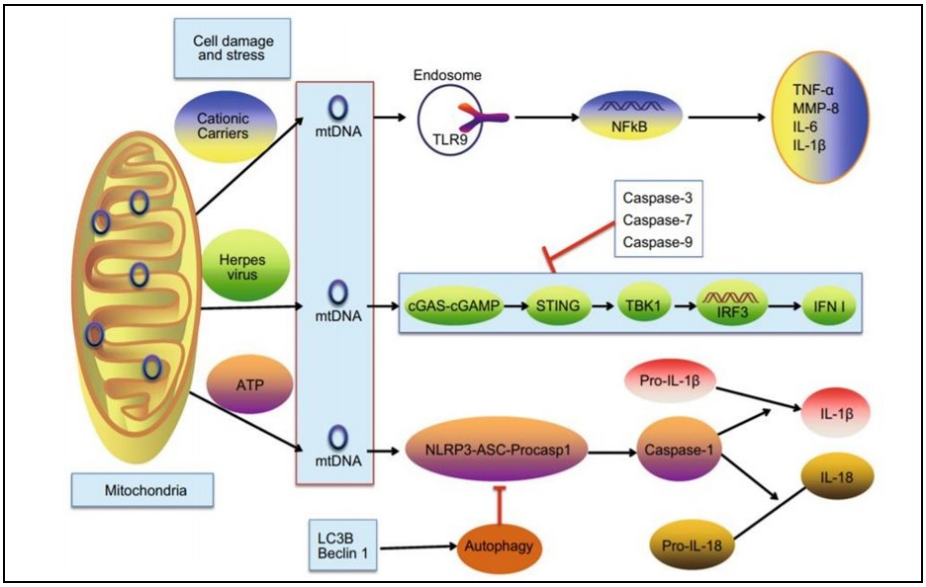

Figure 18. Immune response pathways induced by mtDNA release (107).

According to research, release of mtDNA in the cytoplasm plays an important role in the development of several inflammatory disorders such as rheumatoid arthritis, atherosclerosis, SLE, and AGS (107,109).

Aberrant mitochondria metabolism in AGS has been recently linked to increased production of reactive oxygen species (ROS) (110,111). Under physiological settings, the equilibrium between ROS creation and ROS antioxidant scavenging is tightly regulated. In such case, ROS are required for a wide range of biological activities including adaptation to hypoxia, regulation of autophagy, regulation of immunity and regulation of cell differentiation (112). On the other hand, excessive ROS generation induce oxidative damage to multiple cellular compartments, including mitochondria, nuclear and plasma membrane. As a result, apoptotic cell death pathway is activated and exacerbates mtDNA leakage into the cytoplasm, thus worsening IFNα-associated inflammatory response (110). Despite the growing interest in mitochondrial dysfunction in AGS, there is still a gap in knowledge regarding their role in AGS pathogenesis.

4.7 Therapeutic options for Aicardi-Goutières Syndrome

As previously discussed, AGS-affected patients present a variety of autoimmune and inflammatory symptoms due to different genotypes and phenotypes (17). Moreover, pediatric drug development is mainly based on prescription of adult medicines which often results in multiple side effects (113). For these reasons, it may be challenging to assess the efficacy of some immune-modulating therapies in AGS children. Since AGS is defined by an aberrant reaction to endogenous nucleic acids, there are two ways to reduce the pathological type I IFN response: the first involves the inhibition of the synthesis of endogenous NAs stimuli or enhancing their elimination, whilst the second involves the suppression of the downstream signaling derived from self-nucleic acid stimuli (114).

However, these therapies only represent palliative treatments and no definitive cure for AGS has been developed yet (114).

4.7.1 Reverse transcriptase inhibitors

A large portion of human DNA contains endogenous retroelements that still have the potential to replicate themselves (115), so they need to be controlled (Figure 19). Some of the genes involved in this mechanism are related to AGS pathogenesis. For this reason, AGS individuals may benefit from reverse transcriptase inhibitors (RTIs) therapy. Recently, AGS patients with variants of *TREX1*, *RNASEH2A*, *RNASEH2B*, *RNASEH2C*, and *SAMHD1* were treated with a combination of three RTIs (abacavir, lamivudine, and zidovudine) and most of them exhibited a decrease in type I IFN production without experiencing any adverse consequence. Interestingly, the positive effects of the treatment were more significant among the subjects with mutations in components of the RNase H2 complex (116). Although no results have been reported yet, researchers at the Children's Hospital of Philadelphia are currently investigating the safety and effectiveness of the other two RTIs (tenofovir and emtricitabine) in AGS subjects (117).

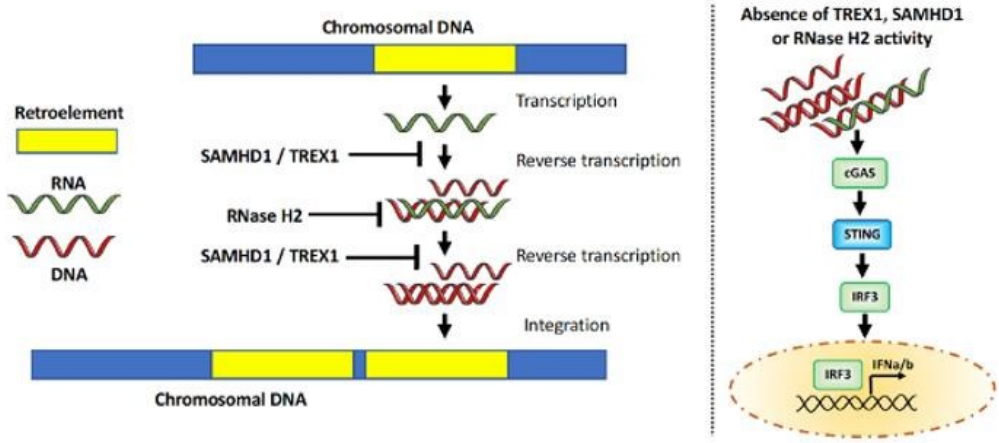

Figure 19. In physiological conditions (left) SAMHD1, RNase H2 complex, and TREX1 block endogenous retroelements, preventing immune response. Absence or mutations of these genes (right) result in overproduction retroelements that are recognized by immune system as 'foreign'. Thus, leading to the production of type I IFN (114).

4.7.2 JAK-STAT inhibitors

AGS patients may also benefit from the use of Janus Kinases Inhibitors (JAK-STAT inhibitors), which include baricitinib and ruxolitinib. JAK1 is a crucial component of the type I IFN signaling cascade which is involved in production of multiple proinflammatory cytokines. JAK1 inhibitors are currently used to treat SLE and other type I interferonopathies including rheumatoid arthritis and familial chilblain lupus (118,119). AGS-affected patients treated with ruxolitinib and baricitinib who presented mutations in *RNASEH2B* (120), *SAMHD1* (121), and *IFIH1* (122) all exhibited improvements regarding both neurological and non-neurological symptoms. Given the pivotal role that IFNα plays in the pathogenesis of AGS, using antibodies directed against the type I interferon

receptor could be an additional method to prevent IFNα activity. Although promising investigations have been undertaken in the setting of SLE, no clinical results regarding AGS have been published yet (123,124).

4.7.3 Hydroxychloroquine

Chloroquine and its synthetic analogue hydroxychloroquine (HCQ) are derivatives of the heterocyclic aromatic compound quinoline currently employed as antimalarial drugs (125). Recently, they have been approved for use as monotherapy or in conjunction with other therapies for the treatment of autoimmune diseases such as SLE, rheumatoid arthritis, and Sjögren's syndrome as immunosuppressive drugs (126,127). Since HCQ modulates the activity of NAs receptor, this compound has recently gained more and more attention regarding its potential role in AGS (128). *In silico* tests indeed revealed that multiple antimalarial drugs could act as inhibitors of cGAS-STING and TLRs molecular pathways, and HCQ was indicated as one of strongest compounds (128,129). By preventing TLR activation and obstructing TLR processing, HCQ lowers proinflammatory cytokines secretion. Moreover, it has been demonstrated that HCQ suppresses secretion of TNF-α, IFN-γ, and IL-6 in peripheral blood mononuclear cells (PBMCs) (130) as well as in human monocytes *in vitro* (131). In 2021, Garau and colleagues also demonstrated the beneficial effects of HCQ in lymphoblastoid cell lines derived from AGS patients mutated in *RNASEH2A* and *RNASEH2B* (132).

4.7.4 Metformin

Metformin (1,1-dimethylbiguanide hydrochloride) is the first-choice oral medication for treating type 2 diabetes. However, it is also used to treat multiple types of disorders, such as cancer, aging, cardiovascular diseases, and neurological conditions (133). Recent research shown that metformin reduces inflammation by regulating the autophagy process through the AMP-activated protein kinase (AMPK)-dependent pathway which in turn inhibits mTOR and activates the ULK complex (Figure 20) (134). As a consequence, the NF-kB/NLRP3 cascade is inhibited, thus leading to a decrease of proinflammatory cytokines production (134,135). Metformin can also reduce oxidative stress by scavenging mtDNA and mitochondrial-derived ROS (mtROS) via the inhibition of mitochondrial complex I (134). This drug also presented neuroprotective effects in patients affected of Alzheimer's disease and traumatic brain injury (135) and it has been recently demonstrated that it is a valid approach to reduce inflammatory response in AGS (136).

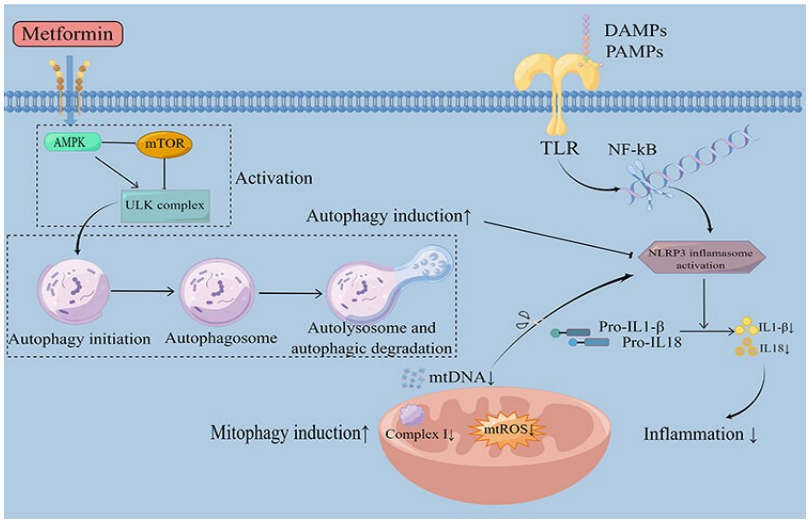

Figure 20. Metformin reduces inflammation by regulating the autophagy process (134).

5. AIMS

Aicardi-Goutières syndrome (AGS) is a rare genetic disorder that usually manifests itself between the first six months to 3 years of life (1,17). The primary characteristics of this condition include increased interferon-α (IFNα) levels in CSF and serum, bilateral spasticity, dystonia, acquired microcephaly, white matter abnormalities, basal ganglia calcifications, chronic lymphocytosis, and progressive brain atrophy (15). Since the signaling pathway of IFNα plays a central role in more than 85% of AGS-affected patients, this syndrome belongs to a class of disorders defined as type I interferonopathies (7). Indeed, most of AGS subjects show increased expression of interferon-stimulated genes (ISGs) in multiple tissues, and this expression is defined with the term "interferon signature" (IS) (29). Recent studies confirmed that 6 ISGs are mainly involved in AGS: *IFI27, IFI44L, IFIT1, ISG15, RSAD2* and *SIGLEC1* (29,137).

Considering genetic aspects, AGS is associated with mutations in 9 genes (*TREX1, RNASEH2A, RNASEH2B, RNASEH2C, SAMHD1, ADAR1, IFIH1, LSM11* and *RNU7-1*), all of which encode for proteins or transcripts involved in metabolism and recognition of nucleic acids (11,32). Even though it is hypothesized that alterations in these genes lead to the over-activation of the innate immune system and type I IFN release (11), some molecular mechanisms underlying the syndrome are still controversial.

Amongst the 9 genes cited above, *RNU7-1* (AGS9) is the least commonly altered gene in the Italian AGS cohort of patients (11) and most of mechanisms involved in AGS9 pathogenesis remain poorly understood. Starting from the evidence that IFNα plays an important role in AGS (1), it is also aimed to investigate IFN-mediated inflammation, its molecular readouts and its respective pathway of induction.

In recent years, a strong correlation between mitochondrial dysfunctions and AGS has been reported (110,111). For this reason, this project aims to define the potential role of mitochondrial alterations in AGS9 pathogenesis with a specific focus on oxidative stress and mitochondrial metabolism.

Lastly, this work aims to identify novel specific pathways involved in AGS9 pathogenesis. To do so, transcriptional changes of AGS9 profiles will be investigated and deregulated pathways will be characterized.

All the experiments cited above will be performed in primary dermal fibroblasts derived from an AGS-affected patient expressing a pathological variant of *RNU7-1* and in control fibroblasts derived from a healthy control subject matched by age and sex.

6. MATERIALS AND METHODS

6.1 Study subjects

After obtaining informed written consent, the Buzzi Children's Hospital recruited 1 AGS-affected patient expressing a pathological variant of *RNU7-1*. Clinical criteria were used to diagnose patients, and genetic analysis has been performed to confirm the pathology. One healthy volunteer matched by age and sex was also recruited. The information regarding the study' subjects involved in this work of thesis are reported in Table 2.
All procedures performed in this study involving human participants were in accordance with the ethical standards of the institutional and/or national research committee and with the 1964 Helsinki declaration and its later amendments or comparable ethical standards.

Patient's ID code	Age (in years)	Gender	Mutated gene	Mutated sequence
CTR VM2012	11	Female	Healthy control	/
AGS9 AG2010	13	Female	RNU7-1	Mutation 1: n.23T>G Mutation 2: n.54G>C

Table 2. AGS patients and healthy controls' relative information.

6.2 Isolation and characterization of human dermal fibroblasts

A punch skin biopsy was obtained from the volar part of the forearm of both the AGS patient and the healthy control. The biopsies were approximately 0.3 cm^2 and, after removal of subcutaneous tissue attached to the epidermis and dermis, the samples were washed twice with PBS and cut into 2 pieces using a sterile blade. One section of the biopsy was placed into a 24-well plate and maintained in culture with DMEM supplemented with 20% FBS, 1% penicillin/streptomycin and 1% L-glutamine to obtain fibroblasts, whilst the other one was frozen into a cryovial with 90% FBS and 10% DMSO.
The characterization of human dermal fibroblasts was performed by flow cytometry for surface antigen expression. Briefly, 2.5×10^5 of total fibroblasts per FACS tube were stained for 30 min at 4°C with anti-human monoclonal antibodies (mAbs) as follows: PerCP-conjugated anti-CD45, APC-conjugated anti-CD31, FITC-conjugated anti-CD90, PE-conjugated anti-EpCAM (all purchased by Miltenyi Biotec). Following Forward/Side Scatter setting, fibroblasts cells were identified as CD45- and CD31- cells (total fibroblasts cells). CD90 and EpCAM expression was evaluated on CD45-CD31- (total fibroblasts) gated cells.

6.3 Cell culture

Human dermal fibroblasts were cultured in DMEM Complete Medium supplemented with 20% of Fetal Bovine Serum (FBS; Euroclone), 1% glutamine (L-GLUT; GIBCO), 1% Penicillin/Streptomycin (P/S, GIBCO) and 1% non-essential Amminoacids (Euroclone) at 37 °C in a 5% CO_2. When cells reached 80% confluency they were split with trypsinization (trypsin-EDTA 1X 0.05% Euroclone) and plated at the appropriate concentration for further experimental procedures.

6.4 Hydroxychloroquine treatment

Fibroblasts were seeded in a 6-well plate at 5×10^5 cells/well density. 24 hours later, a final concentration of 10 µM of hydroxychloroquine sulfate (Thermo Scientific Chemicals) has been added to the standard growth medium. Non treated condition has also been prepared. Cells were incubated for 8 h with the reagent and then RNA was extracted following standard procedure (see total RNA extraction part).

6.5 RNA analysis

6.5.1 Total RNA extraction

Total RNA from human dermal fibroblasts was isolated using TRIzol® reagent (Invitrogen) in accordance with the manufacturer's instructions. TRIzol® is a complete, ready-to-use reagent for the isolation of high-quality total RNA and it consists of a monophasic solution of phenol and guanidinium isothiocyanate which solubilizes biological material and denatures proteins (Figure 21).

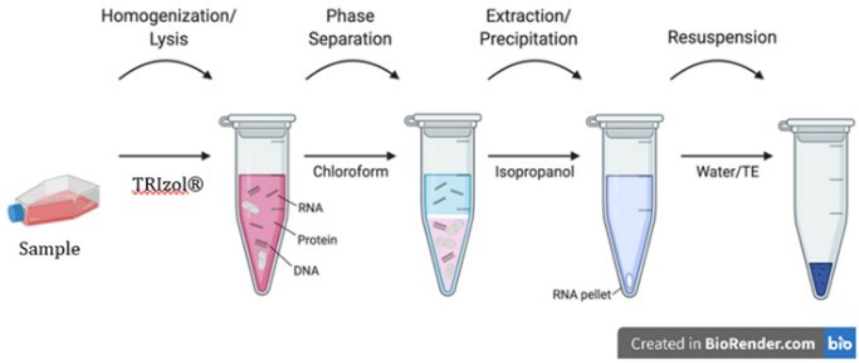

Figure 21. RNA extraction protocol overview. Created with BioRender.com.

6.5.2 RNA subcellular fractioning

Cytoplasmic and nuclear RNA were isolated and purified through the use the Cytoplasmic and Nuclear RNA Purification Kit (Norgen). Briefly, the protocol involves the lysis of the cells or tissue of interest with the provided Lysis Buffer J. The lysate is then separated through centrifugation, with the supernatant containing the cytoplasmic RNA and the pellet containing the nuclear RNA. Buffer SK and ethanol are then added to the desired fraction, and the solution is loaded into a spin-column. Only the RNA will bind to the column, while the contaminating proteins will be removed in the flowthrough or retained on the top of the resin. The bound RNA is then washed with the provided Wash Solution A in order to remove any remaining impurities, and the purified RNA is eluted with the Elution Buffer E (Figure 22).

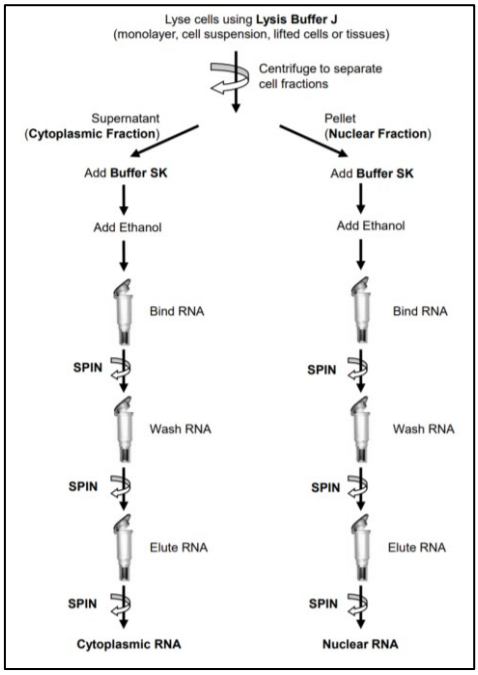

Figure 22. Cytoplasmic and Nuclear RNA Purification Kit (Norgen) protocol.

6.5.3 RNA quantification

The RNA obtained was quantified with the Multiskan GO spectrophotometer (Thermo Fisher Scientific) which can determine the average concentrations of the nucleic acids, as well as their purity through the absorption of purine and pyrimidine bases. Nucleic acids in solution absorb light with a peak in the ultraviolet region of 260 nm. To determine RNA concentration in the sample, a drop (1µl) of the sample is exposed to UV light at a wavelength of 260 nm and a photodetector measures the light which passes through the sample. Some of the ultraviolet light will pass through the sample while some light will be absorbed by the nucleic acid. The more light absorbed by the sample, the higher the nucleic acid concentration in the sample, in line with the Beer-Lambert law.

6.5.4 Reverse transcription

500 ng RNA were retro transcribed using 4 µl of reverse transcriptase Supermix 5X full (Genespin) in a final volume of 20 µl. Then, the RNA was diluted in nuclease-free water to reach the desired final concentration. The mix was incubated in a thermal cycler using the following protocol (Table 3).

Priming	5’ at 25°C
Reverse transcription	30’ at 42°C
RT inactivation	5’ at 85°C

Table 3. Thermal Protocol used for Reverse-transcriptase reaction.

6.5.5 Real-Time PCR

Real-Time PCR was performed with the CFX Connect Real-Time PCR System (Bio-Rad) using Optimum qPCRMaster Mix with SYBR® Green (Genespin). The NCBI's Primer-BLAST tool was used to design primers. Gene expression was calculated using the $2^{-\Delta\Delta Ct}$ method. *GAPDH* was used as endogenous control gene, and the list of primers used in this work is reported in Table 4.

Gene	Forward	Reverse
RNU7-1	CAGTGTTACAGCTCTTTTAG	GGGCTTTCCGGTAAAAAG
TREX1	TGCCTGCTACGGCTCA	AGTGGCCTCCATGTCGAAAAA
RNASEH2A	CGTGAACGTCACCCAGGTAT	TAGAGGGCATCTGCTTTGGC
RNASEH2B	CAGCCTCATTGCCAAATCCTCC	TAGCCAAAGCCTTCTGAGCTGC
RNASEH2C	GGGATAGTGATGGTGACAGAAG	AAGCGGCTGAAGTTGGCATGG
SAMHD1	AGCATAGTCTAGGGGTGGGG	CCCAGTGCGTGAACTAGACA
ADARTOT	AGCTTGGGAACAGGGAATCG	CTTCGCAGTCTGGGAGTTGT
ADAR110	CGCCCTCTTTGACAAGTCCT	GGGATTGTGCCTTCTCCGTT
ADAR150	CACTTCCAGTGCGGAGTAGC	CTGAGGGAATACCCCTGCC
LSM11	GCAAGAATCCTGAGCCCTGT	GAGTAAAGGAGGCCCAACCC
IFIH1	CCCGCTACATGAACCCTGA	TGCAGCAGCAATCCGGT
SIGLEC-1	GGAGGCGTGTTTGTAAGCAG	CAGGATCAATGAGCTGCGTG
IFI44L	TCTGTCTCCAAACCGTGGC	ACTCACACGTGGAAGCTGTTT
IFI27	CTCCTTCTTTGGGTCTGGCT	TGGTCACTGCTGATGAGGTG
IFIT1	CTAATTTACAGCAACCATGAT	TCCCACACTGTATTTGGTGTC
ISG15	CAGCCATGGGCTGGGA	CTCTGACACCGACATGGAGC
RSAD2	ACTCGCCAGTGCAACTACAA	TGATCTTCTCCATACCAGCTTC
cGAS	AAGAAGAGAAATGTTGCAGGA	GACTGTCTTGAGGGTTCTGGG
IRF3	TCTAGAGCTCAGCTGACGGG	TCCCATGGTCCGGCCTAC
STING	GAGTGTGTGGAGTCCTGCTC	CTGGAGTGGGGCATCTTCTG
TBK1	CGGAGACCCGGCTGGTATAA	TGCATCTTGGCTGGATCAGG
H1FX tot.	CGTGGGCTTTTCGGTGTTTT	GGCGTGAGCCGTACAAAATC
HIST1H2AC tot.	GACCGAGAGTCACCACAAGG	CGGGAGCTCAGATACCTGTC
H3F3Atot.	CATTGTTTAGAGGCCGACGC	GTCCGCCGTAGACAACTTGA
HIST1H1tot.	GGAAGCCAAGCCCAAGGTTA	AGCGCTCTTCTTCGGAGTTG
HIST2H3A tot.	CTACCAGAAGTCCACGGAGC	AAGCGCAGGTCCGTCTTAAA
HIST2H3A polyA	CGAAGACACGAACCTGTGCGCC	GGCAAGCGTACAGCTTCTTCCA
HISTH2AC polyA	GACCATGCTCAGGGCGGCGTCCT	CCTTCTACCTACAAGCAGTGAGGTT
H1FX polyA	GTGGTTCGACCAGCAGAATG	GAGCTTGAAGGAACCGTTGG
H3F3A polyA	AAAGCCGCTCGCAAGAGTGCG	ACTTGCCTCCTGCAAAGCAC
HISTH1C polyA	ACACCGAAGAAAGCGAAGAA	GCTTGACAACCTTGGGCTTA
SLBP	GCAGACCCGAGAGCTTTAC	CTTCAACTGCACTTGCCCAG
LSM10	GGGAAAGCGGAAGGAATGTC	CCTGCTTGCACGCGAC
ZFP100	TCACAGCTCCCTTGTGCTTC	TGAGGGTCACAAATTCCTCAGC
GAPDH	ACATCGCTCAGACACCATG	TGTAGTTGAGGTCAATGAAGGG

Table 4. List of primers used in this work.

6.5.6 RNA immunoprecipitation

ZFP100 immunoprecipitation was performed in human dermal fibroblasts. Cells were lysed with lysis buffer (10 mM Tris HCl, 10 mM NaCl, 2 mM EDTA, 0.5 Triton X100) and incubated on ice for 10 min. 120 mM NaCl was then added, and cells were incubated for a further 5 min. Cells were then pelleted at 16,000 g for 15 min and the supernatant was retained for pre-clearing. Following pre-clearing, the lysate was incubated in the presence of ZFP100 (Thermo Fisher Scientific, BS-12242R) or IgG used as negative control. Protein-G magnetic beads (Pierce™ ThermoFisher Scientific) were used to capture ZFP100-RNA complexes. After elution, samples were purified with TRIzol® reagent (Thermo Fisher Scientific) following the manufacturer's instructions. Samples were retrotranscribed and analyzed via Real-Time qPCR (see above). *GAPDH* was used as a negative control. Relative enrichments were calculated with respect to their inputs.

6.5.7 Total protein extraction

Using RIPA buffer (50 mM Tris-HCl [pH 8.0], 150 mM NaCl, 1% NP-40, and 12 mM Deoxycholic acid, supplemented with 1X protease inhibitors (10X PIC)), total soluble protein samples were extracted from $5x10^6$ fibroblasts. Cells were resuspended in 100 µL of RIPA buffer and put on ice for 20 minutes. After ice incubation, cells were centrifuged for 20 minutes at 15000 RPM at 4°C, to separate soluble and insoluble protein fraction. Soluble fraction was then retrieved and used for protein quantification.

6.5.8 Subcellular fractioning

To separate the soluble cytoplasmic fraction and the soluble nuclear fraction of cellular proteins, subcellular fractionation of fibroblasts was performed. Using Nuclear Extraction Buffer mix (NEB) and Cytosol Extraction Buffer mix (CEB) from nuclear isolation kit (Abcam), respectively, supplemented with protease inhibitors and Dithiothreitol (DTT), soluble protein samples were extracted from the nuclear and cytoplasmic fraction of $5x10^6$ living cells. The cells were collected, centrifuged for 15 minutes at 1600 RCF, and then resuspended in 200 µL of CEB. Following 10 minutes ice incubation, the cell suspension was centrifuged at 1000 RCF for 10 minutes at 4 °C after passing through a needle. The pellet, representing the nuclear fraction, was reconstituted in 40 µL of NEB, and the cytosolic fraction was extracted by centrifuging the supernatant at 10,000 RCF for 30 minutes at 4 °C. Both protein contents were measured through the Multiskan GO spectrophotometer (Thermo Fisher Scientific) and the then quantified with the Bradford Assay (see protein quantification section).

6.5.9 Bradford protein assay

The protein content of previously extracted samples was assessed using the Bradford Reagent (Sigma Aldrich). This procedure is based on the formation of a complex between the dye, Brilliant Blue G, and proteins in solution.

The protein-dye complex causes a shift in the absorption maximum of the dye from 465 to 595 nm. The amount of absorption is proportional to the protein present, and the linear concentration range is 0.1–1.4 mg/ml of protein, using BSA (bovine serum albumin) as

the standard. Using the Multiskan GO spectrophotometer (Thermo Fisher Scientific), protein quantity was determined.

6.5.10 Western Blot Analysis

By using the SDS–polyacrylamide gel electrophoresis (SDS-PAGE), western blotting analysis was carried out. 25 µg of solubilized proteins were heated in Laemmli sample buffer (Bio-Rad) containing 70 mM 2-β-mercaptoethanol (Merck), separated by SDS-PAGE gel 6%, 10% or 12% (depending on the molecular weight of investigated proteins) and electroblotted onto a nitrocellulose membrane (Trans-blot, Bio-Rad). Membranes were then fixed with 4% paraformaldehyde (Thermo Fisher Scientific) in 0.1 M PBS and 0.01% Glutaraldehyde (Merck), pH 7.4, for 30 min at room temperature, and then blocked in 5% slim milk (diluted in 1X TBS with 0.05% Tween-20). After that, membranes were probed overnight with the appropriate primary antibody. All the primary antibodies used in the western blot analysis are listed in Table 5. Lastly, membranes were incubated with a specific secondary antibody Peroxidase AffiniPure Goat Anti-Rabbit/Mouse IgG (1:5000 dilution; Jackson Immuno Research). Proteins were then visualized by means of an enhanced chemiluminescence detection solution (Thermo Fisher Scientific). After acquisition by a GelDocTM image capture system (Uvitec, Eppendorf), densitometric analysis of the bands was performed using the ImageJ software.

Antibody	Dilution	Host	Brand and code
ADAR1	1:500	Mouse	Thermo Fisher Scientific MA5-17285
SIGLEC1	1:1000	Rabbit	Abclonal, A17533
IFI44L	1:1000	Rabbit	Abclonal, A13210
RSAD2	1:1000	Rabbit	Abclonal, A8271
IFI27	1:1000	Rabbit	Abclonal, A14174
IFIT1	1:1000	Rabbit	Abclonal, A8551
ISG15	1:500	Rabbit	Abclonal, A2416
B-ACTIN	1:3000	Mouse	Sigma Aldrich, A5441
VINCULIN	1:2000	Rabbit	Genetex, GTX113294
H4	1:1000	Rabbit	Abclonal, A1131
H1	1:1000	Rabbit	Abclonal, A3298
H3	1:2000	Rabbit	Abclonal, A2348
H2AX	1:1000	Rabbit	Abclonal, A2082
H2B	1:1000	Rabbit	Abclonal, A1981

Table 5. List of specific antibody and dilution used for WB experiments.

6.5.11 Immunocytochemistry

$3x10^5$ fibroblasts were seeded on ethanol-washed glass coverslips, maintained in standard culture medium, and then processed for immunocytochemistry. Briefly, cells were fixed with 4% paraformaldehyde in 0.1 M PBS (Life Technologies, Thermo Fisher Scientific, Waltham, MA, USA), pH 7.4, for 20 min at room temperature, and then washed with PBS.

The coverslips were incubated overnight at 4 °C in PBS containing 10% normal goat serum (NGS, Thermo Fisher Scientific), 0.3% Triton X-100 (BDH, VWR, Radnor, PA,

USA), and the appropriate primary antibody. List of specific antibobies used in this work for immunocytochemistry is reported in Table 6. Cells were thoroughly rinsed with PBS and 10% NGS and reacted with the appropriate secondary antibody (Alexa Fluor® 488 and 546, Life Technologies) and DAPI at a final concentration of 1 µg/mL for 1.5 h. Glass coverslips were mounted using the FluorSave Reagent (Calbiochem, Merck Chemical, Darmstadt, Germany) and analyzed by confocal microscopy (Confocal laser scanning microscopy platform Leica TCS SP8, Leica Microsystems). As control, the appropriate secondary antibody was administrated omitting the primary one (Alexa Fluor® 488 or 546, Life Technologies). Assessment of fluorescence intensity was performed using the FIJI software.

Antibody	Dilution	Host	Brand and code
ZFP100	1:200	Mouse	Thermo Fisher Scientific, BS-12242R
SIGLEC1	1:200	Rabbit	Abclonal, A17533
IFI44L	1:300	Rabbit	Abclonal, A13210
RSAD2	1:200	Rabbit	Abclonal, A8271
IFI27	1:200	Rabbit	Abclonal, A14174
IFIT1	1:250	Rabbit	Abclonal, A8551
ISG15	1:100	Rabbit	Abclonal, A2416
VIMENTIN	1:300	Mouse	Cell signaling mAb #5741
H4	1:100	Rabbit	Abclonal, A1131
H1	1:100	Rabbit	Abclonal, A3298
H3	1:300	Rabbit	Abclonal, A2348
H2AX	1:250	Rabbit	Abclonal, A2082
H2B	1:200	Rabbit	Abclonal, A1981
B-ACTIN	1:300	Mouse	Sigma Aldrich, A5441
cGAS	1:300	Rabbit	Abclonal, A8335
STING	1:200	Rabbit	Abclonal, A20175
IRF3	1:250	Rabbit	Abclonal, A11373
TBK1	1:300	Rabbit	Abclonal, A3458

Table 6. List of specific antibody and dilution used for immunocytochemistry experiments.

6.5.12 ELISA assay

The level of IFNα was detected on supernatant of fibroblasts using a commercial ELISA kit (Thermo Fisher Scientific), according to the manufacturer's protocols. Absorption was measured at 450 nm with Multiskan™ multimode plate reader (Thermo Fisher Scientific), and it was subsequently converted to the concentrations of IFNα following manufacturer's instructions.

6.5.13 Nascent protein labeling (Click-It assay)

For Click-iT metabolic protein labeling, cells were seeded on glass coverslips, left overnight, treated with 1µM dexamethasone for 2 hours to induce circadian synchronization and then incubated in growth medium.

22 hours after dexamethasone treatment, cells were incubated for 1 hour with DMEM methionine-free medium (Thermo Fisher Scientific) and then incubated for 4 hours with

DMEM methionine-free medium additioned with 50 μM of L-Azidohomoalanine (AHA).
Cells were then fixed for 30 minutes with 4% paraformaldehyde (Merck) and then Click-it reaction was performed following manufacturer instructions (Click-iT® Cell Reaction Buffer Kit, Thermo Fisher Scientific). At the end of the procedure, nascent proteins were labeled with 488 Alexa fluor, and nuclei were stained with DAPI at a final concentration of 1 μg/mL for 30 minutes. Glass coverslips were mounted using the FluorSave Reagent (Calbiochem, Merck Chemical, Darmstadt, Germany) and analyzed by confocal microscopy (Confocal laser scanning microscopy platform Leica TCS SP8, Leica Microsystems). As control, cells were reacted with Click-iT® Cell Reaction Buffer Kit without prior incubation with AHA. Assessment of fluorescence intensity was performed using the FIJI software.

6.6 Mitochondrial assays

6.6.1 Mitotracker assay

$3x10^5$ fibroblasts were seeded on ethanol-washed glass coverslips and maintained in standard culture medium for 24 hours. Cells were then incubated with 100 nM MitoTracker® Deep Red (Invitrogen™) for 45 minutes at 37 °C in a 5% CO_2. Cells were then washed twice with 1X PBS and fixed with 4% paraformaldehyde in 0.1 M PBS (Life Technologies, Thermo Fisher Scientific, Waltham, MA, USA), pH 7.4, for 20 min at room temperature. Lastly, samples were incubated with DAPI at a final concentration of 1 μg/mL for 1.5 h at room temperature and analyzed by confocal microscopy (Confocal laser scanning microscopy platform Leica TCS SP8, Leica Microsystems). As a control, cells were reacted with DAPI without prior incubation with MitoTracker® Deep Red. Assessment of fluorescence intensity was performed using the FIJI software.

6.6.2 Mitosox assay

The MitoSOX™ Red Mitochondrial Superoxide Indicator (Invitrogen™) is a novel fluorogenic dye for highly selective detection of superoxide in the mitochondria of live cells. $3x10^5$ fibroblasts were seeded on ethanol-washed glass coverslips and maintained in standard culture medium for 24 hours. Cells were then incubated with 500 nM MitoSOX™ Red for 30 minutes at 37 °C in a 5% CO_2. Cells were then washed twice with 1X PBS and fixed with 4% paraformaldehyde in 0.1 M PBS (Life Technologies, Thermo Fisher Scientific, Waltham, MA, USA), pH 7.4, for 20 min at room temperature. Lastly, the samples were incubated with DAPI at a final concentration of 1 μg/mL for 1.5 h at room temperature and analyzed by confocal microscopy (Confocal laser scanning microscopy platform Leica TCS SP8, Leica Microsystems). As a control, cells were reacted with DAPI without prior incubation with MitoSOX™ Red. Assessment of fluorescence intensity was performed using the FIJI software.

6.7 MTT assay

The MTT assay is a colorimetric assay used as an indicator of cell viability of all cells by measuring the growth rate of cells comparing with the absorbance.

The MTT assay is based on the reduction of MTT (3-(4-(4, 5-dimethylthiazolyl-2)-2, 5-diphenyltetrazolium bromide) a yellow water-soluble tetrazolium salt created by mitochondrial dehydrogenases in metabolically active cells that is reduced to purple formazan-stained crystals (Figure 23) (138).

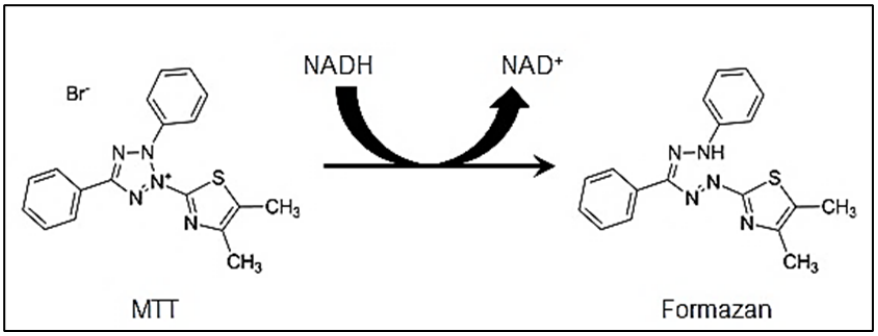

Figure 23. Chemical structure of MTT and colored formazan product (138).

Human dermal fibroblasts were seeded in a 96-well plate at 2×10^5 cells/well density. After 24 hours period of incubation at 37 °C in a 5% CO_2, 10 µl MTT assay kit reagent (Merck) was added to each well, and cells were incubated for 3 h. MTT crystals were eluted with 100 µl of elution solution, composed of 4 mM HCl, 0.1% (v/v) NP40 all in isopropanol for 30 min. The relative absorbance was measured with Multiskan™ multimode plate reader (Thermo Fisher Scientific) at $\lambda = 570$ nm. The results are expressed as a percentage of the absorbance read in healthy fibroblasts cells (CTR).

6.8 Transmission Electron Microscopy (TEM) analysis

After being cleaned with 1X PBS, around $3x10^6$ live cells were gently scraped from the culture flasks and fixed in 2.5% glutaraldehyde in 0.13 M phosphate buffer, pH 7.2–7.4, for 2 h. Following this process, cells were post-fixed in 1% (w/v) osmium tetroxide, dehydrated through graded ethanol and propylene oxide, and embedded in Epon-Araldite. Several semithin sections (about 70 nm thick) were prepared from each sample and stained with 0.5% toluidine blue in 1% sodium borate. Ultrathin sections of 50 nm were then generated and counterstained with uranyl acetate and lead citrate, to be observed using a Tecnai Spirit BT transmission electron microscope (Thermo Fisher Scientific).

6.9 RNA sequencing workflow

The primary challenge with RNA-seq is the experiment design, where accuracy and cost need to be balanced. To produce dependable analysis, the ideal number of biological and technical duplicates must be selected, together with the necessary sequencing depth.

The decision to use "single-reads" or "paired-end" is especially noteworthy as it influences whether the fragments are read from one end to the other or from both ends. To increase sequence coverage, "paired-end" sequencing is advised where it is feasible (139).

An RNAseq experiment typically includes of many fields of biology: experimental biology, computational biology, and systems biology (Figure 24).

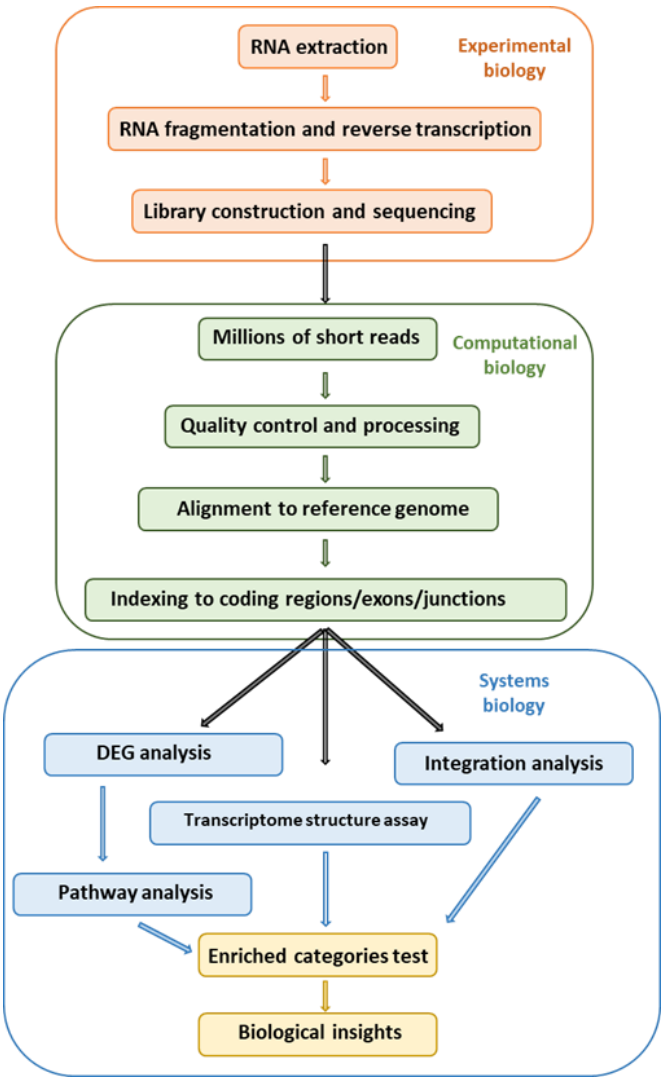

Figure 24. Schematic representation of RNAseq workflow. The three primary sections: Experimental Biology (orange), Computational Biology (green), and System Biology (blue) are displayed in different boxes. As shown by the arrows, the workflow begins with sample preparation and moves on to the sequencing and analysis phases. Created with BioRender.

RNA samples were isolated from human dermal fibroblasts and their quality were determined using the Agilent 4200 TapeStation System (Agilent, Santa Clara, CA, USA). Four samples per patients were analyzed (N = 4). RNA-seq libraries were prepared with the CORALL Total RNA-Seq Library Prep Kit (Lexogen, Austria) using 750 ng total RNA. To remove ribosomal RNA, a RiboCop rRNA Depletion Kit (Lexogen, Austria) was used. The quality and quantity of the sequencing libraries was assessed with D1000 ScreenTape Assay using the 4200 TapeStation System (Agilent, USA). Libraries were

sequenced using 75 bp paired end reads on the Illumina NextSeq 500 platform (Illumina, San Diego, CA, USA).
FastQ files were generated via Illumina bcl2fastq2 (v. 2.17.1.14). The quality of the raw data output was examined on a FastQC.
The bioinformatic data analysis pipeline included unique molecular identifier (UMI) extraction, trimming, alignment, and quality control steps. Because CORALL libraries contain N12 UMIs at the start of Read 1, UMIs were removed in the first step using the UMI tools software.
Adapter sequences, poly-A sequences at the 3′ end of Read 1, and poly-T sequences at the 5′ end of Read 2 were then trimmed using the Cutadapt software. Subsequent steps to assess gene and transcript intensities were carried out using the STAR software and transcripts were aligned on the GRCh38 version of the genome. Gene and transcript abundance were computed using the FeatureCounts software, with the "stranded forward" option.
A differential expression analysis was performed using R package DESeq.2; coding and non-coding genes were considered differentially expressed and retained for further analysis when $|\log2 \text{ group2/group1})| \geq 1$ and FDR ≤ 0.1.
The R software was used to generate heatmaps (the heatmap.2 function from the R ggplots package), PCA plots (the prcomp function from the R ggplots package), and biotype plots. Over-representation analysis (ORA) for Gene Ontology, Reactome and KEGG were carried out using ClusterProfiler (140). A Venn diagram for shared genes was constructed using the InteractiVenn webtool (141). The differentially expressed lncRNAs and coding genes were loaded on the ncpath webtool and an integrated KEGG enrichment analysis which includes all three classes of RNAs was performed (142).

6.10 Statistical analysis for *in vitro* experiments

Statistics was evaluated using GraphPad Prism version 9.0a (GraphPad Software Inc, La Jolla, USA). Student's unpaired t-test was used if two conditions were to be analyzed during data collection, and one-way ANOVA followed by Tukey's post-test was used when three or more conditions were to be analyzed. For all in vitro experiments, data are reported as mean ± Standard Error Mean (SEM). The statistical significance level was set at $p=0.05$.

7. RESULTS

7.1 Setup of the experimental model

Thanks to the collaboration with the Pediatric Neurology Unit at the Buzzi Children's Hospital in Milan (Dr. Davide Tonduti), we enrolled one AGS-affected patient (AGS9) in this study and obtained a sample of skin biopsy from which we isolated primary dermal fibroblasts (see material and methods section for detailed protocol and patients' relative information). These cells indeed represent a reliable *in vitro* model to study type I interferonopathies (143,144), and they can be obtained with a minimally invasive procedure. Fibroblasts of an age and sex matched control (CTR) were already available for this study and used to obtain the results presented thereafter (see materials and methods section for patient and control's relative information).

7.1.1 Fibroblast characterization

To confirm that the isolated cell population from the skin biopsy was purely composed of fibroblasts, an immunophenotypic characterization was performed via Fluorescence-activated cell sorting (FACS) analysis (Figure 24). Specifically, the cells were tested for the potential expression of two hematopoietic markers, CD45 and CD31 to exclude the potential presence of hematopoietic cells. Results confirm that the totality of the cell population do not express these markers (Figure 25A), indicating that there wasn't a contamination of hematopoietic cells. CD45-/CD31- cells were also tested for CD90 and EpCAM (epithelial cell adhesion marker). EpCAM is an antigen mainly expressed in cancer stem cells and epithelial tumors, while CD90 is a specific dermal fibroblast marker (145,146). Results demonstrate that fibroblasts express CD90 marker but not EpCAM (Figure 25B), indicating that the isolation process was successful.

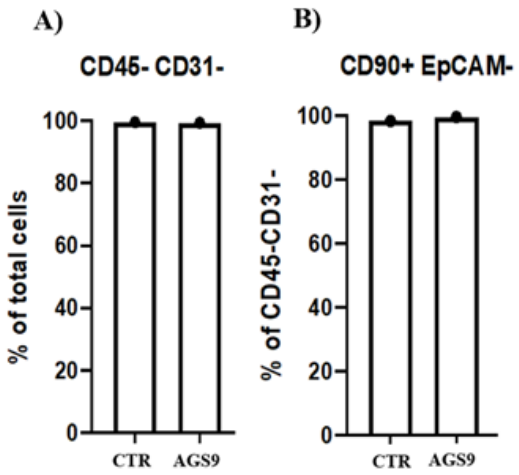

Figure 25. Phenotypic analysis of cell surface markers. Fibroblast characterization was performed via flow cytometry. Hematopoietic markers CD45 and CD31(A); CD90 and EpCAM (B). Y-axis represents the percentage of cells positive or negative to the markers. CTR: fibroblasts derived from the healthy control's biopsy; AGS9: fibroblasts derived from the AGS patient's biopsy carrying the mutation in *RNU7-1*. The results refer to two experiments (N=2).

7.1.2 Metabolic state and membrane permeability assay

MTT assay was performed to test fibroblasts' metabolic activity consequently to *RNU7-1* mutation and it was conducted at three time-points: 24 hours, 48 hours, and 72 hours after plating.

The MTT reagent (3-[4,5-dimethylthiazol-2-yl]-2,5-diphenyl-2H-tetrazolium bromide) is a mono-tetrazolium salt that can reach the mitochondrial inner membrane of metabolically active cells where it is reduced to formazan through a colorimetric-based reaction (147). Results highlight a reduced metabolic activity in fibroblasts derived from the AGS9 patient compared to CTR (Figure 26).

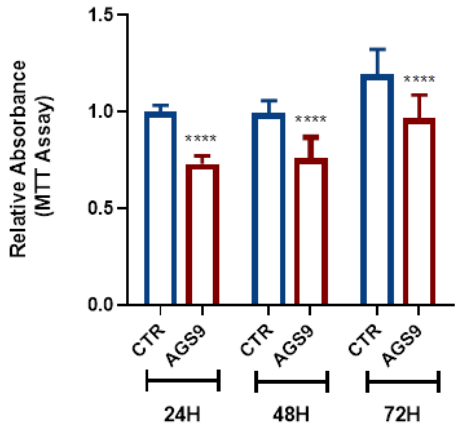

Figure 26. Metabolic feature of both CTR and AGS fibroblasts. MTT assay in control (CTR) and AGS patient (AGS9). MTT assay was performed at different time point (24h, 48h, 72h). Histograms show the results of three independent experiment, eight wells per experiments (N=24, ****p<0.0001 vs CTR). Data are expressed as mean ± SEM.

7.2 Impact of RNU7-1 pathologic variant on U7 snRNA

7.2.1 Folding prediction of U7 snRNA following RNU7-1 mutation

Through Whole Exosome Sequencing (WES) conducted from our collaborators at Buzzi Children's Hospital, two homozygous transitions have been identified in the *RNU7-1* gene of the enrolled AGS-affected patient: n.23T>G and n.54G>C (Figure 27A).

RNU7-1 is one of the 9 AGS-related genes and encodes for the U7 small nuclear RNA (U7 snRNA) (89).

U7 snRNA folding prediction was obtained through the software package RNAfold 2.6.4 and highlighted some structural differences between the Wild-Type (WT) RNA sequence and the mutated one (n.23T>G; n.54G>C) (Figure 27B).

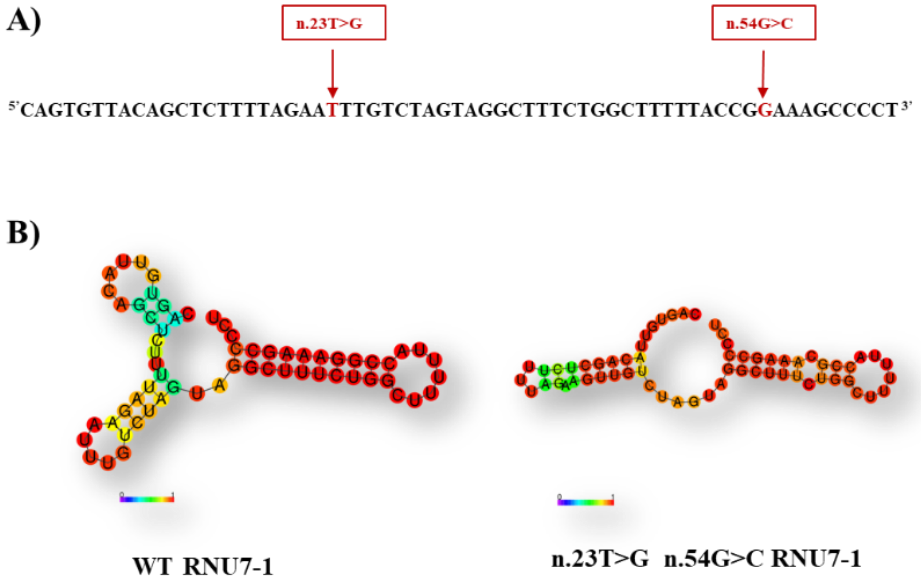

Figure 27. A) Schematic representation of the *RNU7-1* gene with localization of the investigated mutations reported in red. (B) Structure prediction of wild-type (WT) U7 snRNA (left) and mutated U7 snRNA (right). RNA minimum free energy (MFE) structure. Created with RNAfold 2.6.4.

7.2.2 Investigation of U7 snRNA expression and localization in primary fibroblasts carrying mutations in RNU7-1

As altered RNA morphology could affect both the expression and the localization of U7 snRNA, a standard Real-Time qPCR analysis and a nuclear-cytoplasmic mRNA quantification have been conducted on dermal fibroblasts. Results demonstrates that global expression of *RNU7-1* does not significantly change between AGS9 and CTR conditions (Figure 28A). On the other hand, *RNU7-1* pathologic variant affects the localization in subcellular compartment of the U7 snRNA, thus leading to an increase of the cytoplasmic isoform at the expense of the nuclear one (Figure 28B).

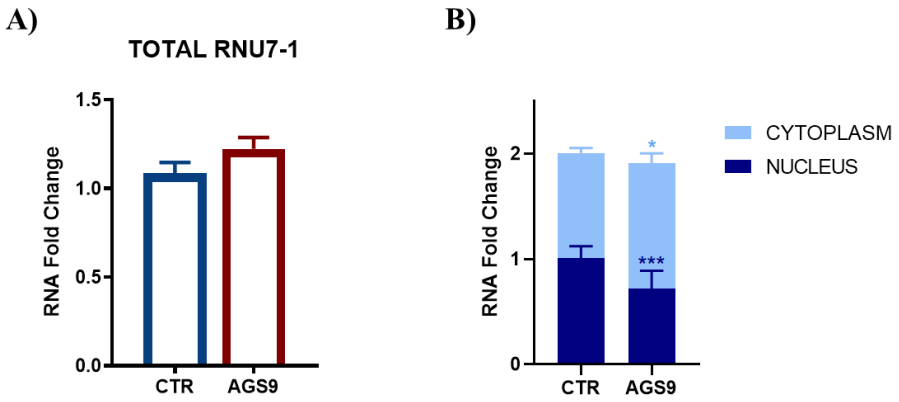

Figure 28. Altered RNU7-1 morphology affects U7 snRNA subcellular localization. A) Real-Time qPCR of RNU7-1 in AGS9-affected patient (AGS9) vs healthy (CTR) fibroblasts (N=9). GAPDH was used as

housekeeping gene. Data are expressed as means ± SEM of 3 replicate values in 3 independent experiments. (B) Absolute quantification of RNU7-1 in either cytosol (N=9, *p<0.05 vs CTR) or nucleus (N=9, ***p<0.001 vs CTR) of fibroblasts of a CTR and AGS9 patient. GAPDH and MALAT were used as housekeeping genes for cytosol and nuclei, respectively.

7.3 Impact of RNU7-1 pathologic variant on other AGS-related genes

The 9 AGS-related genes are strongly dependent with one another as they all encode for proteins or transcripts involved in metabolism and nucleic acids uptake (11,32). To investigate whether mutations in *RNU7-1* impacted other AGS genes, the mRNA expression of *IFIH1, TREX1, SAMHD1, RNASEH2A, LSM11* and the two isoforms of *ADAR1* (p150 and p110) have been measured through Real-Time qPCR. Results report that fibroblasts expressing the pathologic variant of *RNU7-1* present an increased expression of *LSM11,* and the two isoforms of *ADAR1* (p150 and p110) (Figure 29). Our data confirms the strong relationship between *RNU7-1* and *LSM11* as they both encode for components of the U7 snRNP complex. Moreover, the overexpression of *ADAR1* emphasizes the hypothesis according to which multiple members of the ADAR family form large multicomponent protein complexes with nuclear ribonucleoproteins to cooperate during the pre-mRNA processing machinery (148). Taken together, these data suggest a broader impact of the *RNU7-1* variant on the molecular landscape associated with AGS.

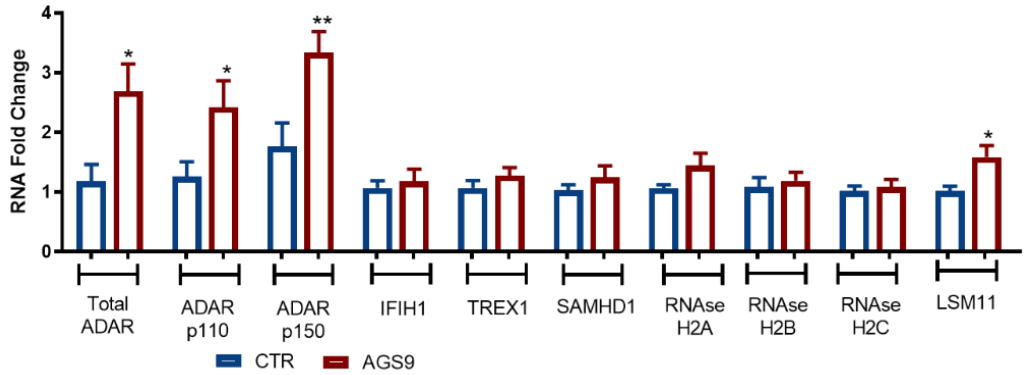

Figure 29. Mutations in RNU7-1 impact the expression of other AGS-related genes. Real-Time qPCR of AGS genes in AGS9 and CTR fibroblasts. Total ADAR1, ADARp110, ADARp150, IFIH1, TREX1, SAMHD1, RNASEH2A, RNASEH2B, RNASEH2C, and LSM11 levels were assessed by Real Time qPCR. GAPDH was used as housekeeping gene. Results are reported as means ± SEM of 3 replicate values in 3 independent experiments. (N=9, *p<0.05, **p<0.01 vs CTR).

7.4 Investigation of AGS canonic features

7.4.1 Production of IFNα in fibroblasts carrying mutations in RNU7-1

Increased expression of IFNα in CSF and serum is a key aspect in over 85% of AGS patients (28). IFNα has the function of activating the transcription of ISGs. ISGs are a panel of more than 100 genes which encode for several components involved in the inflammatory process and in the activity of innate and adaptive immune systems (149). To determine whether IFNα is overexpressed in the AGS9 condition, we set out an ELISA (enzyme-linked immunosorbent assay) test to quantify the amount of IFNα in the

supernatant derived from both AGS9 and CTR fibroblasts (Figure 30). Results highlight the increased production of IFNα in AGS9 condition.

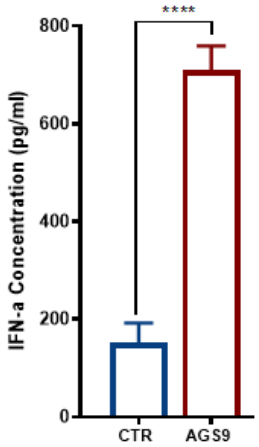

Figure 30. Interferon overproduction in RNU7-1 pathologic variant. ELISA (enzyme-linked immunosorbent assay) to target IFNα in the secretome derived from AGS9 and CTR fibroblasts after 72h of incubation (N=6, ****p<0.0001 vs CTR). Data are expressed as means ± SEM of 3 replicate values in 2 independent experiments.

7.4.2 Evaluation of interferon signature in AGS9 fibroblasts

mRNA expression of the 6 ISGs mostly related to AGS (*SIGLEC-1, IFI44L, IFI27, IFIT1, ISG15* and *RSAD2*) (29) was assessed via Real-Time qPCR, and these targets resulted upregulated (Figure 31A). Expression of ISGs is often used to calculate an important parameter of AGS, the interferon score. The interferon score defines the level of dysregulation of IFN, and it can be measured to test the effectiveness of a therapy or to monitor the state of the disorder (137). In this study, the interferon score has been analyzed in both fibroblast cells and in a whole blood sample of the AGS9 patient and the respective CTR. The analysis confirms the overall increased transcription of the ISGs in fibroblasts (Figure 31B) and in whole blood (Figure 31C) derived from the affected subject in respect to the control. Protein expression of these ISGs was also assessed via Western Blot (Figure 31D) and Immunofluorescence (Figure 31E), confirming an overall increased expression of these targets.

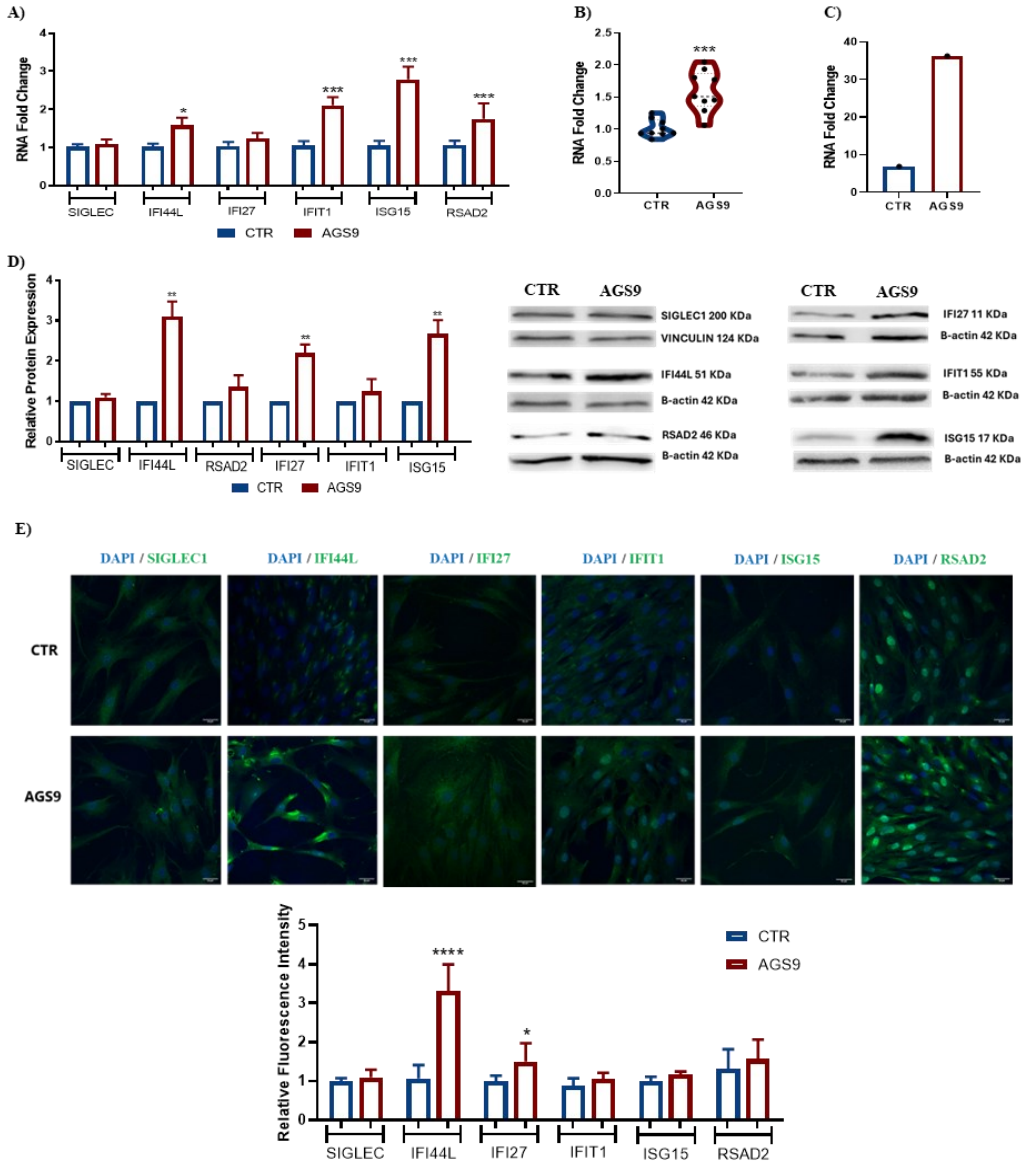

Figure 31. Activation of the IFN signature in fibroblasts of the AGS9 patient. A) Real-Time qPCR of ISGs in AGS9 and CTR fibroblasts. SIGLEC1, IFI44L, IFI27, IFIT1, ISG15 and RSAD2 levels were assessed. GAPDH was used as housekeeping gene. Results are reported as means ± SEM of 3 replicate values in 3 independent experiments. (N=9, *p<0.05, ***p<0.001 vs CTR). B) IFN SCORE mRNA expression in AGS9 and CTR fibroblasts (N=9, ***p<0.001 vs CTR). IFN SCORE levels were assessed by Real Time qPCR. GAPDH was used as housekeeping gene. Data are expressed as means ± SEM of 3 replicate values in 3 independent experiments. C) IFN score calculated in whole blood with the IFN Signature type 1 One Step Multiplex assay (N=1). D) Western Blot (right) and relative protein quantification (left) of ISGs. Representative images showing SIGLEC1 (N=3), IFI44L (N=3, **p<0.01), RSAD2 (N=3), IFI27 (N=3, **p<0.01), IFIT1 (N=2) and ISG15 (N=3, **p<0.01). β-actin was used as housekeeping protein. Data are expressed as means ± SEM. E) Immunofluorescence images (top) and relative fluorescence quantification (bottom) of ISGs in CTR and AGS9 cells. Nuclei are stained with DAPI (blue) and ISGs are shown in green. Data are expressed as mean ± SEM of three independent experiments, with three fields per experiment (N=9, *p<0.05, ****p<0.0001 vs CTR). Scale bar = 30 µm.

7.5 Effects of Hydroxychloroquine on interferon signaling and cell viability

Chloroquine (CQ) and its synthetic analogue hydroxychloroquine (HCQ) are currently employed as antimalarial drugs (125). Recently, they have been approved for use as monotherapy or in conjunction with other therapies for the treatment of autoimmune diseases such as systemic lupus erythematosus (SLE), rheumatoid arthritis, and Sjögren's syndrome as immunosuppressive drugs (126,127).

7.5.1 Hydroxychloroquine reduces interferon signature and secretion of IFNα

Given some similarities between SLE and AGS (150), we wanted to investigate the possible therapeutic effect of hydroxychloroquine (HCQ) on AGS outcomes. Specifically, we investigated if this compound could reduce IFN production and interferon signature in AGS9 fibroblasts. Basing on a previous reported protocol (151), we treated fibroblasts obtained from the AGS9 patient and the CTR with hydroxychloroquine sulfate (see material and methods for detailed protocol). Results obtained via ELISA confirm the increased production of IFNα in non-treated AGS9 cells (NT) and its subsequent decrease following hydroxychloroquine treatment (TR) (Figure 32A). Moreover, expression of ISGs and IFN score in AGS9 condition significantly decrease in AGS9 treated condition (Figures 32B and 32C). On the other hand, this treatment seems to not affect the overall expression of IFNα and ISGs in CTR cells.

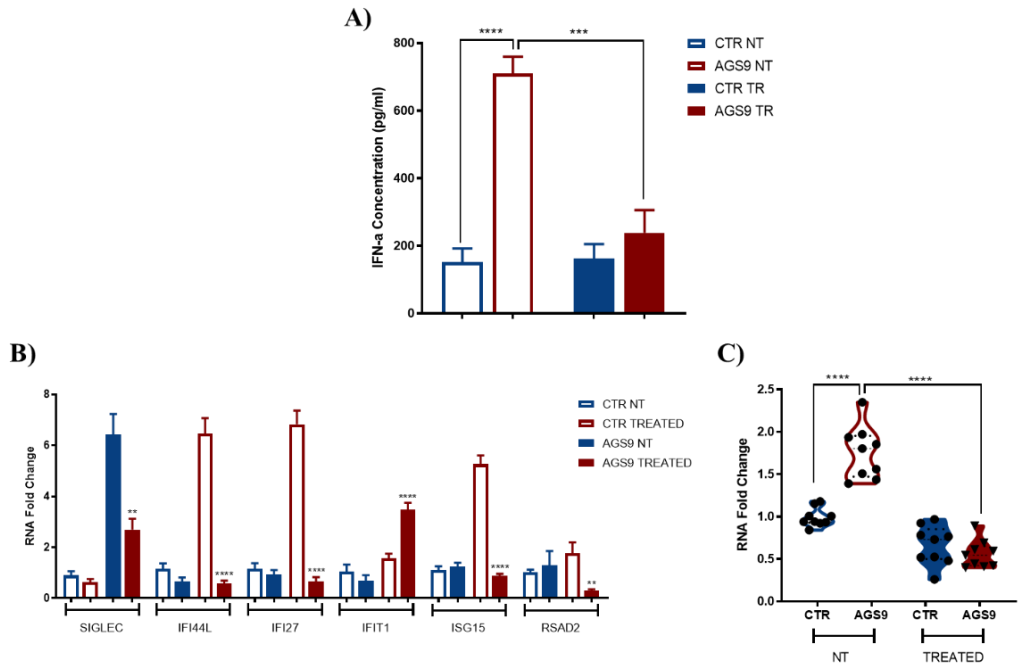

Figure 32. Hydroxychloroquine effectively reduces IFN production and its signaling pathway. A) ELISA (enzyme-linked immunosorbent assay) to target IFNα in non-treated (NT) AGS9 and CTR conditions and after chloroquine treatment (TR). Experiments were performed in duplicates in two experiments (N=4). Results are reported as mean ± SEM. B) SIGLEC, IFI44L, IFI27, IFIT1, ISG15 and RSAD2 mRNA expression in CTR and AGS9 with and without hydroxychloroquine treatment. GAPDH was used as housekeeping gene. Results are reported as means ± SEM of 2 replicate values in 3 independent experiments (N=6, **p<0.01;

****p<0.0001). C) Interferon score mRNA expression in CTR and AGS9 fibroblasts with and without hydroxychloroquine treatment. SIGLEC, IFI44L, IFI27, IFIT1, ISG15 and RSAD2, INTERFERON SCORE levels were assessed by Real-Time qPCR. GAPDH was used as housekeeping gene. Experiments were performed in duplicates in three independent experiments (N=6, ****p<0.0001). Results are reported as mean ± SEM. NT=non treated; TR=treated with hydroxychloroquine.

7.5.2 Hydroxychloroquine improves overall metabolism of AGS9 cells

As reported in the setup of the experimental model, AGS9 fibroblasts presented a strongly reduced metabolism measured through MTT assay. Recent research indicate that inflammation is one of the major contributors in cell viability as it has been demonstrated that cells subject to inflammation stimuli present higher mortality risk (152). To test the potential effects of hydroxychloroquine on cell survival, viability, and metabolism, an MTT assay has been conducted on supernatant of fibroblasts treated with this drug. A standard MTT assay without any drug treatment has also been set out as a negative control (Figure 33). Results confirm the improvement of cell viability in AGS9 condition after hydroxychloroquine treatment, giving more credit to role of inflammation in overall cell survival.

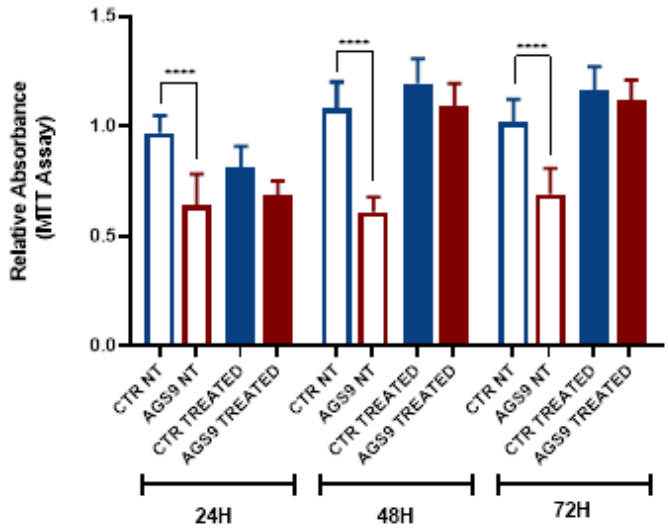

Figure 33. Hydroxychloroquine ameliorates cell viability. MTT assay performed in control (CTR) and AGS fibroblasts (AGS9) in both non-treated (NT) and treated conditions. Treated condition refers to the addition of 10 μ hydroxychloroquine in cell media for 8h. MTT assay was performed at different time point (24h, 48h, 72h). Histograms show the results of three independent experiment, eight wells per experiments (N=24, ****p<0.0001 vs CTR). Data are expressed as mean ± SEM. NT=non treated; TR=treated with hydroxychloroquine.

7.6 Importance of the cGAS-STING signaling cascade in IFN production

Amongst all the molecular pathways that lead to the production of IFNα, the cGAS-STING signaling cascade has emerged as a key mediator of inflammation in AGS pathogenesis (153,154).
The primary effector of this signaling cascade is the cyclic GMP-AMP synthase (cGAS) which catalyzes the production of the 2′,3′-linked dinucleotide cGAMP (55).

The endoplasmic reticulum (ER) transmembrane adaptor protein stimulator of interferon genes (STING) is then activated by cGAMP and subsequently reaches the Golgi apparatus (56).

At this point, the C-terminal tail of STING recruits and activates the TANK-binding kinase 1 (TBK1) that in turn phosphorylates the IFN regulatory factors 3 (IRF3). Lastly, IRF3 translocates to the nucleus and causes the transcription of IFNα and its autocrine signaling cascade (53,54,56).

To point out the potential activation of the cGAS-STING pathway in AGS9 fibroblasts, the expression of the players implicated in this cascade have been investigated. Results demonstrate the overall upregulation of both mRNAs (Figure 34A) and proteins (Figure 34B) of cGAS, STING and TBK1 in AGS9 condition.

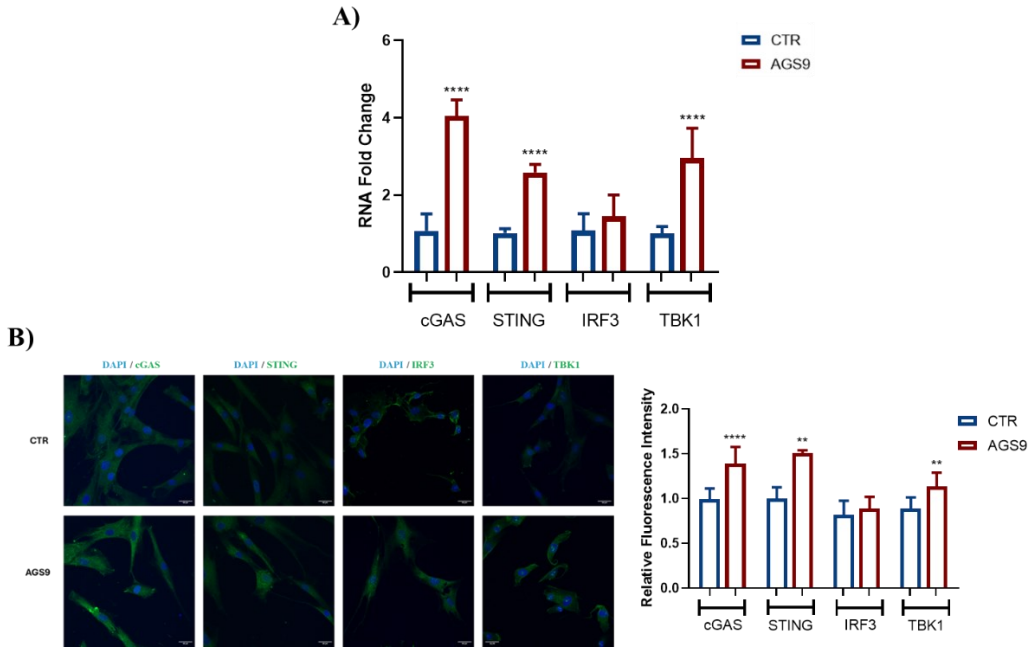

Figure 34. Major IFNα expression in AGS9-derived cells. A) cGAS, STING, IRF3 and TBK1 mRNA expression was assessed via Real-Time qPCR, GAPDH was used as housekeeping gene. Data are expressed as mean ± SEM of three independent experiments performed in duplicates (N=6, ****p<0.0001 vs CTR). B) Immunofluorescence analysis of IFN activators in CTR and AGS9 cells. Nuclei are stained with DAPI (blue) and target proteins are shown in green. Data are expressed as mean ± SEM of three independent experiments, with three fields per experiment (N=9, **p<0.01, ****p<0.0001). Scale bar = 30 µm.

7.7 Investigation of AGS specific features following RNU7-1 variation

Increased production of IFNα and interferon signature, as well as activation of the cGAS-STING represent canonic AGS readouts but do not explain how pathologic variations in *RNU7-1* are involved in AGS pathogenesis. To overcome this aspect, this part of the study is focused on the characterization of specific functional readouts triggered by variations of *RNU7-1*.

7.7.1 RNU7-1 variations affect expression of U7 snRNP-related genes

The U7 small nuclear RNA (U7 snRNA), encoded by the *RNU7-1* gene, is an essential component of the U7 small nuclear ribonucleoprotein (U7 snRNP) complex (91) (Figure 35A). Besides the U7 snRNA, the other components of U7 snRNP are LSM10 and LSM11 proteins. Other essential proteins for U7 snRNP functioning are ZFP100 (also called ZNF473) and SLBP that allows the cut of poly-A of replication-dependent histones (92). Specifically, ZFP100 stabilizes the binding of U7 snRNP to the poly-A cleavage site whilst SLBP is a trans-acting factors that binds the stem-loop structure and cooperates with U7 snRNP to the cut (90).

In this part of the study, we wanted to investigate the effects of mutated *RNU7-1* on the components of U7 snRNP. Real-Time qPCR conducted on the genes that encode for the components of the U7 complex shows an increase of *LSM11* and *ZFP100* in AGS9 fibroblasts (Figure 35B).

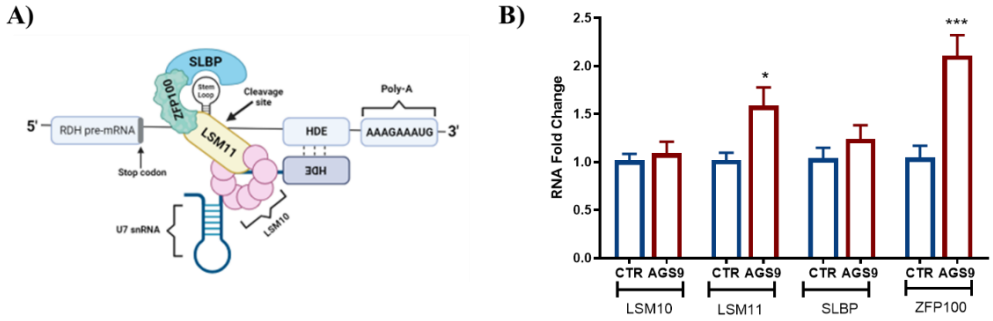

Figure 35. Effects of RNU7-1 mutation on U7snRNP complex A) Representative image of the U7 complex. Created with BioRender.com. B) LSM10 (N=9), LSM11 (N=9, *p<0.05 vs CTR), SLBP (N=9), and ZFP100 (N=9, ***p<0.001 vs CTR) mRNA expression in fibroblasts were assessed via Real-Time qPCR; GAPDH was used as housekeeping gene. Results are reported as mean ± SEM of three different experiments performed in triplicates.

To better understand how aberrant U7 snRNA leads to the overexpression of *LSM11* and *ZFP100*, the IntAct Molecular Interaction Database (IMID) was used. IMID is a tool used to study molecular interaction data derived from literature curation (155). Through this database, it was possible to discover that the U7 snRNA physically binds ZFP100 during the functioning of U7 snRNA (Figure 36). Moreover, recent research indicates that variants of *ZFP100* (here reported as its alias ZNF473) could affect its binding with U7 snRNA, overall leading to U7 snRNP misfunctioning (97).

Molecule A	Molecule B	Type A	Type B	Positive interaction	Publication IDs	Interaction Type	Aliases A	Aliases B
rnu7_human	ZNF473	rna	protein	✔	11782445	physical association	gene name synonym RNU7-1 gene name synonym U7.1 Show more (1)	gene name ZNF473 gene name synonym ZFP100 Show more (2)

Figure 36. IntAct search results for "RNU7-1 human". Schematic representation of RNU7-1 and ZFP100 (ZNF473) interaction (top) and interaction table with specific information about the two interactors (bottom).

7.7.2 Variations of RNU7-1 impair physical association between U7 snRNA and ZFP100

To verify whether variations *RNU7-1* could affect the binding between U7 snRNA and ZP100, RNA immunoprecipitation (RIP) was conducted (see materials and methods section for detailed protocol). Results highlight the decrease in physical association between U7 snRNA and ZFP100 in AGS9 fibroblasts (Figure 37). Thus, leading to a potential U7 snRNP misfunctioning.

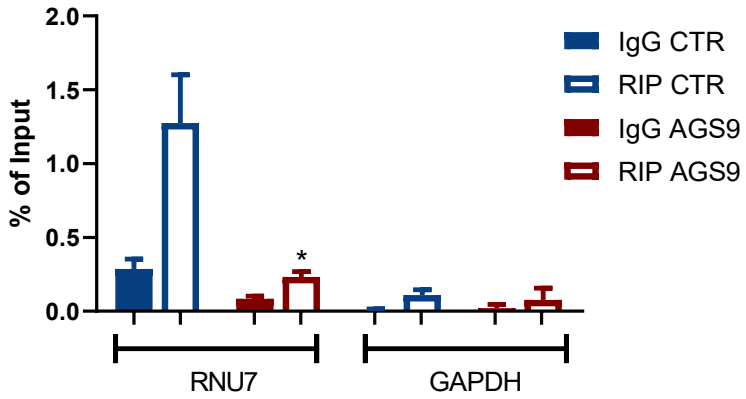

Figure 37. Effects of RNU7-1 mutation on ZFP100-RNU7 binding. RNA immunoprecipitation analysis of ZFP100. RNU7-1 (N=9, *p<0.05 vs CTR) mRNA expression in fibroblasts were assessed via Real-Time qPCR; GAPDH was used as housekeeping gene and results were normalized according to ZFP100 antibody or isotype immunoglobulin G (Isotype IgG; negative control). Results are reported as mean ± SEM of three different experiments performed in triplicates.

7.8 Identification of novel molecular pathways involved in AGS9 pathology

7.8.1 RNA-sequencing analysis highlights differences in AGS9 transcriptome

To investigate whether novel pathologic pathways could be involved in *RNU7-1* mediated AGS, we performed a total RNA-sequencing (RNAseq) analysis in fibroblasts obtained from either the AGS9 patient or the matched control.

Principal Component Analysis (PCA) highlighted a separation amongst conditions (Figure 38A), and the heatmap reports the top 30 up- and down-regulated genes (Figure 38B). Specifically, differential expression analysis highlighted 663 transcripts as differentially expressed (DEGs), of which 344 are down-regulated and 319 are up-regulated. Moreover, Figure 38C shows the distribution of the different biotypes of DEGs, and it is possible to see how the vast majority (535) are protein coding, 68 are lncRNAs, and the remaining ones are other types of RNAs.

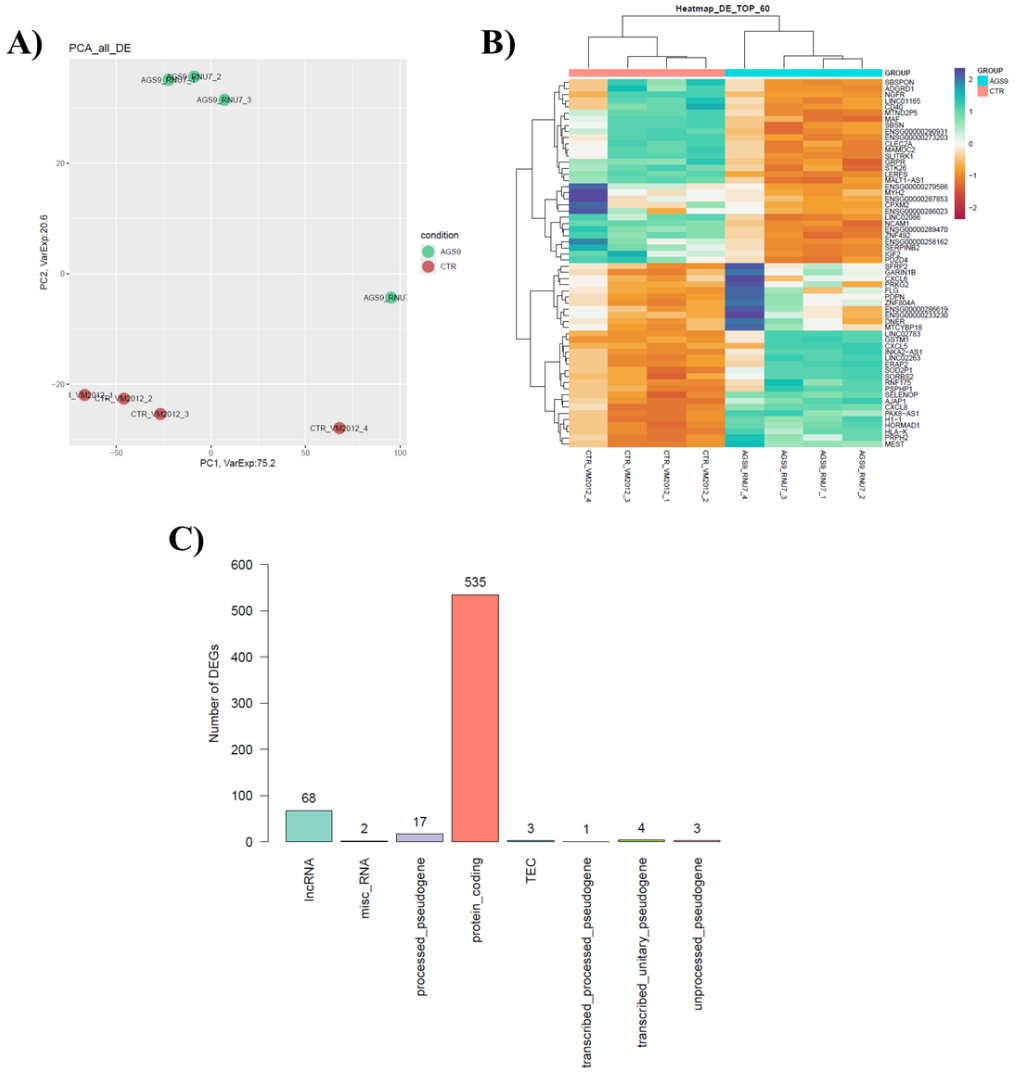

Figure 38. RNA-sequencing analysis indicates transcriptional perturbations following AGS9 mutation. A) Principal Component Analysis (PCA) of differentially expressed genes (DEGs) in AGS9 vs. CTR. We considered as differentially expressed genes with $|\log2FC| \geq 1$ and a False Discovery Rate (FDR) ≤ 0.1. B) Heatmap of the top 30 up- and down-regulated genes in AGS9 vs. CTR. C) Biotype of DEGs reported as barplot indicating on the y axis the number of DEGs and on the x axis the different biotypes.

7.8.2 AGS9 fibroblasts present alterations in multiple neural pathways

Gene Ontology (GO) analysis was then performed to assess implicated biological processes in which differentially expressed genes are involved. Interestingly, Biological Processes analyses highlighted multiple neuro-related pathways such as neurogenesis, neuron differentiation and nervous system development, which are main neurologic features in AGS patients (Figure 39).
Thus, confirming the role of aberrant neurologic pathways in AGS pathogenesis. Moreover, GO data indicates that fibroblasts represent a good *in vitro* model for the study of this disorder as they reflect specific molecular AGS aspects.

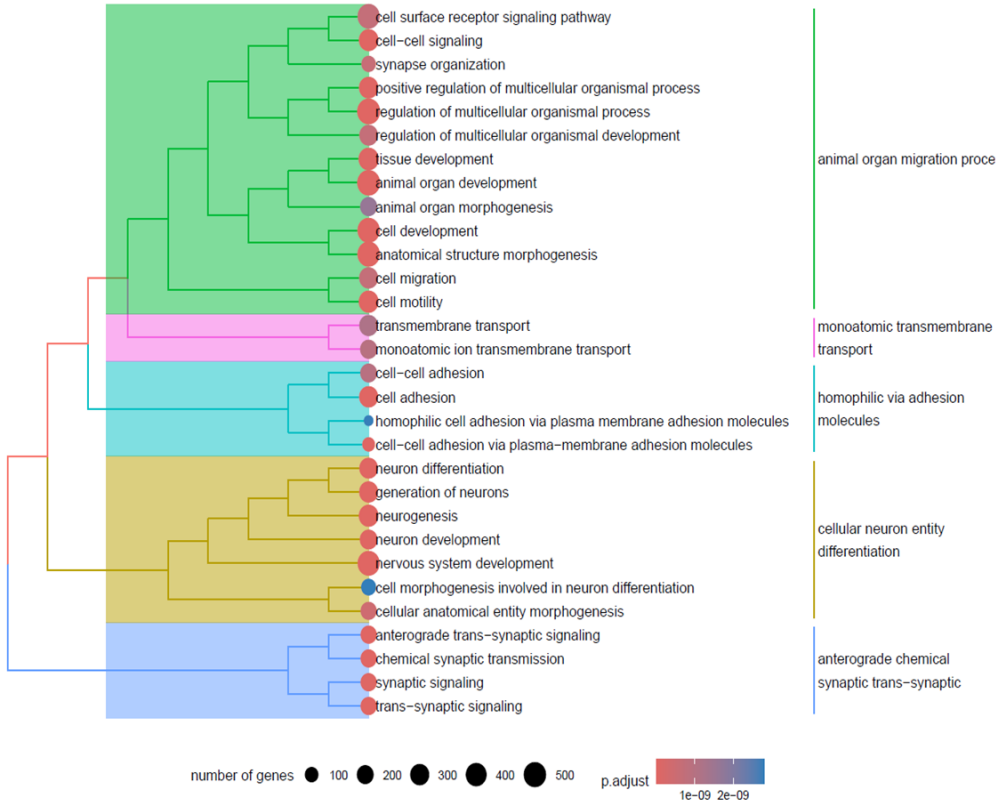

Figure 39. Differentially expressed genes in AGS9 are mainly involved in neural-related pathways. Treeplot showing the hierarchical clustering of enriched terms in GO Biological Processes. Pathways are clustered according to pairwise similarities which are calculated according to the Jaccardi's similarity index; dot size represents the number of different DEGs in the pathway, and the color indicates the adjusted p-value.

Reactome pathway enrichment analysis also confirmed dysregulation in neuron-related mechanisms and pointed out differentially expressed genes involved in interferon α and β signaling, a key feature in AGS pathology (Figure 40). Specifically, multiple ISGs resulted to be upregulated, including *ISG15, IFI27*, and *RSAD2,* confirming previously reported results regarding interferon-signature.

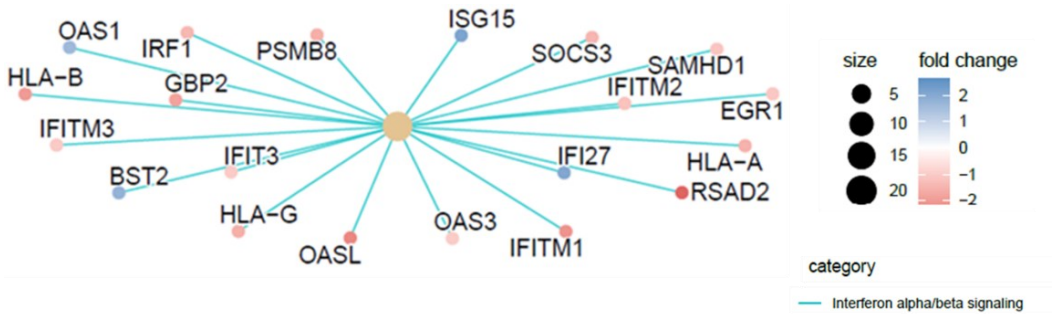

Figure 40. Cnet plot of enriched Reactome pathway. This plot was produced in ClusterProfiler based on the results of the "EnrichDAVID" function. Category = the enriched Reactome pathway. Size = the number of differentially expressed genes which belong to the enriched Reactome pathway. Fold change = the fold change difference between AGS9 and CTR.

7.8.3 Transcriptional changes in AGS9 cells affect chromatin modifications

GO analysis also highlighted multiple events related to chromatin modifications which are affected by transcriptional changes in AGS9 cells with respect to CTR. Specifically, the "structural constituent of chromatin" pathway resulted to be the most altered one. Figure 41 illustrates a cnet plot that includes the genes included in this pathway and, interestingly, most of them are genes involved in histone post-translational modifications.

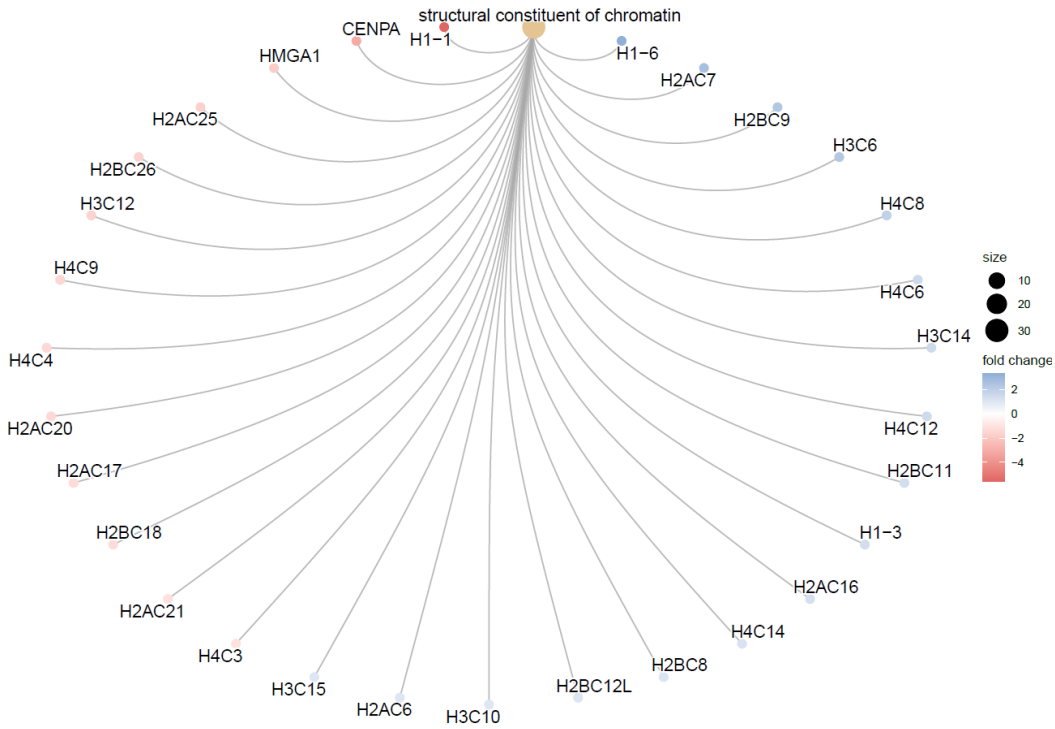

Figure 41. Cnetplot showing the clustering of enriched terms in GO Molecular Functions. This plot was produced in ClusterProfiler based on the results of the "EnrichDAVID" function. Category = the enriched

Reactome pathway. Size = the number of differentially expressed genes which belong to the enriched Reactome pathway. Fold change = the fold change difference between AGS9 and CTR.

7.9 Variations in RNU7-1 gene affect histone mRNA maturation and translation

Given the results previously reported in RNAseq analysis, this part of the study was focused on the impact of *RNU7-1* variations on histone transcription and translation.

7.9.1 Misprocessing of RDH pre-mRNAs in AGS9 fibroblasts

U7snRNP is a complex that mediates replication-dependent histone (RDH) pre-mRNA processing (14). The RDH genes encode the four core histones (H2A, H2B, H3 and H4) and the linker histone family (H1).

A distinctive feature of RDH is that they encode the only known eukaryotic mRNAs without a poly-A tail at the 3′ end, terminating instead with a stem-loop structure (89). This unique 3′ end is formed by a U7-dependent endonucleolytic cleavage of the pre-mRNAs between the stem-loop and a purine-rich sequence called histone downstream element (HDE) (90). A failure in this mechanism can lead to the production of aberrant mRNA isoforms that possess a poly-A (156).

To investigate functional consequences of the *RNU7-1* variant on U7 snRNP functioning, we performed a Real-Time qPCR in patient and control fibroblasts using primers that span the endonucleolytic cleavage site between the stem-loop site and HDE to determine the presence of misprocessed RDH transcripts. Compared to controls, patient cells were enriched for forms of RDH mRNAs that still present the poly-A tail. On the other hand, expression of replication-independent histones (RIH) mRNAs, which are normally polyadenylated and do not require the U7 snRNP complex, was unaffected (Figure 42).

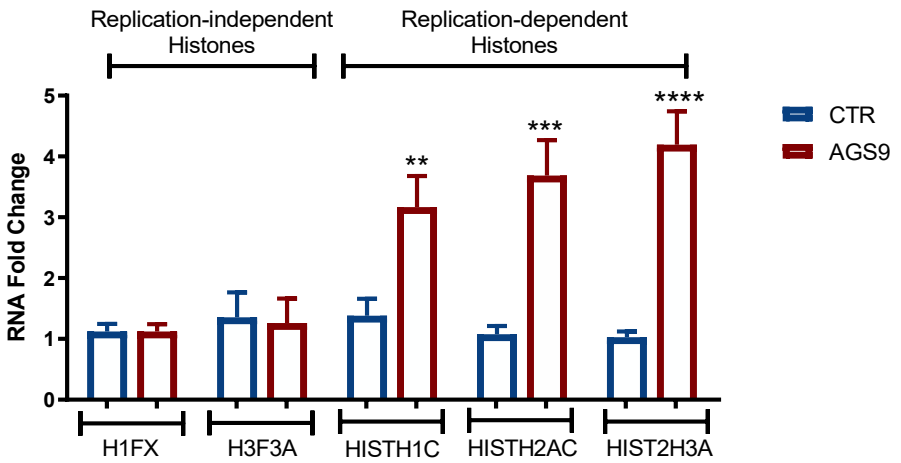

Figure 42. Enrichment in poly-A of RDH pre-mRNAs following RNU7-1 mutation. H1FX (N=9), H3F3A (N=9), HISTH1C (N=9, **p<0.01 vs CTR), HISTH2AC (N=9, ***p<0.001 vs CTR), and HIST2H3A (N=9, ****p<0.0001 vs CTR) mRNA expression in fibroblasts were assessed via Real-Time qPCR; GAPDH was used as housekeeping gene. Results are reported as mean ± SEM of three different experiments performed in triplicates.

To demonstrate that the increase in poly-A tail was a direct consequence of U7 snRNA misfunctioning and not a result of a potential basal overexpression of histone genes in AGS9, a standard Real-Time qPCR on both RDH and RIH transcripts has been performed. No significant differences were found among AGS9 and CTR conditions in terms of total histone transcription (Figure 43), suggesting a normal transcription of RDH genes and an aberrant maturation of their transcripts that could have consequences in term of histone translation.

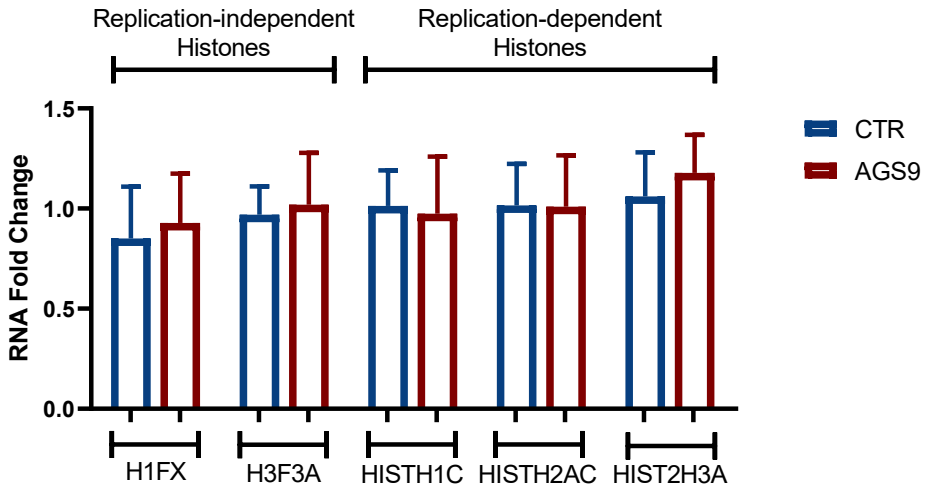

Figure 43. Histone mRNA basal expression is not affected by U7 snRNP misfunctioning. Real-Time qPCR of RDHs and non RDHs histones in AGS9 and CTR fibroblasts. H1FX (N=9), H3F3A (N=9), HISTH1C (N=9), HISTH2AC (N=9), and HIST2H3A (N=9) mRNA expression in fibroblasts were assessed; GAPDH was used as housekeeping gene. Data are expressed as means ± SEM of 3 replicate values in 3 independent experiments.

7.9.2 Histone translation is reduced because of RNU7-1 pathologic variations

As maturation of RDH transcripts resulted to be compromised by U7 snRNP misfunctioning, this part of the study focused on the consequences of altered RDH mRNA maturation on histone protein production. To this end, western blot on protein nuclear extracts (Figure 44A) and immunocytochemistry (Figure 44B) were conducted on both AGS9 and CTR fibroblasts. Results report a significant decrease of histone proteins in AGS9 condition, suggesting a link between RNU7-1 mutation and histone translation.

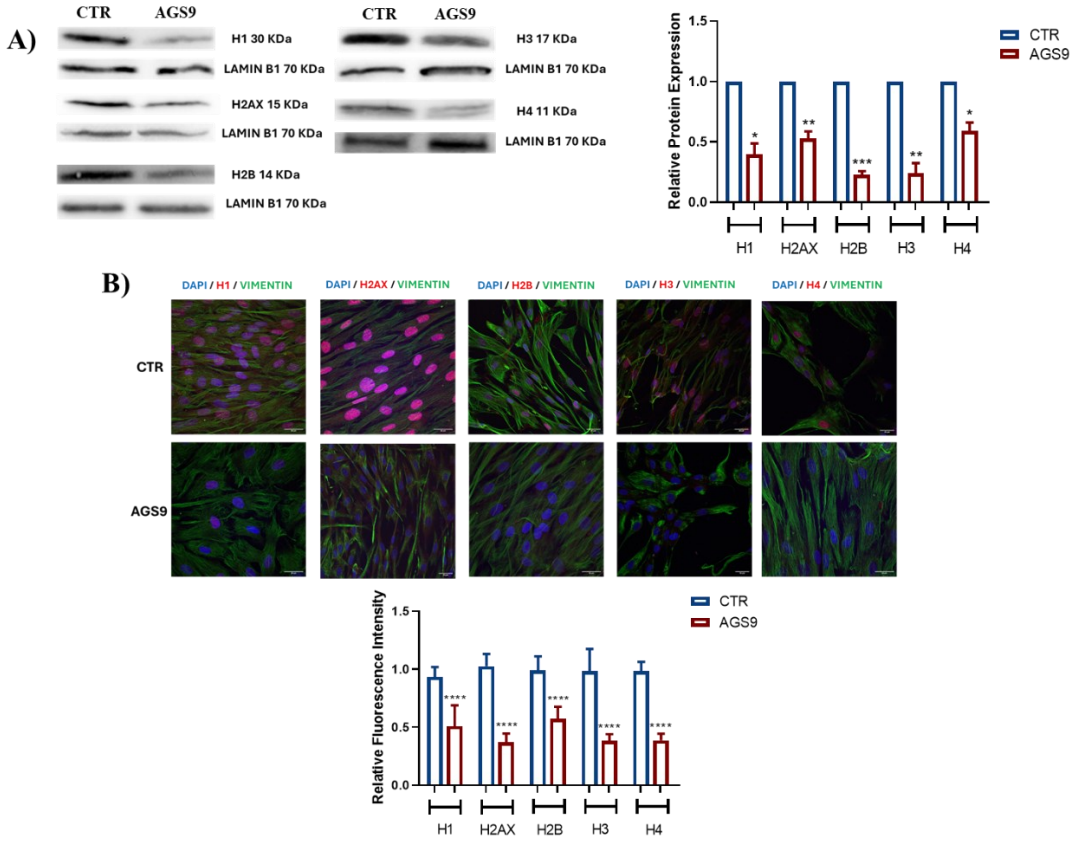

Figure 44. RNU7-1 pathologic variations affect histone protein expression in AGS9 fibroblasts. A) Western Blot (left) and relative protein quantification (right) of H1 (N=2, *p<0,05 vs CTR), H2AX (N=2, **p<0.01 vs CTR), H2B (N=2, ***p<0,001 vs CTR), H3 (N=2, **p<0.01 vs CTR) and H4 (N=2, *p<0.05 vs CTR). Lamin B1 was used as housekeeping protein. Data are expressed as means ± SEM. D) Immunofluorescence images (top) and relative analysis (bottom) of histones in CTR and AGS9 cells. Nuclei are stained with DAPI (blue), histones are represented in red, and vimentin is shown in green. Data are expressed as mean ± SEM of three independent experiments, with three fields per experiment (N=9, *p<0.05, ****p<0.0001 vs CTR). Scale bar = 30 µm.

7.10 TEM analysis reveals morphological alterations in AGS9 fibroblasts

Since histones are essential proteins for the package of genomic DNA and for gene regulation (157), their dysfunction could affect chromatin structure and expression.
Transmission electron microscopy (TEM) analysis on AGS9 and CTR fibroblasts revealed a lack of chromatin in AGS9 nuclei, confirming previously reported RNAseq results. Smaller mitochondria and reduced localization of ribosomes on ER membranes in AGS9 cells were also reported (Figure 45).

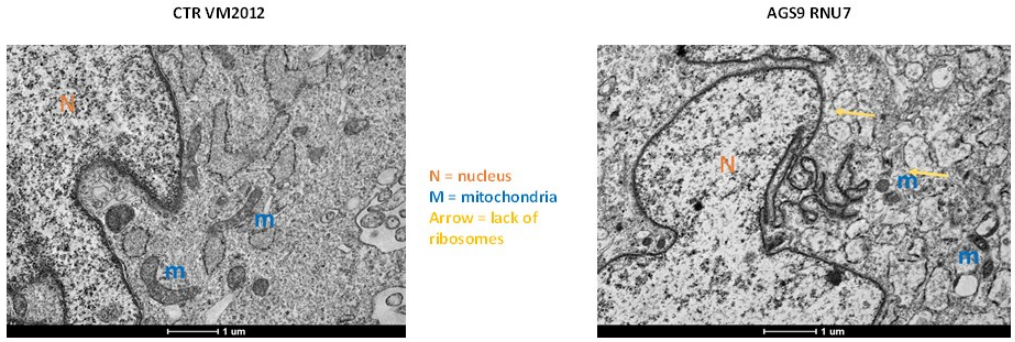

Figure 45. Representative transmission electron microscopy (TEM) images of fibroblasts from an AGS patient carrying mutations in RNU7-1 and a healthy control. Chromatin lack (in nucleus (orange), reduced dimensions of mitochondria (blue) and ribosome lack (yellow arrow) have been reported in AGS9 condition.

7.10.1 AGS9 fibroblasts present dysfunctions in mitochondrial metabolism

Several studies have recently demonstrated the involvement of mitochondrial impairment in multiple inflammatory disorders and AGS, with a close correlation between altered mitochondrial metabolism and the induction of an aberrant IFNα-dependent immune response (107,108,110). However, there is still a cap in knowledge regarding the potential role of mitochondrial alterations in *RNU7-1* mediated AGS.

For this reason, this part of the study is focused on the investigation of mitochondrial alterations in AGS9 context. Firstly, to understand whether morphologic alterations in mitochondria reported with TEM analysis affect mitochondria basal activity, we performed Mitotracker staining assay. Results report a decrease in fluorescence signaling in fibroblasts from AGS9 patients, supporting the findings highlighting a decrease in mitochondrial metabolic activity (Figure 46A).

Moreover, as aberrant mitochondria metabolism in AGS has been recently linked to increased production of reactive oxygen species (ROS) (110,111), Mitosox assay was also performed. Results confirm an increased release of ROS in AGS9 cells, confirming the implication of oxidative stress in AGS pathogenesis.

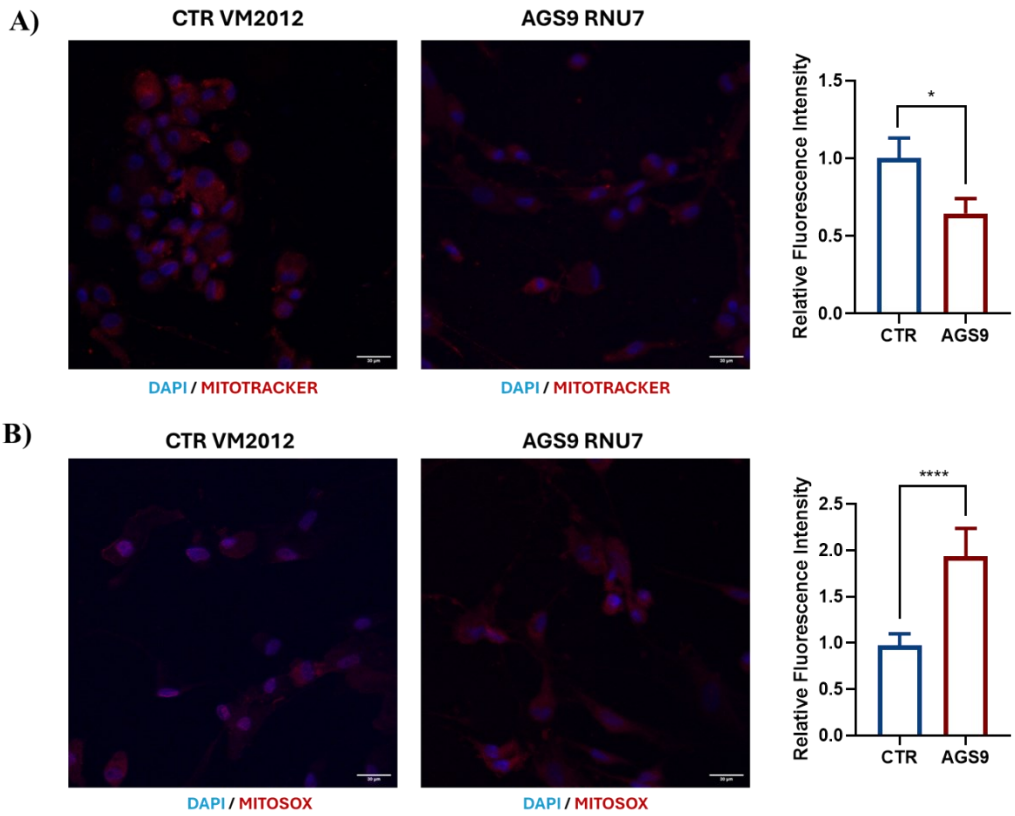

Figure 46. Mitochondrial dysfunctions in AGS9 cells. A) Mitotracker staining assay in AGS9 vs CTR fibroblasts (left) and relative quantification (right). Nuclei are stained with DAPI (blue) and mitochondria are labelled in red. Data are expressed as mean ± SEM of two independent experiments, with three fields per experiment (N=6, *p<0.05). Scale bar = 30 μm. B) Mitosox staining assay in AGS9 vs. CTR fibroblasts (left) and relative quantification (right). Nuclei are stained with DAPI (blue) and mitochondria are labelled in red. Data are expressed as mean ± SEM of two independent experiments, with three fields per experiment (N=6, ****p<0.0001). Scale bar = 30 μm.

7.10.2 Nascent protein synthesis is decreased in AGS9 cells

TEM results revealed a lack of ribosomes in nuclei of AGS9-derived fibroblasts. As ribosomes are essential for protein synthesis (158), their damage or decrease could impact nascent protein synthesis. Therefore, nascent protein synthesis in AGS9 and CTR fibroblasts has been assessed via Click-iT Metabolic Labeling Reagents for Proteins which enables the tagging of novel proteins with an azide-containing biomolecule (L-azidohomoalanine). Results report a decrease in nascent protein production in AGS9 fibroblasts, confirming an alteration in this process (Figure 47).

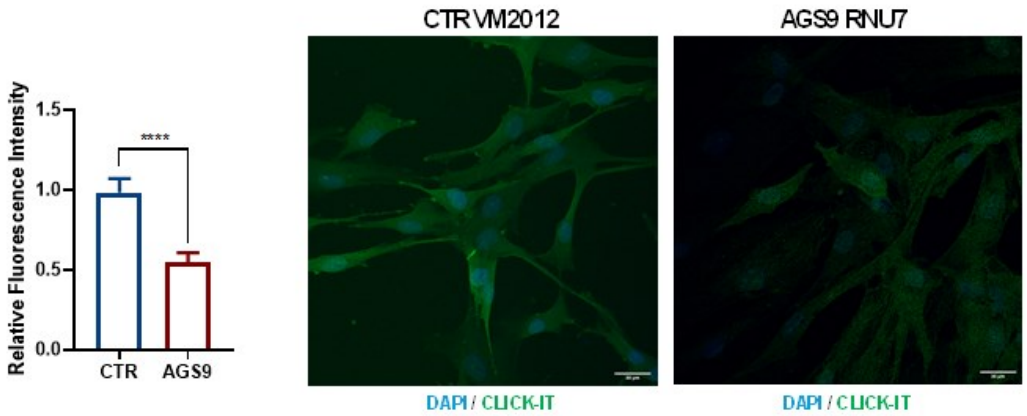

Figure 47. Decreased protein synthesis in AGS9 cells. Click-iT staining assay in AGS9 vs. CTR fibroblasts (right) and relative quantification (left). Nuclei are stained with DAPI (blue) and nascent proteins are labelled in green. Data are expressed as mean ± SEM of two in-dependent experiments, with three fields per experiment (N=6, *p<0.05). Scale bar = 30 μm.

8. DISCUSSION

Aicardi-Goutières syndrome (AGS) is a rare pediatric-onset disorder that usually occurs during the first 3 years of life. AGS is characterized by a progressive encephalopathy related to motor impairment and alteration of normal neurodevelopment (64). This condition is classified as a type 1 interferonopathy because of the increased alpha interferon (IFNα) production in CSF and blood of more than 85% of affected individuals (7). AGS presents a hereditary component and it is currently associated with mutations in 9 genes (*TREX1, RNASEH2A, RNASEH2B, RNASEH2C, SAMHD1, ADAR1, IFIH1, LSM11* and *RNU7-1*), all coding for proteins or transcripts involved in nucleic acids (NAs) metabolism and signaling (11,32). Mutations in one of these genes indeed compromise the ability of the organism to discriminate endogenous from exogenous NAs, triggering an aberrant immune response that results in elevated production and release of IFNα (13,14). Amongst the 9 commonly mutated genes underlying AGS, the least frequently mutated gene is *RNU7-1* (AGS9), that is indeed responsible of less than 1% of AGS cases (2,190). This gene encodes for the U7 small nuclear RNA (U7 snRNA) which is an essential component of the U7 small nuclear ribonucleoprotein (U7 snRNP) complex. U7 snRNP mediates replication-dependent histone (RDH) pre-mRNA processing (91,92).

During the last two decades, multiple studies documented the role of IFNα dependent immune response in multiple inflammatory disorders, including AGS (29,41,58). Specifically, it has been discovered the relationship between this disease and the interferon signature (IS), described as the chronic upregulation of multiple interferon-stimulated genes (ISGs) (11). Many specific molecular pathways involved in AGS pathogenesis have also been identified for most of the genes related to this disorder (63,69,80,153). However, no study has already focused on the pathogenic role of *RNU7-1* (AGS9) in AGS, thus making this gene the least characterized one in this disease.

For these reasons, this work aimed to dissect the role of *RNU7-1* in AGS pathogenesis by exploiting dermal fibroblasts derived from an AGS patient carrying a pathological variant of *RNU7-1* and comparing them to fibroblasts derived from a healthy control subject matched by age and sex with the patient. Specifically, this work highlighted multiple common molecular mechanisms of AGS, such as the increased production of IFNα and the activation of ISGs, but also identifying novel pathways uniquely related to *RNU7-1* through innovative approaches such as RNA-sequencing.

As AGS is a rare condition that affects infants as early as birth, sample recruitment is a limiting factor in the research of this disease and especially in the molecular factors underlying its genesis. We first obtained fibroblasts from a skin biopsy of the AGS patient carrying a mutation in *RNU7-1* and a healthy control matched by age and sex. Through FACS analysis, we characterized these cells using CD45, CD31, CD90 and EpCAM as specific markers, confirming that the isolated lines are purely composed of fibroblasts without any other cell contamination.

Before working with a new primary cell line, it is always important to verify their vitality and overall metabolic activity.

MTT assay was conducted at different times (24 hours, 48 hours, 72 hours) to test cell metabolic activity consequently to *RNU7-1* mutation and it revealed a reduced metabolic activity of fibroblasts derived from the AGS patient compared to CTR.

Through whole exosome sequencing we identified two homozygous transitions in the *RNU7-1* gene of the enrolled AGS-affected patient (n.23T>G and n.54G>C) and predicted the folding structure of the transcript derived from the mutated gene with the one obtained from the wild-type (WT) one. Results revealed some differences between the WT transcript and the mutated one.

As altered RNA morphology could affect both the expression and the localization of U7 snRNA, a standard Real-Time qPCR analysis and a nuclear-cytoplasmic mRNA quantification have been conducted on dermal fibroblasts, revealing an altered localization of U7 snRNA in AGS9 condition that could potentially affect its biological activity.

Since all the 9 AGS genes are involved in metabolism and nucleic acids uptake (15), we investigated if the variant of *RNU7-1* could affect the expression of the rest of AGS genes. Real-Time qPCR conducted on AGS genes highlighted a significative increase of *LSM11, ADAR p150, ADAR p110* and total *ADAR1*, thus confirming the strong relationship between *RNU7-1* and *LSM11* as they both encode for components of the U7 snRNP complex and the role of ADAR family components in cooperating with during the pre-mRNA processing (148).

As previously mentioned, AGS is a disease classified as interferonopathy (1) and interferon plays a crucial role in its pathogenesis (137). For this reason, we analyzed IFNα levels and its signature. In AGS, interferon is produced due to deficits in nucleic acid recognition, editing or breakdown pathways, which activate a series of processes that establish inflammation and trigger IFNα production, which in turn activates transcription of ISGs (59). IFNα and ISGs expression levels were then investigated in fibroblasts, and results reported the overexpression of both IFNα and multiple ISGs in AGS9 condition. Basing on these results, we also determined an important parameter of AGS, the interferon score in fibroblast cells and in a whole blood sample of the AGS patient and the CTR. The interferon score defines the level of dysregulation of IFN, and it can be analyzed to test the effectiveness of a therapy or to monitor the state of the disorder (9). The analysis confirms the increased transcription of the ISGs in AGS9 in both fibroblasts and whole blood. Altogether, this data validates the importance of the "interferon signature" and the role of IFNα in AGS pathogenesis.

Next, we wanted to test hydroxychloroquine (HCQ), a drug currently employed in treatment of multiple inflammatory disorders (129), as potential therapeutic treatment to decrease IFN signature. We demonstrated that HCQ treatment in AGS9 fibroblasts positively reduced their interferon signature and overall interferon production. Moreover, our results show that this drug also restore cell viability in AGS9 fibroblasts.

In the following part of the study, we focused on the study of the molecular pathways involved in production of IFNα. Since recent research hypothesized the involvement of the cGAS-STING signaling cascade in IFNα production in AGS (150,151), we focused on the investigation of this pathway in AGS9 fibroblasts.

Our Real-Time qPCR and immunochemistry data confirmed the upregulation of *cGAS, STING* and *TBK1*, all players involved in the cGAS-STING pathway.

We then investigated the effects of pathologic variations in *RNU7-1* on U7 snRNP related genes. As previously mentioned, *RNU7-1* encodes for the U7 snRNA that, together with LSM10 and LSM11 composes U7 snRNP (89). Other important factors for U7 snRNP functioning are ZFP100 (also called ZNF473) and SLBP, two proteins that allow U7 snRNP to carry out its biological activities (90). Real-Time qPCR results demonstrate an increased expression of *LSM11* and *ZFP100* in AGS9 fibroblasts. To better understand these data, the IntAct Molecular Interaction Database (IMID) was used, and it pointed out the physical interaction between U7 snRNA and ZFP100. To verify whether variations *RNU7-1* could affect the binding between U7 snRNA and ZP100, an RNA immunoprecipitation (RIP) was conducted, and results highlighted the decreased physical association between U7 snRNA and ZFP100 in AGS9 condition. Thus, indicating that the previously discussed misfolding of U7 snRNA could affect its ability to bind ZFP100.

One of the aims of this thesis work was to identify novel pathologic pathways potentially involved in AGS9 pathogenesis, so we conducted an RNA-sequencing (RNAseq) analysis on fibroblasts obtained from either the AGS9 patient or the matched control. This analysis provided a comprehensive view of the transcriptomic differences between AGS9 and control cells. In addition, RNAseq was useful for the identification of differentially expressed genes (DEGs), their categorization into various biotypes, and offered insights into the molecular processes affected by the *RNU7-1* variant. The enrichment of pathways related to neuron function and interferon signaling further emphasized the role of aberrant neurologic pathways in AGS pathogenesis and validated fibroblasts as a good *in vitro* model for the study of this disorder. RNAseq also confirmed the upregulation of multiple ISGs, giving even more credit to our preliminary data. Interestingly, transcriptional changes in AGS9 cells were related to chromatin structural components. Specifically, it was highlighted that genes involved in histone post-translational modifications were strongly affected.

Keeping in mind RNAseq results, we investigated the impact of *RNU7-1* pathologic variations on histone transcription and translation. It is known that U7 snRNP mediates replication-dependent histone (RDH) pre-mRNA processing (13). Mature RDH transcripts indeed are not polyadenylated at the 3′ end, terminating instead with a stem-loop structure (87). This unique 3′ end is formed by a U7-dependent endonucleolytic cleavage of the pre-mRNAs between the stem-loop and a purine-rich sequence called histone downstream element (HDE) (88, 153). Through Real-Time qPCR conducted with primers that span the endonucleolytic cleavage site between the stem-loop site and HDE, we determined the presence of misprocessed RDH transcripts that still present the poly-A in AGS9 cells. On the other hand, expression of replication-independent histones (RIH) mRNAs (which are normally polyadenylated and do not require the U7 snRNP functioning) and total histone expression were the same in AGS9 and CTR cells, suggesting a normal transcription of RDH genes and an aberrant maturation of their transcripts that could have consequences in term of histone translation. WB and immunocytochemistry analysis were then performed to investigate whether aberrant RDH maturation affects histone translation, revealing a significant decrease of histone protein expression in AGS9 condition.

As histone expression could affect chromatin folding and expression (154), transmission electron microscopy (TEM) analysis was performed to visualize overall chromatin content in AGS9 and CTR fibroblasts. TEM results revealed a lack of chromatin in AGS9 nuclei, confirming previously reported RNAseq results.

Since TEM analysis also revealed smaller mitochondria and reduced localization of ribosomes on ER membranes in AGS9 cells, we started to investigate the potential role of this organelles in this disorder. Several studies have already demonstrated the potential involvement of mitochondrial dysfunctions in AGS, with a close correlation between altered mitochondrial metabolism, increased production of reactive oxygen species (ROS), and the induction of an aberrant IFNα-dependent immune response in AGS (105,106,108). For this reason, Mitotracker and Mitosox staining assays were carried out, and results demonstrated a reduced basal metabolic activity together with an increase production of ROS in AGS9 condition. Lastly, Click-iT Metabolic assay was conducted to assess if the reported lack of ribosomes in ER of AGS9 cells could affect overall nascent protein synthesis. Results revealed a decrease in nascent protein production in AGS9 fibroblasts, confirming an alteration in this mechanism that could be involved in pathogenesis of this disease.

In conclusion, this study confirms the key role of IFN-signaling in AGS pathogenesis, and it also proposes novel mechanisms related to *RNU7-1* variations, including mitochondrial and histone dysfunctions.

9. REFERENCES

1. Crow YJ, Manel N. Aicardi–Goutières syndrome and the type I interferonopathies. Nat Rev Immunol. 2015 Jul;15(7):429–40.

2. Kroner BL, Preiss LR, Ardini MA, Gaillard WD. New Incidence, Prevalence, and Survival of Aicardi Syndrome From 408 Cases. J Child Neurol. 2008 May;23(5):531–5.

3. Zubairi MS, Carter RF, Ronen GM. A Male Phenotype With Aicardi Syndrome. J Child Neurol. 2009 Feb;24(2):204–7.

4. Shetty J, Fraser J, Goudie D, Kirkpatrick M. Aicardi syndrome in a 47 XXY male – A variable developmental phenotype? European Journal of Paediatric Neurology. 2014 Jul;18(4):529–31.

5. Stephenson JBP. Aicardi–Goutières syndrome (AGS). European Journal of Paediatric Neurology. 2008 Sep;12(5):355–8.

6. Tolmie JL, Shillito P, Hughes-Benzie R, Stephenson JB. The Aicardi-Goutieres syndrome (familial, early onset encephalopathy with calcifications of the basal ganglia and chronic cerebrospinal fluid lymphocytosis). Journal of Medical Genetics. 1995 Nov 1;32(11):881–4.

7. Crow YJ, Chase DS, Lowenstein Schmidt J, Szynkiewicz M, Forte GMA, Gornall HL, et al. Characterization of human disease phenotypes associated with mutations in *TREX1* , *RNASEH2A* , *RNASEH2B* , *RNASEH2C* , *SAMHD1* , *ADAR* , and *IFIH1*. American J of Med Genetics Pt A. 2015 Feb;167(2):296–312.

8. Aicardi J, Goutières F. A Progressive familial encephalopathy in infancy with calcifications of the basal ganglia and chronic cerebrospinal fluid lymphocytosis. Annals of Neurology. 1984 Jan;15(1):49–54.

9. Ashrafi MR, Amanat M, Garshasbi M, Kameli R, Nilipour Y, Heidari M, et al. An update on clinical, pathological, diagnostic, and therapeutic perspectives of childhood leukodystrophies. Expert Rev Neurother. 2020 Jan;20(1):65–84.

10. Orcesi S, La Piana R, Fazzi E. Aicardi-Goutieres syndrome. British Medical Bulletin. 2008 Nov 13;89(1):183–201.

11. Garau J, Cavallera V, Valente M, Tonduti D, Sproviero D, Zucca S, et al. Molecular Genetics and Interferon Signature in the Italian Aicardi Goutières Syndrome Cohort: Report of 12 New Cases and Literature Review. JCM. 2019 May 26;8(5):750.

12. Liu A, Ying S. AICARDI–GOUTIÈRES syndrome: A monogenic type I interferonopathy. Scand J Immunol. 2023 Oct;98(4):e13314.

13. Crow YJ, Jackson AP, Roberts E, Van Beusekom E, Barth P, Corry P, et al. Aicardi-Goutières Syndrome Displays Genetic Heterogeneity with One Locus (AGS1) on Chromosome 3p21. The American Journal of Human Genetics. 2000 Jul;67(1):213–21.

14. Uggenti C, Lepelley A, Depp M, Badrock AP, Rodero MP, El-Daher MT, et al. cGAS-mediated induction of type I interferon due to inborn errors of histone pre-mRNA processing. Nat Genet. 2020 Dec;52(12):1364–72.

15. Crow YJ. Aicardi-Goutières Syndrome. In: Adam MP, Feldman J, Mirzaa GM, Pagon RA, Wallace SE, Bean LJ, et al., editors. GeneReviews® [Internet]. Seattle (WA): University of Washington, Seattle; 1993 [cited 2024 Apr 27]. Available from: http://www.ncbi.nlm.nih.gov/books/NBK1475/

16. Rice G, Patrick T, Parmar R, Taylor CF, Aeby A, Aicardi J, et al. Clinical and Molecular Phenotype of Aicardi-Goutières Syndrome. The American Journal of Human Genetics. 2007 Oct;81(4):713–25.

17. Crow YJ, Livingston JH. Aicardi-Goutières syndrome: an important Mendelian mimic of congenital infection. Develop Med Child Neuro. 2008 Jun;50(6):410–6.

18. Garrec ML, Doret M, Pasquier JC, Till M, Lebon P, Buenerd A, et al. Prenatal diagnosis of Aicardi-Goutières syndrome: PRENATAL DIAGNOSIS OF AICARDI-GOUTIERES SYNDROME. Prenat Diagn. 2005 Jan;25(1):28–30.

19. Pomar L, Ochoa J, Cabet S, Huisman TAGM, Paladini D, Klaritsch P, et al. Prenatal diagnosis of Aicardi syndrome based on a suggestive imaging pattern: A multicenter case-series. Prenatal Diagnosis. 2022 Apr;42(4):484–94.

20. Bourgon N, Lefebvre M, Kuentz P, Thevenon J, Jouan T, Duffourd Y, et al. Prenatal presentation of Aicardi-Goutières syndrome: Nonspecific phenotype necessitates exome sequencing for definitive diagnosis. Prenatal Diagnosis. 2019 Aug;39(9):806–10.

21. Goutières F. Aicardi–Goutières syndrome. Brain and Development. 2005 Apr;27(3):201–6.

22. Cerebral Calcification International Study Group, Tonduti D, Panteghini C, Pichiecchio A, Decio A, Carecchio M, et al. Encephalopathies with intracranial calcification in children: clinical and genetic characterization. Orphanet J Rare Dis. 2018 Dec;13(1):135.

23. De Barcelos IP, Woidill S, Gavazzi F, Modesti NB, Sevagamoorthy A, Vanderver A, et al. Systematic analysis of genotype-phenotype variability in siblings with Aicardi Goutières Syndrome (AGS). Molecular Genetics and Metabolism. 2024 May;142(1):108346.

24. Świerczyńska M, Tronina A, Filipek E. Aicardi–Goutières Syndrome with Congenital Glaucoma Caused by Novel TREX1 Mutation. JPM. 2023 Nov 15;13(11):1609.

25. Zhang L, Hu XZ, Li H, Li X, Smerin S, Benedek DM, et al. Startle response related genes. Medical Hypotheses. 2011 Oct;77(4):685–91.

26. Abdel-Salam GMH, El-Kamah GY, Rice GI, EL-Darouti M, Gornall H, Szynkiewicz M, et al. Chilblains as a Diagnostic Sign of Aicardi-Goutières Syndrome. Neuropediatrics. 2010 Feb;41(01):18–23.

27. Wong BKY, Sutton VR. Aicardi syndrome, an unsolved mystery: Review of diagnostic features, previous attempts, and future opportunities for genetic examination. Am J Med Genet. 2018 Dec 10;ajmg.c.31658.

28. Sutton VR, Van den Veyver IB. Aicardi Syndrome. In: Adam MP, Feldman J, Mirzaa GM, Pagon RA, Wallace SE, Bean LJ, et al., editors. GeneReviews® [Internet]. Seattle (WA): University of Washington, Seattle; 1993 [cited 2024 Jul 26]. Available from: http://www.ncbi.nlm.nih.gov/books/NBK1381/

29. Rice GI, Forte GMA, Szynkiewicz M, Chase DS, Aeby A, Abdel-Hamid MS, et al. Assessment of interferon-related biomarkers in Aicardi-Goutières syndrome associated with mutations in TREX1, RNASEH2A, RNASEH2B, RNASEH2C, SAMHD1, and ADAR: a case-control study. The Lancet Neurology. 2013 Dec;12(12):1159–69.

30. Livingston JH, Stivaros S, Warren D, Crow YJ. Intracranial calcification in childhood: a review of aetiologies and recognizable phenotypes. Dev Med Child Neurol. 2014 Jul;56(7):612–26.

31. La Piana R, Uggetti C, Roncarolo F, Vanderver A, Olivieri I, Tonduti D, et al. Neuroradiologic patterns and novel imaging findings in Aicardi-Goutières syndrome. Neurology. 2016 Jan 5;86(1):28–35.

32. Lanzi G, D'Arrigo S, Drumbl G, Uggetti C, Fazzi E. Aicardi-Goutières syndrome: differential diagnosis and aetiopathogenesis. Funct Neurol. 2003;18(2):71–5.

33. Govil-Dalela T, Kumar A, Agarwal R, Chugani HT. Agenesis of the Corpus Callosum and Aicardi Syndrome: A Neuroimaging and Clinical Comparison. Pediatr Neurol. 2017 Mar;68:44-48.e2.

34. Tumani H, Huss A, Bachhuber F. The cerebrospinal fluid and barriers - anatomic and physiologic considerations. Handb Clin Neurol. 2017;146:21–32.

35. van Heteren JT, Rozenberg F, Aronica E, Troost D, Lebon P, Kuijpers TW. Astrocytes produce interferon-alpha and CXCL10, but not IL-6 or CXCL8, in Aicardi-Goutières syndrome. Glia. 2008 Apr;56(5):568–78.

36. Blau N, Bonafé L, Krägeloh-Mann I, Thöny B, Kierat L, Häusler M, et al. Cerebrospinal fluid pterins and folates in Aicardi-Goutières syndrome: a new phenotype. Neurology. 2003 Sep 9;61(5):642–7.

37. Murr C, Widner B, Wirleitner B, Fuchs D. Neopterin as a marker for immune system activation. Curr Drug Metab. 2002 Apr;3(2):175–87.

38. Michalak Ł, Bulska M, Strząbała K, Szcześniak P. Neopterin as a marker of cellular immunological response. Postepy Hig Med Dosw (Online). 2017 Aug 24;71(1):727–36.

39. Han VX, Mohammad SS, Jones HF, Bandodkar S, Crow YJ, Dale RC, et al. Cerebrospinal fluid neopterin as a biomarker of treatment response to Janus kinase inhibition in Aicardi-Goutières syndrome. Dev Med Child Neurol. 2022 Feb;64(2):266–71.

40. Rönnblom L, Eloranta ML. The interferon signature in autoimmune diseases. Curr Opin Rheumatol. 2013 Mar;25(2):248–53.

41. Higgs BW, Liu Z, White B, Zhu W, White WI, Morehouse C, et al. Patients with systemic lupus erythematosus, myositis, rheumatoid arthritis and scleroderma share activation of a common type I interferon pathway. Ann Rheum Dis. 2011 Nov;70(11):2029–36.

42. Schoggins JW. Interferon-Stimulated Genes: What Do They All Do? Annu Rev Virol. 2019 Sep 29;6(1):567–84.

43. Ma J, Zhao F, Su W, Li Q, Li J, Ji J, et al. Zinc finger and interferon-stimulated genes play a vital role in TB-IRIS following HAART in AIDS. Per Med. 2018 Jul 1;15(4):251–69.

44. Negishi H, Taniguchi T, Yanai H. The Interferon (IFN) Class of Cytokines and the IFN Regulatory Factor (IRF) Transcription Factor Family. Cold Spring Harb Perspect Biol. 2018 Nov 1;10(11):a028423.

45. Isaacs A, Lindenmann J. Virus interference. I. The interferon. Proc R Soc Lond B Biol Sci. 1957 Sep 12;147(927):258–67.

46. Baron S, Tyring SK, Fleischmann WR, Coppenhaver DH, Niesel DW, Klimpel GR, et al. The interferons. Mechanisms of action and clinical applications. JAMA. 1991 Sep 11;266(10):1375–83.

47. Belardelli F, Gresser I. The neglected role of type I interferon in the T-cell response: implications for its clinical use. Immunol Today. 1996 Aug;17(8):369–72.

48. Manry J, Laval G, Patin E, Fornarino S, Itan Y, Fumagalli M, et al. Evolutionary genetic dissection of human interferons. J Exp Med. 2011 Dec 19;208(13):2747–59.

49. Swiecki M, Colonna M. Type I interferons: diversity of sources, production pathways and effects on immune responses. Curr Opin Virol. 2011 Dec;1(6):463–75.

50. Niewold TB, Clark DN, Salloum R, Poole BD. Interferon Alpha in Systemic Lupus Erythematosus. Journal of Biomedicine and Biotechnology. 2010;2010:1–8.

51. Akiyama H, Ikeda K, Katoh M, McGeer EG, McGeer PL. Expression of MRP14, 27E10, interferon-alpha and leukocyte common antigen by reactive microglia in postmortem human brain tissue. J Neuroimmunol. 1994 Mar;50(2):195–201.

52. Lieberman AP, Pitha PM, Shin HS, Shin ML. Production of tumor necrosis factor and other cytokines by astrocytes stimulated with lipopolysaccharide or a neurotropic virus. Proc Natl Acad Sci U S A. 1989 Aug;86(16):6348–52.

53. Akwa Y, Hassett DE, Eloranta ML, Sandberg K, Masliah E, Powell H, et al. Transgenic expression of IFN-alpha in the central nervous system of mice protects against lethal neurotropic viral infection but induces inflammation and neurodegeneration. J Immunol. 1998 Nov 1;161(9):5016–26.

54. Motwani M, Pesiridis S, Fitzgerald KA. DNA sensing by the cGAS-STING pathway in health and disease. Nat Rev Genet. 2019 Nov;20(11):657–74.

55. Mankan AK, Schmidt T, Chauhan D, Goldeck M, Höning K, Gaidt M, et al. Cytosolic RNA:DNA hybrids activate the cGAS-STING axis. EMBO J. 2014 Dec 17;33(24):2937–46.

56. Sun L, Wu J, Du F, Chen X, Chen ZJ. Cyclic GMP-AMP synthase is a cytosolic DNA sensor that activates the type I interferon pathway. Science. 2013 Feb 15;339(6121):786–91.

57. Dobbs N, Burnaevskiy N, Chen D, Gonugunta VK, Alto NM, Yan N. STING Activation by Translocation from the ER Is Associated with Infection and Autoinflammatory Disease. Cell Host Microbe. 2015 Aug 12;18(2):157–68.

58. d'Angelo DM, Di Filippo P, Breda L, Chiarelli F. Type I Interferonopathies in Children: An Overview. Front Pediatr. 2021;9:631329.

59. Schneider WM, Chevillotte MD, Rice CM. Interferon-stimulated genes: a complex web of host defenses. Annu Rev Immunol. 2014;32:513–45.

60. Fryer AL, Abdullah A, Taylor JM, Crack PJ. The Complexity of the cGAS-STING Pathway in CNS Pathologies. Front Neurosci. 2021;15:621501.

61. Crow YJ, Hayward BE, Parmar R, Robins P, Leitch A, Ali M, et al. Mutations in the gene encoding the 3'-5' DNA exonuclease TREX1 cause Aicardi-Goutières syndrome at the AGS1 locus. Nat Genet. 2006 Aug;38(8):917–20.

62. Richards A, van den Maagdenberg AMJM, Jen JC, Kavanagh D, Bertram P, Spitzer D, et al. C-terminal truncations in human 3'-5' DNA exonuclease TREX1 cause autosomal dominant retinal vasculopathy with cerebral leukodystrophy. Nat Genet. 2007 Sep;39(9):1068–70.

63. Yan N. Immune Diseases Associated with TREX1 and STING Dysfunction. Journal of Interferon & Cytokine Research. 2017 May;37(5):198–206.

64. Rice G, Newman WG, Dean J, Patrick T, Parmar R, Flintoff K, et al. Heterozygous Mutations in TREX1 Cause Familial Chilblain Lupus and Dominant Aicardi-Goutières Syndrome. The American Journal of Human Genetics. 2007 Apr;80(4):811–5.

65. Ali M. A second locus for Aicardi-Goutieres syndrome at chromosome 13q14-21. Journal of Medical Genetics. 2005 Sep 9;43(5):444–50.

66. Crow YJ, Leitch A, Hayward BE, Garner A, Parmar R, Griffith E, et al. Mutations in genes encoding ribonuclease H2 subunits cause Aicardi-Goutières syndrome and mimic congenital viral brain infection. Nat Genet. 2006 Aug;38(8):910–6.

67. Hiller B, Achleitner M, Glage S, Naumann R, Behrendt R, Roers A. Mammalian RNase H2 removes ribonucleotides from DNA to maintain genome integrity. Journal of Experimental Medicine. 2012 Jul 30;209(8):1419–26.

68. Sase S, Takanohashi A, Vanderver A, Almad A. Astrocytes, an active player in Aicardi-Goutières syndrome. Brain Pathol. 2018 May;28(3):399–407.

69. Rice GI, Bond J, Asipu A, Brunette RL, Manfield IW, Carr IM, et al. Mutations involved in Aicardi-Goutières syndrome implicate SAMHD1 as regulator of the innate immune response. Nat Genet. 2009 Jul;41(7):829–32.

70. Ahn J. Functional organization of human SAMHD1 and mechanisms of HIV-1 restriction. Biological Chemistry. 2016 Apr 1;397(4):373–9.

71. Hansen EC, Seamon KJ, Cravens SL, Stivers JT. GTP activator and dNTP substrates of HIV-1 restriction factor SAMHD1 generate a long-lived activated state. Proc Natl Acad Sci USA [Internet]. 2014 May 6 [cited 2024 Jul 30];111(18). Available from: https://pnas.org/doi/full/10.1073/pnas.1401706111

72. Calonge E, Bermejo M, Diez-Fuertes F, Mangeot I, González N, Coiras M, et al. Different Expression of Interferon-Stimulated Genes in Response to HIV-1 Infection in Dendritic Cells Based on Their Maturation State. J Virol. 2017 Apr 15;91(8):e01379-16.

73. Li M, Zhang D, Zhu M, Shen Y, Wei W, Ying S, et al. Roles of SAMHD1 in antiviral defense, autoimmunity and cancer. Reviews in Medical Virology. 2017 Jul;27(4):e1931.

74. Lengyel P, Speyer JF, Ochoa S. Synthetic polynucleotides and the amino acid code. Proc Natl Acad Sci U S A. 1961 Dec 15;47(12):1936–42.

75. Savva YA, Rieder LE, Reenan RA. The ADAR protein family. Genome Biol. 2012 Dec 28;13(12):252.

76. Chen CX, Cho DSC, Wang Q, Lai F, Carter KC, Nishikura K. A third member of the RNA-specific adenosine deaminase gene family, ADAR3, contains both single- and double-stranded RNA binding domains. RNA. 2000 May;6(5):755–67.

77. Nakahama T, Kawahara Y. The RNA-editing enzyme ADAR1: a regulatory hub that tunes multiple dsRNA-sensing pathways. Int Immunol. 2023 Mar 14;35(3):123–33.

78. Bahn JH, Ahn J, Lin X, Zhang Q, Lee JH, Civelek M, et al. Genomic analysis of ADAR1 binding and its involvement in multiple RNA processing pathways. Nat Commun. 2015 Mar 9;6(1):6355.

79. Zhang D, Zhu L, Gao Y, Wang Y, Li P. RNA editing enzymes: structure, biological functions and applications. Cell Biosci. 2024 Mar 16;14(1):34.

80. Guo X, Wiley CA, Steinman RA, Sheng Y, Ji B, Wang J, et al. Aicardi-Goutières syndrome-associated mutation at ADAR1 gene locus activates innate immune response in mouse brain. J Neuroinflammation. 2021 Jul 31;18(1):169.

81. Bazak L, Haviv A, Barak M, Jacob-Hirsch J, Deng P, Zhang R, et al. A-to-I RNA editing occurs at over a hundred million genomic sites, located in a majority of human genes. Genome Res. 2014 Mar;24(3):365–76.

82. Rice GI, Del Toro Duany Y, Jenkinson EM, Forte GM, Anderson BH, Ariaudo G, et al. Gain-of-function mutations in IFIH1 cause a spectrum of human disease phenotypes associated with upregulated type I interferon signaling. Nat Genet. 2014 May;46(5):503–9.

83. Barrat FJ, Elkon KB, Fitzgerald KA. Importance of Nucleic Acid Recognition in Inflammation and Autoimmunity. Annu Rev Med. 2016 Jan 14;67(1):323–36.

84. Dias Junior AG, Sampaio NG, Rehwinkel J. A Balancing Act: MDA5 in Antiviral Immunity and Autoinflammation. Trends in Microbiology. 2019 Jan;27(1):75–85.

85. Oda H, Nakagawa K, Abe J, Awaya T, Funabiki M, Hijikata A, et al. Aicardi-Goutières Syndrome Is Caused by IFIH1 Mutations. The American Journal of Human Genetics. 2014 Jul;95(1):121–5.

86. Sharma A, Kontodimas K, Bosmann M. The MAVS Immune Recognition Pathway in Viral Infection and Sepsis. Antioxidants & Redox Signaling. 2021 Dec 1;35(16):1376–92.

87. Al Mutairi F, Alfadhel M, Nashabat M, El-Hattab AW, Ben-Omran T, Hertecant J, et al. Phenotypic and Molecular Spectrum of Aicardi-Goutières Syndrome: A Study of 24 Patients. Pediatric Neurology. 2018 Jan;78:35–40.

88. Gadgil A, Raczyńska KD. U7 snRNA: A tool for gene therapy. J Gene Med. 2021 Apr;23(4):e3321.

89. Ryu I, Kim YK. AU-rich element–mediated mRNA decay via the butyrate response factor 1 controls cellular levels of polyadenylated replication-dependent histone mRNAs. Journal of Biological Chemistry. 2019 May;294(19):7558–65.

90. Marzluff WF, Wagner EJ, Duronio RJ. Metabolism and regulation of canonical histone mRNAs: life without a poly(A) tail. Nat Rev Genet. 2008 Nov;9(11):843–54.

91. Naesens L, Nemegeer J, Roelens F, Vallaeys L, Meuwissen M, Janssens K, et al. Mutations in RNU7-1 Weaken Secondary RNA Structure, Induce MCP-1 and CXCL10 in CSF, and Result in Aicardi-Goutières Syndrome with Severe End-Organ Involvement. J Clin Immunol. 2022 Jul;42(5):962–74.

92. Ideue T, Adachi S, Naganuma T, Tanigawa A, Natsume T, Hirose T. U7 small nuclear ribonucleoprotein represses histone gene transcription in cell cycle-arrested cells. Proc Natl Acad Sci USA. 2012 Apr 10;109(15):5693–8.

93. Stark GR, Kerr IM, Williams BRG, Silverman RH, Schreiber RD. HOW CELLS RESPOND TO INTERFERONS. Annu Rev Biochem. 1998 Jun;67(1):227–64.

94. Stetson DB, Medzhitov R. Type I Interferons in Host Defense. Immunity. 2006 Sep;25(3):373–81.

95. Rigby RE, Webb LM, Mackenzie KJ, Li Y, Leitch A, Reijns MAM, et al. RNA:DNA hybrids are a novel molecular pattern sensed by TLR9. The EMBO Journal. 2014 Mar 18;33(6):542–58.

96. Stein H, Hausen P. Enzyme from Calf Thymus Degrading the RNA Moiety of DNA-RNA Hybrids: Effect on DNA-Dependent RNA Polymerase. Science. 1969 Oct 17;166(3903):393–5.

97. Dominski Z, Erkmann JA, Yang X, Sànchez R, Marzluff WF. A novel zinc finger protein is associated with U7 snRNP and interacts with the stem–loop binding protein in the histone pre-mRNP to stimulate 3′-end processing. Genes Dev. 2002 Jan 1;16(1):58–71.

98. Tisdale S, Van Alstyne M, Simon CM, Mentis GZ, Pellizzoni L. SMN controls neuromuscular junction integrity through U7 snRNP. Cell Reports. 2022 Sep;40(12):111393.

99. Meister G, Bühler D, Pillai R, Lottspeich F, Fischer U. A multiprotein complex mediates the ATP-dependent assembly of spliceosomal U snRNPs. Nat Cell Biol. 2001 Nov;3(11):945–9.

100. Al Amir Dache Z, Thierry AR. Mitochondria-derived cell-to-cell communication. Cell Rep. 2023 Jul 25;42(7):112728.

101. Andrieux P, Chevillard C, Cunha-Neto E, Nunes JPS. Mitochondria as a Cellular Hub in Infection and Inflammation. IJMS. 2021 Oct 20;22(21):11338.

102. Anesti V, Scorrano L. The relationship between mitochondrial shape and function and the cytoskeleton. Biochim Biophys Acta. 2006;1757(5–6):692–9.

103. Annesley SJ, Fisher PR. Mitochondria in Health and Disease. Cells. 2019 Jul 5;8(7):680.

104. Frey TG, Mannella CA. The internal structure of mitochondria. Trends Biochem Sci. 2000 Jul;25(7):319–24.

105. Bai J, Liu F. The cGAS-cGAMP-STING Pathway: A Molecular Link Between Immunity and Metabolism. Diabetes. 2019 Jun 1;68(6):1099–108.

106. Chen R, Du J, Zhu H, Ling Q. The role of cGAS-STING signalling in liver diseases. JHEP Rep. 2021 Oct;3(5):100324.

107. Fang C, Wei X, Wei Y. Mitochondrial DNA in the regulation of innate immune responses. Protein Cell. 2016 Jan;7(1):11–6.

108. Gambardella S, Limanaqi F, Ferese R, Biagioni F, Campopiano R, Centonze D, et al. ccf-mtDNA as a Potential Link Between the Brain and Immune System in Neuro-Immunological Disorders. Front Immunol. 2019;10:1064.

109. Gao D, Li T, Li XD, Chen X, Li QZ, Wight-Carter M, et al. Activation of cyclic GMP-AMP synthase by self-DNA causes autoimmune diseases. Proc Natl Acad Sci USA [Internet]. 2015 Oct 20 [cited 2024 Aug 8];112(42). Available from: https://pnas.org/doi/full/10.1073/pnas.1516465112

110. Riley JS, Tait SW. Mitochondrial DNA in inflammation and immunity. EMBO Rep. 2020 Apr 3;21(4):e49799.

111. Dragoni F, Garau J, Sproviero D, Orcesi S, Varesio C, De Siervi S, et al. Characterization of Mitochondrial Alterations in Aicardi–Goutières Patients Mutated in RNASEH2A and RNASEH2B Genes. IJMS. 2022 Nov 21;23(22):14482.

112. Sena LA, Chandel NS. Physiological Roles of Mitochondrial Reactive Oxygen Species. Molecular Cell. 2012 Oct;48(2):158–67.

113. Domingues C, Jarak I, Veiga F, Dourado M, Figueiras A. Pediatric Drug Development: Reviewing Challenges and Opportunities by Tracking Innovative Therapies. Pharmaceutics. 2023 Oct 6;15(10):2431.

114. Crow YJ, Shetty J, Livingston JH. Treatments in Aicardi–Goutières syndrome. Develop Med Child Neuro. 2020 Jan;62(1):42–7.

115. Cordaux R, Batzer MA. The impact of retrotransposons on human genome evolution. Nat Rev Genet. 2009 Oct;10(10):691–703.

116. Rice GI, Meyzer C, Bouazza N, Hully M, Boddaert N, Semeraro M, et al. Reverse-Transcriptase Inhibitors in the Aicardi–Goutières Syndrome. N Engl J Med. 2018 Dec 6;379(23):2275–7.

117. Tonduti D, Fazzi E, Badolato R, Orcesi S. Novel and emerging treatments for Aicardi-Goutières syndrome. Expert Review of Clinical Immunology. 2020 Feb 1;16(2):189–98.

118. Briand C, Frémond ML, Bessis D, Carbasse A, Rice GI, Bondet V, et al. Efficacy of JAK1/2 inhibition in the treatment of chilblain lupus due to TREX1 deficiency. Ann Rheum Dis. 2019 Mar;78(3):431–3.

119. Zimmermann N, Wolf C, Schwenke R, Lüth A, Schmidt F, Engel K, et al. Assessment of Clinical Response to Janus Kinase Inhibition in Patients With Familial Chilblain Lupus and *TREX1* Mutation. JAMA Dermatol. 2019 Mar 1;155(3):342.

120. Rodero MP, Frémond ML, Rice GI, Neven B, Crow YJ. JAK inhibition in STING-associated interferonopathy. Ann Rheum Dis. 2016 Dec;75(12):e75.

121. Meesilpavikkai K, Dik WA, Schrijver B, Van Helden-Meeuwsen CG, Versnel MA, Van Hagen PM, et al. Efficacy of Baricitinib in the Treatment of Chilblains Associated With Aicardi-Goutières Syndrome, a Type I Interferonopathy. Arthritis & Rheumatology. 2019 May;71(5):829–31.

122. McLellan KE, Martin N, Davidson JE, Cordeiro N, Oates BD, Neven B, et al. JAK 1/2 Blockade in MDA5 Gain-of-Function. J Clin Immunol. 2018 Nov;38(8):844–6.

123. Yao Y, Higgs BW, Morehouse C, De Los Reyes M, Trigona W, Brohawn P, et al. Development of Potential Pharmacodynamic and Diagnostic Markers for Anti-IFN-α Monoclonal Antibody Trials in Systemic Lupus Erythematosus. Innocenti F, editor. Human Genomics and Proteomics [Internet]. 2009 Jan [cited 2024 Aug 9];1(1). Available from: http://www.portico.org/Portico/article?article=pgj2zb96krx

124. Baccala R, Gonzalez-Quintial R, Schreiber RD, Lawson BR, Kono DH, Theofilopoulos AN. Anti–IFN-α/β Receptor Antibody Treatment Ameliorates Disease in Lupus-Predisposed Mice. The Journal of Immunology. 2012 Dec 15;189(12):5976–84.

125. Daily JP, Minuti A, Khan N. Diagnosis, Treatment, and Prevention of Malaria in the US: A Review. JAMA. 2022 Aug 2;328(5):460.

126. Martinez GP, Zabaleta ME, Di Giulio C, Charris JE, Mijares MR. The Role of Chloroquine and Hydroxychloroquine in Immune Regulation and Diseases. CPD. 2020 Oct 16;26(35):4467–85.

127. Taherian E, Rao A, Malemud CJ, Askari AD. The Biological and Clinical Activity of Anti-Malarial Drugs In Autoimmune Disorders. CRR. 2013 Apr 1;9(1):45–62.

128. An J, Woodward JJ, Sasaki T, Minie M, Elkon KB. Cutting Edge: Antimalarial Drugs Inhibit IFN-β Production through Blockade of Cyclic GMP-AMP Synthase–DNA Interaction. The Journal of Immunology. 2015 May 1;194(9):4089–93.

129. Schrezenmeier E, Dörner T. Mechanisms of action of hydroxychloroquine and chloroquine: implications for rheumatology. Nat Rev Rheumatol. 2020 Mar;16(3):155–66.

130. van den Borne BE, Dijkmans BA, de Rooij HH, le Cessie S, Verweij CL. Chloroquine and hydroxychloroquine equally affect tumor necrosis factor-alpha, interleukin 6, and interferon-gamma production by peripheral blood mononuclear cells. J Rheumatol. 1997 Jan;24(1):55–60.

131. Jang CH, Choi JH, Byun MS, Jue DM. Chloroquine inhibits production of TNF-α, IL-1β and IL-6 from lipopolysaccharide-stimulated human monocytes/macrophages by different modes. Rheumatology. 2006 Jun 1;45(6):703–10.

132. Garau J, Sproviero D, Dragoni F, Piscianz E, Santonicola C, Tonduti D, et al. Hydroxychloroquine modulates immunological pathways activated by RNA:DNA hybrids in Aicardi–Goutières syndrome patients carrying RNASEH2 mutations. Cell Mol Immunol. 2021 Jun;18(6):1593–5.

133. Feng J, Wang X, Ye X, Ares I, Lopez-Torres B, Martínez M, et al. Mitochondria as an important target of metformin: The mechanism of action, toxic and side effects, and new therapeutic applications. Pharmacological Research. 2022 Mar;177:106114.

134. Lin H, Ao H, Guo G, Liu M. The Role and Mechanism of Metformin in Inflammatory Diseases. JIR. 2023 Nov;Volume 16:5545–64.

135. Gillespie ZE, Wang C, Vadan F, Yu TY, Ausió J, Kusalik A, et al. Metformin induces the AP-1 transcription factor network in normal dermal fibroblasts. Sci Rep. 2019 Mar 29;9(1):5369.

136. Dragoni F, Garau J, Rizzo B, Orcesi S, Varesio C, Gerlando RD, et al. Metformin reduces oxidative damage in RNASEH2-mutant Aicardi-Goutières cells [Internet]. 2024 [cited 2024 Aug 9]. Available from: https://www.authorea.com/users/803342/articles/1191201-metformin-reduces-oxidative-damage-in-rnaseh2-

mutant-aicardi-gouti%C3%A8res-cells?commit=9b869329ab99bfc2250c3a92dd261fef233499b1

137. Baechler EC, Batliwalla FM, Karypis G, Gaffney PM, Ortmann WA, Espe KJ, et al. Interferon-inducible gene expression signature in peripheral blood cells of patients with severe lupus. Proc Natl Acad Sci USA. 2003 Mar 4;100(5):2610–5.

138. Riss TL, Moravec RA, Niles AL, Duellman S, Benink HA, Worzella TJ, et al. Cell Viability Assays. In: Markossian S, Grossman A, Arkin M, Auld D, Austin C, Baell J, et al., editors. Assay Guidance Manual [Internet]. Bethesda (MD): Eli Lilly & Company and the National Center for Advancing Translational Sciences; 2004 [cited 2024 Aug 29]. Available from: http://www.ncbi.nlm.nih.gov/books/NBK144065/

139. Giannopoulou EG, Elemento O, Ivashkiv LB. Use of RNA sequencing to evaluate rheumatic disease patients. Arthritis Res Ther. 2015 Dec;17(1):167.

140. Wu T, Hu E, Xu S, Chen M, Guo P, Dai Z, et al. clusterProfiler 4.0: A universal enrichment tool for interpreting omics data. The Innovation. 2021 Aug;2(3):100141.

141. Heberle H, Meirelles GV, Da Silva FR, Telles GP, Minghim R. InteractiVenn: a web-based tool for the analysis of sets through Venn diagrams. BMC Bioinformatics. 2015 May 22;16(1):169.

142. Li Z, Zhang Y, Fang J, Xu Z, Zhang H, Mao M, et al. NcPath: a novel platform for visualization and enrichment analysis of human non-coding RNA and KEGG signaling pathways. Kendziorski C, editor. Bioinformatics. 2023 Jan 1;39(1):btac812.

143. Franzolin E, Coletta S, Ferraro P, Pontarin G, D'Aronco G, Stevanoni M, et al. SAMHD1-deficient fibroblasts from Aicardi-Goutières Syndrome patients can escape senescence and accumulate mutations. FASEB j. 2020 Jan;34(1):631–47.

144. Ferraro RM, Lanzi G, Masneri S, Barisani C, Piovani G, Savio G, et al. Generation of three iPSC lines from fibroblasts of a patient with Aicardi Goutières Syndrome mutated in TREX1. Stem Cell Research. 2019 Dec;41:101580.

145. Ho JD, Chung HJ, Ms Barron A, Ho DA, Sahni D, Browning JL, et al. Extensive CD34-to-CD90 Fibroblast Transition Defines Regions of Cutaneous Reparative, Hypertrophic, and Keloidal Scarring. The American Journal of Dermatopathology. 2019 Jan;41(1):16–28.

146. Hwang HS, Yoo JE, Han DH, Choi JS, Lee JG, Joo DJ, et al. Circulating Cancer Stem Cells Expressing EpCAM/CD90 in Hepatocellular Carcinoma: A Pilot Study for Predicting Tumor Recurrence after Living Donor Liver Transplantation. Gut and Liver. 2022 May 15;16(3):443–55.

147. Ghasemi M, Turnbull T, Sebastian S, Kempson I. The MTT Assay: Utility, Limitations, Pitfalls, and Interpretation in Bulk and Single-Cell Analysis. IJMS. 2021 Nov 26;22(23):12827.

148. Raitskin O, Cho DS, Sperling J, Nishikura K, Sperling R. RNA editing activity is associated with splicing factors in lnRNP particles: The nuclear pre-mRNA processing machinery. Proc Natl Acad Sci U S A. 2001 Jun 5;98(12):6571–6.

149. De Jesus AA, Hou Y, Brooks S, Malle L, Biancotto A, Huang Y, et al. Distinct interferon signatures and cytokine patterns define additional systemic autoinflammatory diseases. Journal of Clinical Investigation. 2020 Feb 24;130(4):1669–82.

150. Pendergraft WF, Means TK. AGS, SLE, and RNASEH2 mutations: translating insights into therapeutic advances. J Clin Invest. 2015 Jan 2;125(1):102–4.

151. Schaer CA, Laczko E, Schoedon G, Schaer DJ, Vallelian F. Chloroquine Interference with Hemoglobin Endocytic Trafficking Suppresses Adaptive Heme and Iron Homeostasis in Macrophages: The Paradox of an Antimalarial Agent. Oxidative Medicine and Cellular Longevity. 2013;2013:1–10.

152. Bonaccio M, Di Castelnuovo A, Pounis G, De Curtis A, Costanzo S, Persichillo M, et al. A score of low-grade inflammation and risk of mortality: prospective findings from the Moli-sani study. Haematologica. 2016 Nov;101(11):1434–41.

153. Pokatayev V, Hasin N, Chon H, Cerritelli SM, Sakhuja K, Ward JM, et al. RNase H2 catalytic core Aicardi-Goutières syndrome-related mutant invokes cGAS-STING innate immune-sensing pathway in mice. J Exp Med. 2016 Mar 7;213(3):329–36.

154. Mathavarajah S, Dellaire G. LINE-1: an emerging initiator of cGAS-STING signalling and inflammation that is dysregulated in disease. Biochem Cell Biol. 2024 Feb 1;102(1):38–46.

155. Hermjakob H, Montecchi-Palazzi L, Lewington C, Mudali S, Kerrien S, Orchard S, et al. IntAct: an open source molecular interaction database. Nucleic Acids Res. 2004 Jan 1;32(Database issue):D452-455.

156. Sullivan E, Santiago C, Parker ED, Dominski Z, Yang X, Lanzotti DJ, et al. *Drosophila* stem loop binding protein coordinates accumulation of mature histone mRNA with cell cycle progression. Genes Dev. 2001 Jan 15;15(2):173–87.

157. Sokolova V, Sarkar S, Tan D. Histone variants and chromatin structure, update of advances. Computational and Structural Biotechnology Journal. 2023;21:299–311.

158. Dvořáčková M, Fajkus J. Visualization of the Nucleolus Using 5′ Ethynyl Uridine. In: Heitkam T, Garcia S, editors. Plant Cytogenetics and Cytogenomics [Internet]. New York, NY: Springer US; 2023 [cited 2024 Sep 4]. p. 377–85. (Methods in

Molecular Biology; vol. 2672). Available from: https://link.springer.com/10.1007/978-1-0716-3226-0_24

10. LIST OF PUBLICATIONS

1) Rey F, Messa L, **Maghraby E**, Casili G, Ottolenghi S, Barzaghini B, Raimondi MT, Cereda C, Cuzzocrea S, Zuccotti G, Esposito E, Paterniti I, Carelli S. *Oxygen Sensing in Neurodegenerative Diseases: Current Mechanisms, Implication of Transcriptional Response, and Pharmacological Modulation*. Antioxid Redox Signal. 2023 Jan;38(1-3):160-182. doi: 10.1089/ars.2022.004

2) Rey F*, **Maghraby E***, Messa L, Esposito L, Barzaghini B, Pandini C, Bordoni M, Raimondi MT, Mazza M, Zuccotti G, Cereda C, Carelli S. *Identification of a novel pathway in sporadic Amyotrophic Lateral Sclerosis mediated by the long non-coding RNA ZEB1-AS1*. Neurobiol Dis. 2023 Mar;178:106030. doi: 10.1016/j.nbd.2023.106030. * These authors contributed equally to the work.

3) Barzaghini B, Carelli S, Messa L, Rey F, Avanzini MA, Jacchetti E, **Maghraby E**, Berardo C, Zuccotti G, Raimondi MT, Cereda C, Calcaterra V, Pelizzo G. *Bone Marrow Mesenchymal Stem Cells Expanded Inside the Nichoid Micro-Scaffold: a Focus on Anti-Inflammatory Response*. Regen Eng Transl Med. 2023 Mar 20:1-12. doi: 10.1007/s40883-023-00296-

4) Rey F, Berardo C, **Maghraby E**, Mauri A, Messa L, Esposito L, Casili G, Ottolenghi S, Bonaventura E, Cuzzocrea S, Zuccotti G, Tonduti D, Esposito E, Paterniti I, Cereda C, Carelli S. *Redox Imbalance in Neurological Disorders in Adults and Children*. Antioxidants (Basel). 2023 Apr 20;12(4):965. doi: 10.3390/antiox12040965.

5) Carelli S, Rey F, **Maghraby E**, Cereda C. *Insights on ZEB1-AS1: emerging roles from cancer to neurodegeneration*. Neural Regen Res. 2024 Jun 1;19(6):1187-1188. doi: 10.4103/1673-5374.385856.

6) Rey F, Esposito L, **Maghraby E**, Mauri A, Berardo C, Bonaventura E, Tonduti D, Carelli S, Cereda C. *Role of epigenetics and alterations in RNA metabolism in leukodystrophies.* Wiley Interdiscip Rev RNA. 2024 May-Jun;15(3):e1854. doi: 10.1002/wrna.1854

7) Rey F, Monti L, Bruno A, Gallazzi M, Roncoroni R, **Maghraby E**, Carelli S, Cereda C, Acquati F. Mutant alleles in Aicardi-Goutières Syndrome patients produce a dysfunctional RNASET2 protein associated with alterations in interferon signaling. In preparation.

8) Pirota V, Rey F, Esposito L, Fantini V, Pandini C, **Maghraby E**, Di Gerlando R, Doria F, Mella M, Pansarasa O, Gandellini P, Freccero M, Carelli S, Cereda C. *Effective lowering of α-synuclein expression by targeting G-quadruplex structures within the SNCA gene*. Int J Biol Macromol. 2024 Oct;277(Pt 4):134417. doi: 10.1016/j.ijbiomac.2024.134417.

9) Calcaterra V, Loretelli C, Biganzoli D, Abdelsalam A, Marano G, Carelli S, Fiori L, Mannarino S, D'Auria E, Verduci E, De Santis R, Dilillo D, Fabiano V, Carlucci P, **Maghraby E**, Messa L, Cereda C, Fiorina P, Biganzoli E, Zuccotti G. *Long-term*

cytokine profile in multisystem inflammatory disease among children. Cytokine. 2024 Aug 27;183:156744. doi: 10.1016/j.cyto.2024.156744.

10) Berardo C, Mauri A, Esposito L, Rey F, **Maghraby E**, Messa L, Vasco A, Benedetti S, Zuccotti G, Carelli S, Cereda C. *Cutting-edge approaches and emerging therapies for conditions identified through newborn screening programs*. In preparation.

11) **Maghraby E**, Rey F, Esposito L, Leone M, Messa L, Allevi R, Mazzucchelli S, Jacchetti E, Zuccotti G, Tonduti D, Carelli S, Cereda C. *Novel insights in Aicardi-Goutières syndrome: characterization of new players in primary fibroblasts carrying a RNU7-1 (AGS9) mutation*. In preparation.

12) Rey F, Esposito L, Messa L, **Maghraby E**, Bianchi V, Pandini C, Allevi R, Mazzucchelli S, Gandellini P, Zuccotti G, Cereda C, Carelli S. *Unraveling the Role of SNCA-AS1: insights into α-Synuclein Regulation, Synaptic Dysfunction, and Dopaminergic Targets*. In preparation.

13) Rey F, **Maghraby E**, Espostio L, Mauri A, Panzeri G, Gallazzi M, Bruno A, Zuccotti G, Tonduti D, Cereda C, Carelli S. *Novel players in Aicardi-Goutières Syndrome: Insights from IFIH1 Mutation associated targets*. In preparation.

14) Rey F, **Maghraby E**, Girau A, Zuccotti G, Cereda C, Carelli S. The lncRNA ZEB1-AS1 interacts with Amyotrophic Lateral Sclerosis-causing protein FUS and it impacts targets of glutamatergic synapse. In preparation.

11. POSTERS AND ORAL PRESENTATIONS

- Functional characterization of IFIH1 mutations in Aicardi-Goutières syndrome: cytosolic RNA sensors and novel molecular regulators. **Maghraby E**, Rey F, Esposito L, Leone M, Allevi R, Mazzucchelli S, Zuccotti GV, Tonduti D, Carelli S, Cereda C. Oral presentation, ULF Congress, Chicago July 2024.
- Novel insights in Aicardi-Goutières syndrome: characterization of new players in primary fibroblasts carrying a RNU7-1 (AGS9) mutation. **Maghraby E**, Rey F, Esposito L, Leone M, Allevi R, Mazzucchelli S, Zuccotti GV, Tonduti D, Carelli S, Cereda C. ULF Congress, Chicago July 2024.
- New insights in Aicardi-Goutières Syndrome: characterization of novel players in a RNU7-1 mutation. **Maghraby E**, Rey F, Esposito L, Panzeri G, Zuccotti GV, Tonduti D, Carelli S, Cereda C. ESHG Congress, Berlin June 2024.
- Novel frontiers in Aicardi-Goutières sydrome: Characterization of a RNU7-1 mutation. **Maghraby E**, Rey F, Esposito L, Panzeri G, Zuccotti GV, Tonduti D, Carelli S, Cereda C. Brayn Congress, Napoli September 2023.
- Oxygen sensing in neurodegenerative diseases: current mechanisms, implication of transcriptional response and pharmacological modulation. **Maghraby E**, Rey F, Messa L, Casili G, Ottolenghi S, Barzaghini B, Raimondi MT, Cereda C, Cuzzocrea S, Zuccotti GV, Esposito E, Carelli S, AD/PD™ 2023 Advances in Science & Therapy, Gothenburg March 2023.

- Investigation of the lncRNA ZEB1-AS1 in sporadic ALS: deregulation in neuronal differentiation and characterization of a novel disease pathway. **Maghraby E**, Rey F, Messa L, Esposito L, Barzaghini B, Pandini C, Bordoni M, Gagliardi S, Diamanti L, Raimondi MT, Mazza M, Zuccotti GV, Carelli S, Cereda C, ARISLA 2022, Milano 3-4 November 2022.